Graphene and Glass Flake Nanocomposites Coatings for Corrosion Mitigation in Chloride Rich Environments

by

Hesham Alhumade

A thesis
presented to the University of Waterloo
in fulfillment of the
thesis requirement for the degree of
Doctor of Philosophy
in
Chemical Engineering

Waterloo, Ontario, Canada, 2018

© Hesham Alhumade 2018

Examining Committee Membership

The following served on the Examining Committee for this thesis. The decision of the Examining Committee is by majority vote.

External Examiner	NAME	Jiangning Wu
	Title	Professor
Supervisor(s)	NAME	Ali Elkamel
	Title	Professor
	NAME	Aiping Yu
	Title	Professor
Internal Members	NAME	Leonardo Simon
	Title	Professor
	NAME	Yuning Li
	Title	Professor
Internal-external Member	NAME	Sagar Naik
	Title	Professor

AUTHOR'S DECLARATION

I hereby declare that I am the sole author of this thesis. This is a true copy of the thesis, including any required final revisions, as accepted by my examiners.

I understand that my thesis may be made electronically available to the public.

Abstract

Inspired by the needs for the preparation of protective coatings with enhanced protection properties especially corrosion resistance in the oil and gas industry, the research focuses on the synthesis and the evaluation of various polymer composites on different metals substrates as protective coatings in Chloride rich environment. In various areas of application including oil and gas industry, metals substrates are continuously exposed to various deterioration factors including corrosion, impact, thermal and UV degradation. In addition, the rates of deterioration based on those factors can be further accelerated in certain environment. For example, the rate of metal deterioration due to corrosion can be accelerated in a Chloride rich environment causing significant reduction in the life span of metal substrates in different fields including oil and gas industry. For instance, in off shore oil and gas operation, drilling rigs are continently exposed to the Chloride rich ocean's wave, which may accelerates the corrosion process on various metals based items of the rigs. Therefore, various corrosion mitigation techniques including the use of protective coatings are utilized to attenuate the corrosion rate and extend the life span of metal substrates. In particular areas, protective coatings can be exposed to various degradation factors including UV, Thermal degradations as well as deterioration due to impact. Therefore, it was important to evaluate other protection properties of the prepared protective coatings in addition to corrosion resistance. The studies focused on the incorporation of pristine Graphene and Glass Flake in different polymer resin such as Epoxy and Polyetherimide and evaluates the composites as protective coating on different metals substrates such as Copper, Stainless Steel 304 and Cold Rolled Steel. Furthermore, the studies investigated the possibility of enhancing the protective properties of the prepared protective composites coating by surface modification and functionalization of the filler in order to enhance the level of interaction between the polymer resin and the fillers. The synthesized

composites are characterized using X-Ray diffraction (XRD) and Fourier transfer infrared (FTIR) techniques, while the dispersion of the fillers in polymeric matrices are examined using Transition electron microscopy (TEM) and Scanning electron microscopy (SEM). The corrosion protection properties of the prepared protective composites coatings are examined using Electrochemical impedance spectroscopy (EIS) and Cyclic voltammetry (CV) or potentiodynamic techniques. Furthermore, the interface adhesion between metal substrates and the protective coatings is examined and evaluated according to the ASTM-D3359 standard, while the impact resistance and the UV degradation properties are examined and evaluated according to the ASTM -D2794 and ASTM-D4587 standards, respectively. Moreover, the thermal degradation properties of the prepared protective coatings are evaluated by examining the rate of degradation or weight loss of the composites using Thermal Gravimetric Analysis (TGA) techniques and examining the influences of the incorporation of the various fillers in the glass transition temperature of the composites using Differential Scanning Calorimetry (DSC) technique. The studies reveal that the incorporation of the different types of fillers will enhance the corrosion resistance properties of the polymer resin in addition to other properties such as impact resistance, thermal stability and UV degradation. Furthermore, the studies conclude that the level of enhancement in corrosion protection as well as other protection properties can be further excelled by increasing the load of fillers in the composites. Moreover, it was interesting to observe that increasing the load of filler in the composites may negatively impact imperative properties such as interface adhesion, where increasing the load of fillers may attenuate the interface adhesion between the protective coatings and the coated metal substrates. A number of contributions have been reported in this research project including the preparation and the examination of nanocomposites materials as protective coatings on different metals substrates after the incorporation of different pristine nano-fillers such as Graphene and Glass Flake. The contributions also include the reporting for the first time of new

and unique recipes that demonstrate simple steps for the surface functionalization of Graphene Oxide and Glass Flake before utilizing the functionalized fillers in the preparation of nanocomposites coatings with enhanced protective properties including corrosion resistance and thermal stability.

Acknowledgements

I would like to acknowledge the financial support of the Petroleum Institute, Abu Dhabi through research project # 66. I also acknowledge the financial support and the full scholarship from the Ministry of Education, Saudi Arabia.

I would like to record my gratitude to my supervisors Dr. Ali Elkamel and Dr. Aiping Yu for their support, advice, and guidance from the beginning of my program. I am indebted and grateful to Dr. Leonardo Simon for all his encouragement and support, which inspired and enriched my knowledge in various ways. I am also indebted to all fellow colleagues for their support and suggestions on my research work and also grateful to all faculty members, office and technical staff at the department of chemical engineering for their support during last years.

I would also like to thanks my family, especially my parents, for the encouragement, support and their effort during the days of the hard work in making my life more comfortable.

Dedication

To all of my teachers, especially my parents

Table of Contents

List of Figures

List of Tables

List of Abbreviations

A	Surface Area
CE	Counter Electrode
CPE	Constant Phase Element
E	Epoxy Composites
E/FGF	Epoxy/Functional Glass Flake Composites
E/FGO	Epoxy/Functional Graphene Composites
E/G	Epoxy/Graphene Composites
E/GF	Epoxy/Glass Flake Composites
E/GO	Epoxy/Graphene Oxide Composites
E_{corr}	Corrosion Potential
EW	Equivalent Weight
FGF	Functional Glass Flake
FGO	Functional Graphene oxide
FTIR	Fourier Transfer Infra-Red
G	Graphene
GF	Glass Flake
GO	Graphene Oxide
I_{corr}	Corrosion Current

OCP	Open Circuit Potential
P_{EF}	Protection Efficiency
R_{ch}	Charge Transfer Resistance
R_{corr}	Corrosion Rate
RE	Reference Electrode
R_P	Polarization Resistance
R_s	Solution Resistance
SEM	Scanning Electron Microscopy
t	Time
TEM	Transmission Electron Microscopy
W	Warburg Impedance
W_0	Weight in mg at time Zero
WE	Working Electrode
W_t	Weight in mg at time t
XRD	X-Ray Diffraction

List of Symbols

ρ	Density

Chapter 1

Introduction

Corrosion is the destruction of materials by chemical or electrochemical reactions with their environments, typically a transfer of electrons from one material to another. Corrosion mainly occurs because of the natural tendency for most metals to return to their natural state. Metals are produced by applying energy to the basic minerals and ores and therefore, it is natural that these metals tend to release this energy and convert to the natural forms when exposed to the environment. This conversion can be accelerated by various physical and environmental factors such as exposed area, time of exposure, temperature and moisture. For most metals, oxide is more stable than the metal and therefore, the metal oxidizes with oxidation rate that depends on the nature of the oxide. Corrosion is a natural phenomenon that should be believed to be an inevitable process. However, failures from corrosion may cause severe safety hazards or interruptions to operations. Therefore, a great attention is given to the control and prevention of corrosion to extend the life of metallic components exposed to the environment.

Corrosion has negative impacts on various industrial areas such as transportation, utilities, infrastructure as well as production and manufacturing. In the United States, the National Association of Corrosion Engineers (NACE) reported that the direct cost of corrosion on various sectors in 2001 was $276 billion, which corresponds to 3.1% of the States' gross national product (GNP). Considering the same percentage of the gross national product, the cost of corrosion was estimated to be $500.7 billion in 2013 and the cost of corrosion is expected to grow to $1 trillion in 2015. Furthermore, in oil and gas industry, the estimated cost of corrosion was reported to be $1.37 billion where this cost was broken down to $590 million for pipeline and facility, $463 million for downhole piping expenses and the rest in corrosion related capital expenditure [1]. The lack of prevention or mitigation of such a process results in serious threat to both economy and industry. Therefore, an increasing number of studies have focused on strategies to slow the kinetics and/or alternate the mechanism of corrosion. Examples of these strategies are anodic or cathodic

protection [2], [3], the use of protective coatings [4], and the use of corrosion inhibitors [5]. These protection techniques have been utilized in various fields such as marine, pipeline, construction and automobile industries. However, there is a growing demand for more robust techniques with enhanced inhibition efficiency in order to boost the life cycle of various materials for environmental and economic savings. Nanocomposites, hydrophobic and organic-inorganic hybrids coatings have already excelled in extending the life of various materials in corrosive environments [6]–[12].

Copper and steel are extensively utilized in a wide range of technological and industrial applications due to their outstanding electrical and thermal conductivity, ductility, wear and shock resistance, and processabilty. Previous study showed that protective oxides or hydroxides layers form on the surface of the metal under neutral or near neutral pH conditions [13], [14]. However, the formation of these protective layers and the corrosion process will be more complex in the presence of chloride ions [15]. In an oxidative environment, the corrosion mechanism involves dissolution of metals at local areas, which are referred to as the anodic sites and electrochemical reduction of oxygen and water at cathodic sites. The formation of oxide or hydroxide layer will eventually slow down the rates of dissolution and reduction reactions. Indeed, studies have illustrated that the rates of these reactions are proportional to the rate of diffusion of metal ions into the chloride solution. Furthermore, the presence of the oxides or hydroxide insoluble layer will not prevent the diffusion and reduction of corrosive agents such as oxygen [16]. Limiting the diffusion of corrosive agents to the metal substrates can be achieved by coating the metal with anti-corrosive materials that can not only protect from corrosion, but also enhance the mechanical properties of the metal. Polymer based composites, which were first reported in the 1960s are perfect examples of compounds that can improve the properties of metal substrates especially when inorganic materials are incorporated as nanofillers to form organic-inorganic nanocomposites. These inorganic nanomaterials can be found in layered, tubular and spherical forms such as clay, carbon nanotubes and SiO2, respectively [17]–[24].

1.1 Types of corrosion

There are two main types of corrosion the first is the dry chemical corrosion, which takes place in a dry environment and the second is the electrochemical corrosion, which is a combination of chemical reactions and a flow of an electric current. The dry reactions between some atmospheric gases such as Oxygen, Halogen and H_2S and metals are examples of chemical corrosion. These reactions might form solid films of corrosion product, which protect the metal from further corrosion. For example, chlorine reacts with silver to produce a protective film of silver chloride as per the following chemical reaction.

$$2Ag + CL_2 \rightarrow 2AgCl \tag{1.1}$$

Furthermore, the corrosion product can be soluble or volatile, which exposes the metal to further corrosion. Unlike the chemical corrosion, the electrochemical corrosion requires a conductive medium for ionic movements, which is called electrolyte. In addition to the electrolyte, electrochemical corrosion requires an anode, a cathode and an electrical connection between the anode and the cathode for the flow of the electron current. At the anode an oxidization reaction takes place and the released electrons form positive metal ions that dissolved in the electrolyte before a precipitation takes place on the cathode, where this participation is referred to as the reduction reaction (*i.e* the anode corrodes while the cathode remains intact). The oxidation and reduction reactions of Zinc and Copper, respectively are illustrated in equations 1.2, 1.3 and Figure 1.1. It is worth mentioning that anode and cathode phases may actually exist on the same piece of a metal with a potential difference at micro-structural levels as shown in Figure 1.2.

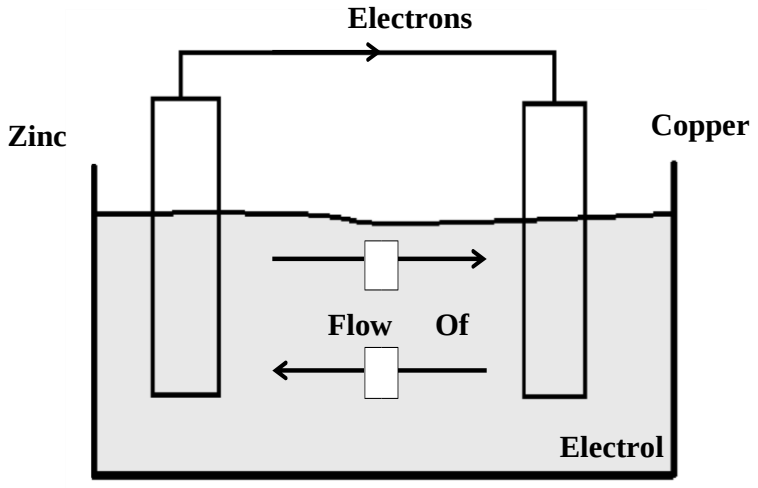

Figure 1.1: Galvanic corrosion between two different materials.

$$Anode : Zn(s) \rightarrow Zn^{2+} + 2e^{-} \quad (1.2)$$

$$Cathode : Cu^{2+} + 2e^{-} \rightarrow Cu(s) \quad (1.3)$$

This potential difference can be a result of different factors such as irregularities of metal surface, differences in the concentration of metal ions or oxygen as well as differences in the residual stress level. Whether the corrosion phenomena occurs on a single metal or between multiple metals, potential difference is what forces the electrons to flow from the anode to the cathode and obviously the corrosion rate increases simultaneously with the potential difference.

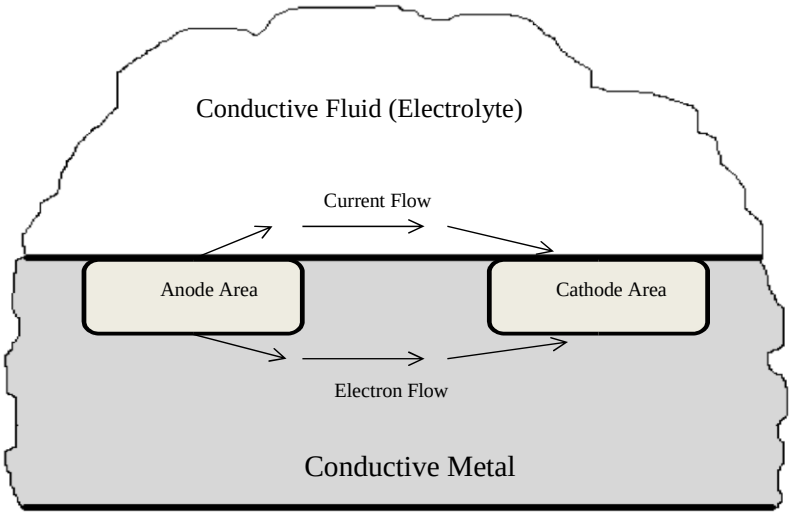

Figure 1.2: Galvanic corrosion within the same material.

1.2 Forms of corrosion

There are different forms in which corrosion can be manifested; therefore it is convenient to classify corrosion based on the appearance of the corroded part of the material. In most cases, visual inspection is good enough to identify the form of corrosion and also to retrieve valuable information, which can be used to take corrective measures. However, magnification is still required for some cases where a naked eye cannot detects or evaluates corrosion. The various forms of corrosion can be classified as follow:

- Uniform corrosion
- Galvanic Corrosion
- Pitting corrosion
- Crevice corrosion
- Erosion corrosion
- Stress corrosion
- Corrosion fatigue

Uniform corrosion is the most commonly observed form of corrosion, which is characterized by an even loss of the metal from the corroding surface. This form of corrosion is usually observed in automobile industry, outdoor appliances and steel structures. This form of corrosion can be easily identified by naked eyes and be characterized by calculating the weight loss. When dissimilar metals are coupled in a presence of an electrolyte the less noble metal corrodes and this corrosion is known as galvanic corrosion. Here too, visual inspection can be enough to identify and evaluate the degree of corrosion. Corrosion may take place in certain areas of the metal and removes a small part of the total volume, which results in craters or pits on the surface of the metal. In this case, corrosion is referred to as pitting corrosion, which is more difficult to detect than the uniform and the galvanic corrosion. Pitting corrosion is considered one of the most dangerous corrosion as the craters or pits can perforate through the metal and results in costly repairs or failures. Crevice corrosion usually takes place in narrow and confined spaced between similar or dissimilar metals and takes the forms of etched patches or pitting. Erosion corrosion is a combination of chemical and mechanical attacks, where the random movements of the liquid above the metal surface first remove the protective film on the surface before the metal oxidizes by reacting with the liquid. Erosion corrosion can be accelerated when solid particles or gaseous bubbles are suspended in the liquid. Both stress corrosion and corrosion fatigue are chemical-mechanical processes where metals crack below their tensile strengths. However, stress corrosion is usually a result of an enduring tensile stress, while corrosion fatigue is a result of repeated mechanical stresses over a period of time. In the proper chemical environment, these forms of corrosion may take place and result in sever damages.

1.3 Electrochemistry of corrosion

When a chemical reaction involves a transfer of electron, the term electrochemical is used to describe such a reaction. This type of reaction is a combination of oxidation and reduction reactions. Since almost all metals corrodes through an electrochemical process, it is crucial to understand the basics of electrochemical reactions. The electrochemical process contains three basic elements, on is the anode, which is the element that gives the electrons, then the cathode which takes the electrons and finally and

electrically conducting path is required between the first two elements in order to complete the electrochemical circuit. Figure 1.1, depicts a typical corrosion cell, where Zinc and Copper are used as anode and cathode, respectively and both metals are connected with an electrical path for the transfer of electrons. In nature, the environment serves as the conducting medium between the anode and the cathode and therefore the conductivity of the various medium Soil, Concrete or natural water is directly related to the degree of corrosion in the medium.

It is important to realize that for a complete electrochemical process, multiple metals are not always required. Indeed, the oxidation and reduction reactions may actually take place on the same piece of metal, where the electrons transfer from the anodic to the cathodic areas on of the metal as illustrated in Figure 1.2. Finally, it should be noted that more than one oxidation reduction reactions might take place at the same time on the same piece of metal and this will accelerate the corrosion. For example, when Zinc is immersed in a Hydrochloride solution, two reduction reactions may take place, first is the evolution of Hydrogen gas and second is the reduction of Oxygen. With two different reduction reactions that consume electrons, a faster oxidation rate will be observed and therefore a Hydrochloride solution with dissolved Oxygen or exposure to the surrounding will be more corrosive than an isolated solution.

1.4 Corrosion Kinetics

In a corrosive medium, predicting the corrosion currents or corrosion rates plays an important role in designing, materials selection and scheduled maintenance. Indeed, the cathodic and anodic currents are the main components in corrosion processes and these two elements are controlled by polarization effects. Polarization is the difference between the observed potential and individual reaction equilibrium potential and the quantitative value of this difference is referred to as overpotential. Total polarization or overpotential consists of three distinct types of polarization, which are activation overpotential, concentration overpotential and ohmic drop and understanding these factors is a key to predict the kinetics of corrosion processes. For example, agitating the electrolyte or stirring will enhance corrosion in systems controlled by concentration polarization as stirring boost the diffusion rate of active species.

1.4.1 Activation Polarization

Activation polarization is a complex function that describes the charge transfer kinetics of electrochemical reactions and this type to polarization is usually dominant in corrosion studies in strong acids, where electrons transfers from the metal surface to the electrolyte is fast. The rates at which electrons can transfer on different metals vary. If the simple reduction reaction of hydrogen is considered, the rate of hydrogen evolution for various metal substrates might highly varies as an effect of the different electron transfer rate on these metals. The variation of hydrogen production on different metals substrates can be explained by the exchange current density or the corrosion current density (I_{corr}), where this variable can be obtained by using a three electrodes configuration and a potentiostat/ galvanostat power controller. Here a current is passed through the working electrode to the auxiliary electrode and the potential is recorded between the working and the reference electrode. The collected current and potential data are used to extract the corrosion current density and the corrosion potential and illustrated in Figure 1.3.

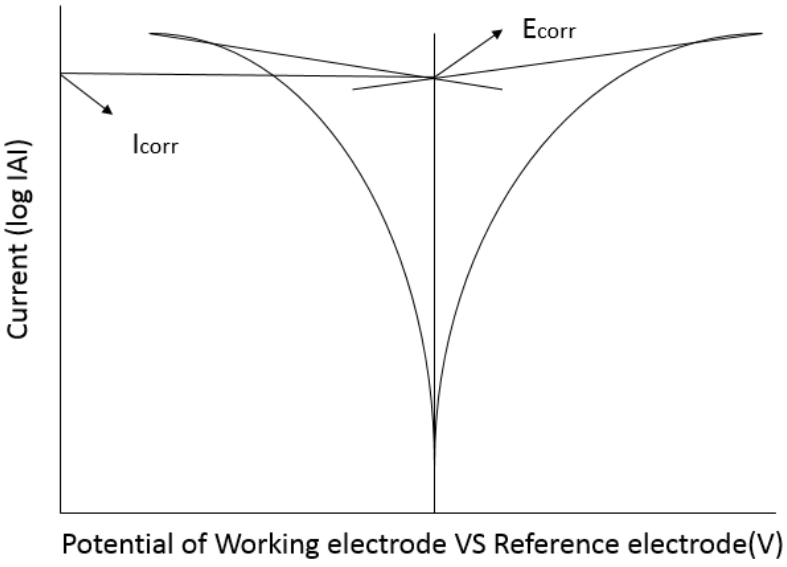

Figure 1.3: Tafel plot representing activation Polarization behavior of Carbon Steel.

1.4.2 Concentration Polarization

The variation in concentrations in the environment close to metal substrate is what drives the concentration polarization. Therefore, concentration potential may limit the overpotential value in a dilute solution where low concentrations of corrosive agents are available. An example of this limitation is an isolated corrosion process where the cathodic process is oxygen reduction. In general, mass transfer is driven by three main forces, which are diffusion, migration and convection. The influences of migration and convection will be negligible in absence of electrical field and in stagnant conditions, respectively. In this case, mass transport will be controlled purely by diffusion. Here, Fick's first law can be used to describe the flux of a certain species from the surrounding to the metal substrate, where the diffusion coefficients for some common elements such as hydrogen and copper are already reported in the literature.

1.4.3 Ohmic Polarization

Ohmic polarization represents the driving force from the environment. Therefore, in situations where the surrounding is a good conductor such as sea water, the influence of ohmic polarization is neglected. Ohmic polarization in significant in studies that focus on the effects of the electrolyte rather than metal substrates or coatings. Furthermore, this type of polarization is also significant in protection method such as cathodic and anodic protection, where a current is passed through the electrolyte in order to force a potential shift. In corrosion studies a Luggin capillary is always used and fixed as close as possible to the working electrode surface in order to minimize the variation in potential caused by the electrolyte

1.5 Electrochemical corrosion testing

1.5.1 Potentiodynamic Polarization

In this testing technique, the potential of the working electrode is scanned over a certain range using a certain scanning rate, where the potential is controlled by applying a current through the electrolyte. Based on the activities on the working electrode, the polarization can be identified as anodic, where the potential is moved in the anodic direction forcing the working electrode to release electrons or cathodic polarization,

where the opposite happens and electrons are added to the working electrode. The most famous form of potetiodynamic polarization is cyclic voltammetry, where the potential is swiped from a certain start value in the positive direction until a predetermined value is reached and the potential reverses back to the original start point. During this sweep of potential, the current is recorded and presented as a function of potential to produce a polarization plot as depicted in Figure 1.4. Linear polarization resistance (R_p) is another parameter that can be computed using the polarization technique. This resistance is defined as the slop of potential-current density at the open circuit potential and it can also be calculated using the corrosion current density (I_{corr}) and the Steam-Geary equation.

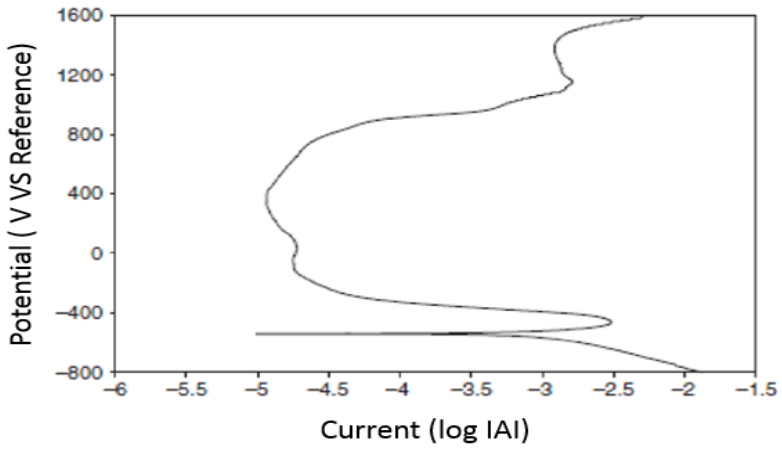

Figure 1.4: Polarization Curve

1.5.2 Electrochemical impedance spectroscopy

Electrochemical Impedance Spectroscopy (EIS) is another powerful and accurate technique that can be used to evaluate the corrosion resistance of metal substrate. In this technique an alternative current is passed through the corrosion system and the resulted resistivity is recorded as a complex number with real and imaginary parts. The main advantage of this technique over others is the possibility of testing the metal substrate without disturbing the properties being measured. In general, the resulted complex resistivity of the tested metal substrate provided qualitative conclusions only, however; these qualitative results can be

interpreted using a model of the metal interface, which might contain various electrical elements such as resistors and capacitors. For instance, R_p is one of the electrochemical variables that can be computed using the model of the metal interface.

1.6 Objectives

The objective of this research is to examine adhesive polymer such as (Polyetherimide) *PEI* and Epoxy as corrosion inhibition coatings after the incorporation of graphene sheets and GF as fillers. These coatings are expected to protect metal substrates through two mechanisms. First, the coatings serve as barrier to water and oxygen permeation. The second protection mechanism is attributed to the ability of the well dispersed graphene nanosheets in the polymer matrix in prolonging the diffusion pathway corrosive agents such as oxygen and water molecules cross to reach metal substrate. In this study, the corrosion prevention ability of graphene nanocomposites is examined through electrochemical corrosion measurements in a 3.5 wt.% sodium chloride aqueous solution. Furthermore, the study investigates the long time performance of the coatings by performing the adhesion test after certain period of exposure to the 3.5 wt.% NaCl solution. In addition to the electrochemical and adhesion tests, other properties such as flexibility and thermal stability of the coatings are examined.

This report is divided as follow, a brief overview about corrosion will be presented first, where the various types, forms, protection techniques of corrosion are illustrated in Part I. In addition, electrochemistry, thermodynamics and kinetics of corrosion are also presented in the same part. Following the general overview on corrosion, a detailed literature about graphene/glass flake and the current studies that focused on using graphene/glass flake composites for corrosion protection purposes will be presented in Part II. The methods used to evaluate the corrosion resistance properties of the prepared coatings in addition to other properties are detailed in Part III Then, Part IV-IX will illustrate the current advances in implementing *PEI* and Epoxy graphene/glass flake composites as anti-corrosion coatings and the various collected results from electrochemical measurements and other tests are presented and described. Finally,

Part X will illustrate the plan for the future work and the proposed ideas to excel the corrosion inhibition property of the prepared coatings.

Chapter 2

Background

2.1 Graphene and Glass Flake

Graphene is a honeycomb lattice of carbon atoms and is believed to be the basic structural unit of various carbon allotropes such as graphite, carbon nanotube and fullerenes. For instance, carbon nanotube is a rolled-up cylinder of graphene, while graphite is viewed as a stack of graphene layers. Since the historical successful identification of single layer graphene, which was once considered to be unstable and could not exist under ambient conditions, by Geim and co-worker in 2004 [25] using a simple tabletop experiment, graphene has attracted remarkable attention as nanofiller for polymer nanocomposites and this is attributed to the extraordinary properties of graphene such as high surface area, aspect ratio, tensile strength, thermal and electrical conductivity, electromagnetic interference shielding ability, flexibility, transparency as well as low coefficient of thermal expansions. Therefore, graphene can be preferred over other nanofillers such as clay and carbon nanotube. There are four various approaches for graphene preparation. First approach is chemical vapor deposition (CVD) and epitaxial growth [26]. The second method, which is the one reported in 2004 by Geim and coworkers is the micromechanical exfoliation of graphite, which is known as the "scotch tape" method [25]. The third is epitaxial growth on electrically insulating surfaces [27], while the fourth and the most currently used method is the thermal exfoliation of graphene oxide [28]. In what follows, the various available methods for graphene composites will be illustrated before current advances in using graphene composites for corrosion inhibition purposes are detailed.

Glass flake is an extremely thin glass platelets that can be produced in various thickness and size using two main approaches. First is the bubble method [29], where the glass marble is turned into liquid form by heating and then shattered into glass flake and filtered by particle size distribution. The second approach is the centrifuge method [30], where the glass is also turned into liquid by heating and the liquid glass flake is rotated creating glass flake due to the centrifuging force.

2.2 Graphene and Glass Flake composites

The development of the incorporation and dispersion of graphene/glass flake particles in a polymer matrix has recently initiated studies in various fields of science and engineering. This is attributed to the considerable improvement in properties that cannot usually be achieved using composites with other nanofillers or virgin polymers. However, the extent of the enhancement in various properties can be directly related to the degree of dispersion of the graphene/glass flake particles in the polymer matrix. Furthermore, it is interesting to observe that such an enhancement in the properties of a polymer matrix can be achieved at a very low loading of the fillers [31]–[34]. These improvements in the properties for example, but not limited to tensile strength, storage modulus and electrical conductivity have been observed on various polymer resin such as epoxy, polyethylene, polypropylene, polystyrene and polyimide. The degree of dispersion of graphene/glass flake in a polymer matrix plays an important role in the degree of the improvement of the various properties. Therefore, various preparation methods have been established in order to maximize dispersion of graphene/glass flake for the purpose of achieving the optimum performances with minimum loadings of fillers.

There are three main approaches for incorporation of graphene/glass flake in a polymer matrix. First is the in situ polymerization method, where graphene/glass flake is first swollen within the liquid monomer. Then based on the hosting polymer a suitable initiator is introduced to the filler solution and polymerization is initiated usually by thermal energy or radiation. The second method is known as the solution method, where a solvent is used in which the polymer or pre-polymer is solubilized and graphene/glass flake is allowed to swell. The advantage of this approach is that graphene/glass flake can be dispersed easily in various solvents such as water, acetone and toluene and this is attributed to the weak forces that stack the layers of graphene/glass flake together. Here, the polymer adsorbs onto the delaminated graphene/glass flake thin sheets and once the solvent is evaporated, the sheets reassemble in a form of sandwiching the resin to form the composites. Another advantage of this method is the possibility of synthesis of intercalated composites using polymers with low or even no polarity. However, a considerable amount of solvent might

be required in order to achieve an optimum dispersion of the fillers and this is considered a disadvantage of the approach since solvent removal can be a critical issue. Finally, graphene/glass flake composites can also be synthesized using the melt intercalation method, where no solvent is required and this is the main advantage of this approach. In this technique, graphene/glass flake is mixed with the hosting polymer matrix in molten state. Typically, a thermoplastic polymer is mixed mechanically with graphene/glass flake at certain temperatures using conventional methods, such as extrusion and injection molding and as a result graphene/glass flake composites are formed.

2.3 Corrosion protection using Graphene and Glass Flake composites

The implementation of graphene and glass flake composites have been widely reported in various fields and applications [35]. However, only studies that have focused on using graphene and glass flake composites for corrosion protection purposes are reported here.

There are different approaches for the implementation of graphene and graphene composites as protective coatings on metals substrates. However, the majority of the previous studies have used the expensive chemical vapor deposition (CVD) approach for deposition of graphene on various metals substrate. For example, a graphene coating on the copper substrate has been prepared by the CVD technique and the study revealed that impedance of the substrate to electrochemical degradation can be improved significantly with a noticeable reduction in the anodic and cathodic current densities [36]. Using the same technique, another study has reported that a graphene coated copper substrate by CVD encountered a significant enhancement in corrosion resistance [32]. In the chemical vapor deposition approach, graphene is synthesized in situ on metal substrate a hydrocarbon element as carbon source in presence of catalyst under high vacuum. Furthermore, CVD operates at high temperature range that usually varies from 650 to 1000 °C based on the source of carbon as well as the nature of the metal substrate. These requirements of high operating temperature and high vacuum have resulted in limitation on the metal substrate sample size. Therefore, CVD technique lacks the potential to be developed for mass production.

Another coating approach is electrophoretic deposition (EPD), which is a colloidal forming process. In EPD, electrostatically charged colloidal particles in a stable suspension are deposited onto an oppositely charged metal substrate by introduction a DC electric field to the system. Furthermore, a post EPD treatment, normally a heat treatment is usually required in order to eliminate the coatings' porosity [37]. EPD has been used to synthesis a graphene composite coating on copper substrate, where a coating thickness of about 40 nm was obtained at 10 V and 30 s deposition time at optimum EPD conditions [33]. In this study, morphological characterization was carried out using SEM, where graphene was observed to be uniformly coated on the copper substrate. Furthermore, the study concluded an enhancement and reduction in the resistance to electrochemical degradation and the corrosion rate, respectively. In comparison to CVD, this approach is very versatile, fast and cost effective in producing a coating with well controlled microstructure on a wide range of metals substrates. This is attributed to easiness in this method in controlling various variables such as dimensions, stoichiometry, deposition time and rate, thickness in addition to uniformity. Therefore, this method can be considered a substitute to other techniques such as slurry dipping, thermal spraying, sputtering as well as CVD [38]. Despite the remarkable advantages of EPD, it has an intrinsic disadvantage compared to other colloidal approaches such as dip and slurry coating, where EPD cannot be used in applications or fields where the liquid medium is water. This is due to the fact that application of a voltage to water will initiate the evolution of hydrogen and oxygen at the metal substrate and consequently attenuate the quality of the deposits. Moreover, it should be noted that the quality of coatings prepared by EPD will also depend on the electrical nature of the electrodes, where metal substrate with low conductivity are usually more difficult to coat.

In addition to graphene based coating prepared using CVD and EPD, promising observations have been reported using graphene based adhesive composites such as epoxy and polyimide graphene composites. The possibility of using adhesive composites in various environments in addition to the low maintenance cost, simple preparation steps and the possibility of applying these coatings on various metal substrates, explain why these coatings are usually more preferable than coatings prepared using CVD or EPD. In

addition to these remarkable properties these resins combine other outstanding properties such as high thermal and chemical stability, temperature durability, low dielectric constant and thermal expansion coefficient [39]–[41]. A number of studies have focused on the probability of enhancing various valuable properties of polymer including corrosion protection by the incorporation of pristine graphene [32]. For example, Polyimide/Graphene composites coatings have been recently prepared by thermal imidization and the incorporation of graphene resulted in remarkable enhancement in the corrosion inhibition property of the coating [32]. In parallel an environmental friendly anti-corrosion epoxy/graphene composite coating on cold rolled steel has been prepared and cured at room temperature without using any type of solvent [31]. Similar to the previous study, the corrosion protection property of the coating has been examined using Tafel polarization and EIS, where both tests revealed an enhancement in both corrosion protection as well as gas barrier properties as a result of incorporating graphene in the epoxy resin. In addition, the hydrophobic property of this coating has been enhanced by modifying the surface of the coating using a cast. As a result of this surface modification, attenuation on the water and corrosive media adsorption has been reported on the epoxy/graphene coating surface.

In addition to the simple incorporation of pristine graphene in polymer composites or CVD coating with graphene, many researchers have focused on the functionalization of graphene and the influences of such functionalization on various properties including corrosion resistance. For instance, a recent study revealed that the corrosion protection of epoxy and graphene oxide (GO) composites coatings can be enhanced the attaching titanium dioxide on the GO surface using 3-aminopropyltriethoxysilane as coupling agents [42]. Another study investigated the incorporation of fluorographene particles into polyvinyl butyral composite coatings for corrosion protection purposes. The study revealed that shielding property of may remarkably enhance the corrosion resistance of the coating by blocking the diffusion paths of corrosive elements and moisture [43]. Recently, the influences of the incorporation of functionalized GO in epoxy composites, through the wet transfer of amino functionalized GO, on the corrosion resistance property of epoxy coating

were investigated. The study demonstrated that significant enhancement in the corrosion mitigation property of epoxy can be achieved by improving both ionic resistance and barrier properties.

A growing number of studies have focused on the utilization of glass flake as filler in polymer composites. This incorporation have delivered enhancement in various properties such as thermal and viscoelastic properties [44] in addition to corrosion mitigation. For example, the long term performance of epoxy/glass composites as corrosion protection coatings on cold rolled steel was investigated in Chloride rich environment and the study illustrated that the incorporation of glass flake in the epoxy resin may extend the life span of the coated metal substrates. Furthermore, the study revealed that glass flake may delivers further corrosion protection compared to other fillers such as clay [45]. In addition to epoxy, the incorporation of glass flake in various polymer composites was assessed and encouraging corrosion resistance properties were observed on different metal substrates [46]–[48].

Chapter 3

Methodology

The objective of this chapter is to describe in details all procedures followed to conduct the various experimental evaluation techniques utilized to evaluate the prepared protective coatings. In all evaluation techniques, tests were performed on coated samples before and after the incorporation of the fillers in order to illustrate the influences of this incorporation on the various properties of the hosting resin.

3.1 Composites Synthesis

Properties of a polymer composite coating may vary dramatically by incorporating a filler in the polymeric matrix. However, the variation in these properties depends intensely on the preparation procedures of the composite coating. Synthesis of a composite comprises different parameters such as reaction time, temperature, load of filler, dispersion time and thickness of the coating. Therefore, it is essential to conduct experimental analysis to identify the key parameters that may deliver major variation in the properties of the prepared composite coating. The identification of these parameters would help maximizing the valuable properties of a coating including, but not limited to corrosion protection. Therefore, a factorial experimental design statistical study was conducted in order to evaluate the impact of various preparation parameters such as load of filler, curing time, dispersion time and coating thickness [49].

In this study, Epoxy was utilized as a resin while Graphene was incorporated in the Epoxy to prepare the protective coatings. Different samples were prepared with high and low levels of each examined preparation parameters various and the prepared coatings were evaluated using the potentiodynamic polarization technique. Previous studies revealed that the load of filler and the dispersion time are the most significant parameters that may influence the corrosion resistance performance of a protective coating, where increasing the load of filler and mixing time enhanced the corrosion protection properties of the coatings. Furthermore, the study illustrated that increasing the dispersion time is more momentous at low loading of

the filler, while the dispersion time is trivial at high load of filler. Therefore, in all studies the various prepared protective coatings were synthesized with different loads of filler in order to maximize the corrosion resistance properties of the coatings and the dispersion time was always high in order to enhance the dispersion of the different fillers in the prepared protective coatings.

3.2 Composites Characterization

The prepared protective polymer composites coatings were characterized using various techniques such as Fourier transfer infrared spectroscopy (FTIR) and X-ray diffraction (XRD). Furthermore, the dispersion of fillers in polymer composites was captured using Scanning electron microscopy (SEM) and Transmission electron microscopy (TEM). The objective here, is to illustrate the sample preparations steps for each technique.

FTIR samples were prepared by scratching the polymer composites with a sharp fine knife in order to collect small amount of the composites. The collected composites samples were then mixed with certain amount of Potassium Bromide (KBr) in order to maintain the sample load to 2-5 wt.% of the mixture. The mixture was then compressed at 5000 pounds for 2 min to form the FTIR disk sample. FTIR data were recorded from 400-2000 wavenumber at 4 cm^{-1} resolution and a scan time of 64 sec. Unlike FTIR, the XRD samples did not require specific procedures to follow in sample preparation. However, the thicknesses of the prepared polymer composites were maintain below 20 μm in order to maximize the quality of diffraction peaks. XRD diffraction patterns for all prepared composites were recorded in the range of $2\theta = 3\text{-}90^{\circ}$ at scan rate of 0.24°/sec and 0.02° step size.

The dispersion of fillers in the polymer composites was captured using SEM and TEM. SEM samples were fixed on SEM stub using conductive carbon tape. Furthermore, gold sputtering technique with sputtering time of 120 sec was utilized to coat non-conductive polymer composites samples. TEM samples were collected by scrapping the prepared polymer composites with a fine sharp knife and the collected samples were dispersed in methanol. The dispersion was sonicated in a sonication bath for 30 min before

the samples were fished with TEM copper grids. Finally, the collected samples in copper grids were allowed to dry under vacuum at room temperature over night before conduction TEM imaging.

3.3 Adhesion

Interface adhesion between polymer composites coatings and the coated metals substrates was evaluated according the ASTM-D3359 standard. An adhesion tape testing kit was used for this purpose with a standard 11-teeth and 1 mm spacing blade. The test was conducted by making parallel cuts on the coating before applying the tape on the cuts. After peeling off the tape from the coatings, SEM technique was utilized to observe the adhesion property of the various prepared coatings. Moreover, adhesion property of each coating was evaluated and rated according to the ASTM standard based on the amount of peeled composites from the coated samples after conducting the adhesion tape test.

3.4 Electrochemical Measurements

All electrochemical measurements were conducted in a 1L double jacked temperature controlled corrosion cell using 3.5 wt.% NaCl solution as electrolyte. A three electrodes configuration was used to conduct electrochemical measurements, where Ag/AgCl electrode was used as a reference electrode, A graphite rod was used as a counter electrode and coated samples were used as the working electrode. Coated samples were cleaned and dried then mounted in a Teflon holder with 1 cm^2 exposed surface area and the potentials of the testing samples were allowed to stabilize for at least 30 min before conducting electrochemical measurements. The potential of the testing samples were recorded after stabilization as the Open Circuit Potentials (OCP). The electrochemical behaviors of coated samples were evaluated using Electrochemical Impedance Spectroscopy (EIS) and Cyclic voltammetry (CV) techniques.

EIS measurements were carried out at frequency range from 200 kHz – 100 mHz and the collected raw impedance data were presented using Bode and Nyquist plots. Furthermore, equivalents circuits with specific combination of elements utilized for fitting raw impedance data and the variations in the magnitude

of the different elements were used to evaluate the corrosion resistance properties of the prepared protective coatings.

Following the non-destructive EIS measurements, CV was also utilized to evaluate the corrosion protection properties of the prepared protective coatings using the similar testing setup. Here, the potentiodynamic measurements were carried out by scanning the potential of the testing sample from -0.5 V to 0.5 V around OCP at a rate of 0.02 V/min. The collected CV measurements were used to generate Tafel plots in order to extract valuable corrosion parameters such as corrosion current (I_{corr}) and potential (E_{corr}). The variation of these parameters corrosion was investigated to evaluate the corrosion resistance properties of the different protective coatings.

3.5 Gravimetric Analysis

The long term performances of the prepared protective coatings were examined by conducting weight loss measurements. A 500 ml temperature controlled 3.5 wt% NaCl solution was used as the corrosion medium. Testing samples were cleaned with acetone, dried with KimTech paper and weighted before conducting the weight loss tests. After that the samples were mounted in Teflon holders with 1 cm^2 exposed surface areas and immersed in the corrosive medium for 60 days. At the end of the exposure period and after removing the samples from the holders, samples were cleaned in order to remove the corrosive residues by washing the samples with distilled water and immersing the sample in bath sonication for 10 min. Samples were allowed to dry under vacuum over night before the final weights were recorded. The corrosion protection properties of the different coatings were evaluated by comparing the weights of the samples before and after exposure to the corrosive medium. Furthermore, all weight loss measurement were conducted in triplicate in order to examine the reproducibility of the results.

3.6 Thermal Analysis and UV Degradation

Some of the prepared protective coatings are intended for utilization in outdoor environment and therefore, it was important to evaluate the thermal stability and UV degradation properties of those coatings.

Thermal stability property was evaluated using Thermal Gravimetric Analysis (TGA) and Differential Scanning Calorimetry (DSC) techniques. TGA analysis were conducted over temperature range of 25-800° C at heating rate of 15° C/min, DSC analysis were conducted over temperature range of 25-200° C at heating rate of 10° C/min. Thermal analysis helped evaluation important thermal properties such Glass Transition temperature (T_g) and the Onset temperature (T_{onset}), which is the temperature, where the composites loss 5% of the original weight.

In addition to thermal behaviors, it was important to evaluate UV degradation properties of the coatings intended for utilization in outdoor applications. UV analysis were conducted and evaluated according to the ASTM standard D4587 using an accelerated weathering tester. In this test, the samples were continuously exposed to repeated cycles of UV light at 60 ± 2.5° C for 8 hours, followed by water condensation at 50 ± 2.5° C for 4 hours over 30 days. The surface morphology of the tested samples were examined by SEM and here too the samples were gold coated using the sputtering technique for 120 sec.

3.7 Impact resistance

In addition to thermal stability and UV degradation, impact resistance was an important property to evaluate for coatings intended for usage in outdoor environments. Two important properties were tested, which are flexibility and resistance to sudden deformation. Flexibility was evaluated by conducting a pending test, where the coated samples were bent with a conical shaped mandrel with diameter range from 3.1 – 38 mm. The diameter at which the coating cracked was noted in order to compare the flexibility of the prepared coatings before and after the incorporation of fillers.

Resistance to sudden deformation was assessed according to the ASTM standard D2794 using a universal impact tester with 2 Ib falling weight attached to a ball with 0.5 inch diameter. The test was conducted by rising the falling weight 1 inch above the surface of the coatings and releasing the falling weight to impact the coating. This process was repeated with 1 inch increment in the distance between the height of the falling weight and the surface of the coating until the coating

cracks. The heights at which the coatings cracked were recorded and compared in order to examine the influences of the incorporated filler on the impact resistance properties of the coatings.

Chapter 4

Optimizing Corrosion Protection of Stainless Steel 304 by Epoxy-Graphene Composite using Factorial Experimental Design

Abstract

Epoxy-Graphene (E/G) composites were synthesized and evaluated as a corrosion protection coating on Stainless Steel type 304 (SS304) using in situ polymerization approach. Coatings were synthesized at various process variables in order to optimize the corrosion protection efficiency of the prepared protective E/G coating. Cyclic voltammetry (CV) electrochemical measurements were conducted to evaluate the protection efficiency of the prepared coatings. In addition, dispersion of graphene in the polymeric matrix was observed using Scanning Electron Microscopy (SEM) and Transmission Electron Microscopy (TEM). The study revealed that load of graphene as well as mixing time significantly influenced the corrosion protection efficiency, where the protection efficiency increased simultaneously with load of graphene.

4.1 Introduction

A growing problematic natural problem in the metallic industry is corrosion, where metals deteriorate due to electrochemical reactions between metals and the surroundings. A growing number of studies focused on various corrosion protection techniques such as the design of advanced coatings that may significantly slow down corrosion rates and extend the lifetime of metals in different environments. Various materials such as nanocomposites, hydrophobic and organic-inorganic hybrid coatings have already been reported as a potential solution to extend the lifespan of metals [50] in addition to different approaches such as corrosion inhibitors [5], and anodic or cathodic protections [3]. The various protection technologies are currently utilized in fields such as construction, pipeline, and automobile industries.

Stainless steel 304 (SS304) is widely utilized in various fields of industry. This is attributed to the valuable properties of SS304 such as formability, weldability as well as the substantial thermal and

electrical conductivity. Furthermore, SS304 may withstand different atmospheric conditions and temperatures up to 1650°F [51]; however, SS304 may corrode intensely in a chloride rich environment [52]. The incorporation of fillers in polymeric composites might slow the process of corrosion. The protection mechanism depends on the ability of the fillers to prolong the diffusion path corrosive agents follow to reach the surfaces of the metals. Graphene is material that has been increasingly investigated in the manufacturing of polymers composites. The growing interest in graphene is attributed to the ability of Graphene in enhancing mechanical, thermal and dielectric properties of different polymers [40], in addition to the low density and a very high aspect ratio of graphene compare to different fillers such as clay [53]. Therefore, graphene based materials have found wide applications in different fields including gas barrier application and the preparation of corrosion protective coatings [32], [54], [55].

The incorporation of graphene in epoxy may enhance the corrosion protection property of the polymer resin. However, there is no study that focuses on the influences of the E/G coating preparation variables on the corrosion protection property of the coatings. In the present study, the influences of the coating preparation variables such as load of graphene, mixing time, curing temperature and the thickness of coating are examined at high (+1) and low (-1) levels using a full factorial experiment design in order to maximize the corrosion protection efficiency of the E/G protective coatings. Here, the corrosion protection efficiency of a coating is evaluated using electrochemical cyclic voltammetry measurements in a 3.5% aqueous Sodium Chloride (NaCl) solution.

4.2 Experimental

4.2.1 Materials

Polished SS304 foil (McMASTER-CARR) was used as substrate. Graphene, prepared by thermal exfoliation/reduction of graphite oxide was utilized (ACS Material). Graphene has surface area of 400-1000 m2/g and electrical resistivity of $\leq$ 0.3 Ω.cm According to the supplier. Bisphenol A diglycidyl ether

(BADGE) and Poly(propylene glycol) bis(2-aminopropyl ether) (Hardner, B230) were supplied by Sigma Aldrich. All chemicals were used as received.

4.2.2 Composites Synthesis and Design of Experiments

The process of E/G composites preparation is schematically presented in Figure 4.1, where high and low loads of graphene sheets were first dispersed in (2.58 g) of the hardner (B230). The graphene suspension was sonicated/mixed at high and low levels before (3.82 g) of the epoxy resin was added to the suspension. The final solution was mechanically mixed and homogenized for 20 min each before it was spin coated at 300 rpm for 1 min and 4 min to produce thick and thin E/G coatings, respectively, on a SS304 substrate. Finally, the graphene solution on SS304 was thermally cured at high and low levels to produce E/G composite coated SS304 substrate.

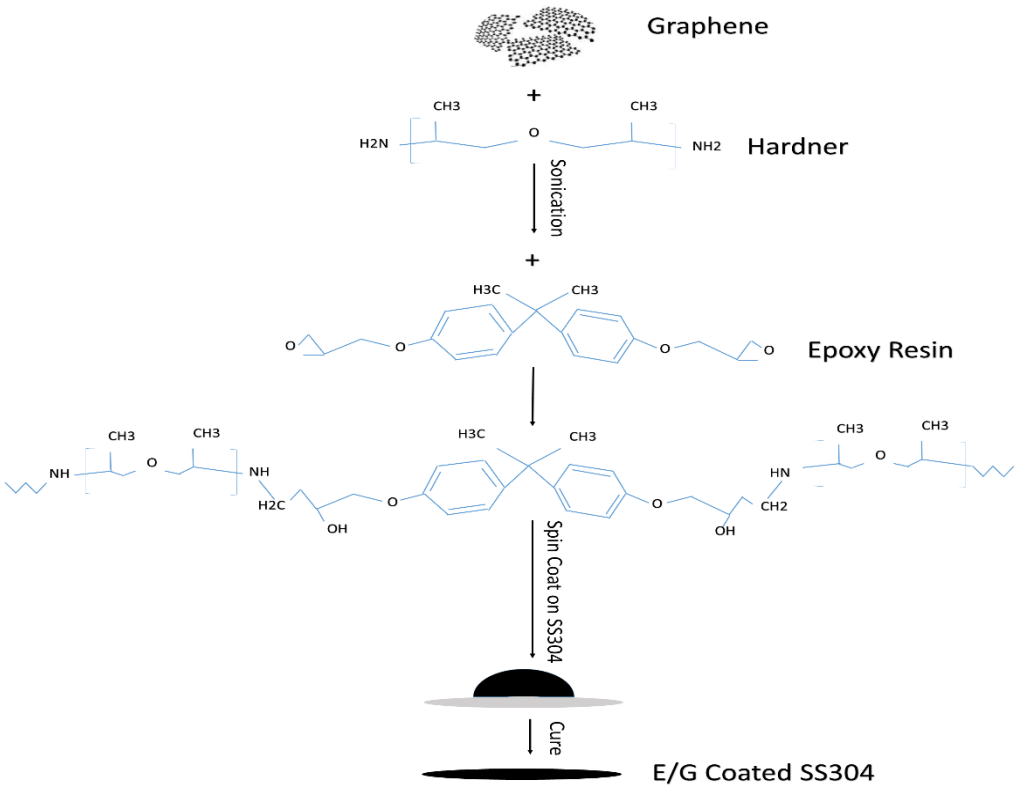

Figure 4.1: Synthesis and coating of E/G composites on SS304 substrates.

E/G coatings were prepared at high (+1) and low (-1) levels of graphene loading, mixing time, curing temperature and coating thickness as illustrated in Table 4.1.

Table 4.1: High and low levels of factors for factorial designed experiments.

Factor	Name	High (+1)	Low(-1)
G	Load of Graphene (mg)	10	2
MT	Mixing time (min)	40	10
T	Curing Temperature (°C)	70	40
TH	Coating Thickness (µm)	100	50

4.2.3 Electrochemical Measurements

Electrochemical measurements were performed at 25 °C in a double-jacketed corrosion cell. One Liter 3.5% NaCl solution was used as electrolyte and experiments were conducted using a three electrode configuration, where the bare and coated SS304 substrates served as the working electrodes with 1 cm2 exposed surface area. Silver/Silver Chloride (Ag/AgCl) and two graphite rods were used as reference (RE) and counter electrodes (CE), respectively. The working electrode (WE) was first washed with acetone and distilled deionized water then, dried and installed in a Teflon sample holder. The open circuit potential was allowed to stabilize for 30 min after immersion of the WE in the electrolyte and after stabilization, the potential was recorded as the corrosion potential (Ecorr). Cyclic voltammetry (CV) technique was utilized to examine the electrochemical behavior of the bare and coated SS304 samples using a VSP-300 workstation (Uniscan instruments ltd.).

4.2.4 Morphology

Dispersion of graphene was observed using SEM (Zesis LEO 1550). In order to enhance the conductivity of E/G coating for SEM imaging, the coated SS304 substrates were further coated with gold using sputtering

technique for 120 sec. The samples were fixed on SEM holders using carbon tape and the dispersion was captured at high and low magnifications. Graphene dispersion in the polymeric matrix was also observed using TEM (Philips CM-10 TEM), where E/G samples were collected by scrapping the coatings with a fine knife, dispersed in methanol for 5 min using sonication technique and collected with TEM copper grid. TEM collected samples were left to dry overnight under vacuum at room temperature.

4.3 Results

4.3.1 Cyclic Voltammetry

CV was used to record raw electrochemical data by scanning the potential of the WE from -0.5 to 0.5 V above the open circuit potential at 10 mV/min. This potential scanning generates Tafel plot, which permits the extraction of the corrosion current (I_{corr}) by extrapolating the straight portions of anodic and cathodic curves through E_{corr} as illustrated in Figure 4.2.

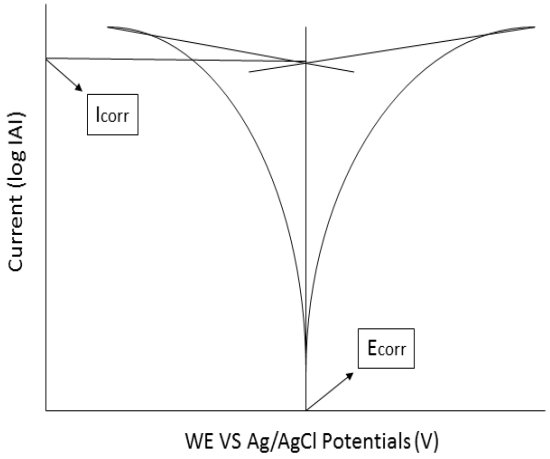

Figure 4.2: Synthesis and coating of E/G composites on SS304 substrates.

4.3.2 Design of Experiment

2^4 full factorial design experiments were conducted in order to illustrate the significance of variable of the preparation process as well as the two factors interactions. The observed I_{corr} was reported for each experiment in Table 4.2 and in general, a drop in I_{corr} represent an enhancement in corrosion protection.

Table 4.2: 2^4 Design levels and corrosion currents.

	Design Factors				
Run	G	MT	T	TH	$I_{corr}(\mu A/cm^2)$
I01	-1	-1	-1	-1	0.2
I02	+1	-1	-1	-1	0.007
I03	-1	+1	-1	-1	0.04
I04	+1	+1	-1	-1	0.0091
I05	-1	-1	+1	-1	0.19
I06	+1	-1	+1	-1	0.0086
I07	-1	+1	+1	-1	0.07
I08	+1	+1	+1	-1	0.0066
I09	-1	-1	-1	+1	0.3
I10	+1	-1	-1	+1	0.0098
I11	-1	+1	-1	+1	0.03
I12	+1	+1	-1	+1	0.0088
I13	-1	-1	+1	+1	0.25

I14	+1	-1	+1	+1	0.013
I15	-1	+1	+1	+1	0.05
I16	+1	+1	+1	+1	0.001

Analysis of variance (ANOVA) approach was adopted to analyze the factorial design experimental and the results are presented in Table 4.3. The total sum of variance was calculated using equation 4.1, where yi and n represent the response of experiment I and the number of experiments, respectively. Furthermore, the sum of square (SS) for each factor and their interaction was calculated using equation 4.2, where k is the number of main factors.

Table 4.3: Analysis of variance for main Effects and two-factor interactions for observed response.

Factor	Effect	SS	df	MS	F
G	-0.133	0.07	1	0.07	14.2^{*}
MT	-0.095	0.036	1	0.036	7.2^{*}
T	-0.002	$1.5e^{-5}$	1	$1.5e^{-5}$	0.003
TH	0.016	0.001	1	0.001	0.2
G×MT	0.092	0.03	1	0.03	6.79^{*}
G×T	0.001	$1.3e^{-6}$	1	$1.2e^{-6}$	$2.5e^{-4}$
G×TH	-0.016	0.001	1	0.001	0.2
MT×T	0.012	$0.5e^{-3}$	1	0.0005	0.11
MT×TH	-0.025	0.003	1	0.003	0.51
T×TH	-0.007	$0.2e^{-3}$	1	0.0002	0.03

Error	-	0.017	5	0.003	-
Total	-	0.164	15	-	-

*Significance factors.

$$SS_{total} = \sum_{i=1}^{n} y_i^2 - (\sum_{i=1}^{n} y_i)/n \quad (4.1)$$

$$SS_{effect} = 2^{k-2}(effect)^2 \quad (4.2)$$

The error sum of square was computed as the difference between the total sum of square and the summation of the sum of squares for main factors and their interactions. The degree of freedom (df) for factors and their interaction is the levels of factors less one. Therefore, main factors degree of freedom is (2-1), while, the interactions degree of freedom is (2-1) × (2-1). The error sum of square degree of freedom equal the total number of experiments less the sum of all main factors and interaction effects less one (16-10-1=5). Finally, the degree of freedom of the total sum of square is the number of experiments less one (16-1=15). The mean squares (MS) are compute by dividing the sum of square over the degree of freedom and the F values for a main factor or an interaction is calculated by diving the mean square of the main factor or the interaction over the mean square of the error. At 95% confidence interval ($F_{1,5}$=6.61) a main factor or an interaction is considered significant when the F value is grater then 6.61 and not otherwise.

From the reported analysis in Table 4.3**,** it can be observed that load of graphene, mixing time and the interaction between these factors are significant. The importance of the significant factors can be observed in the results reported in Table 4.2, where the corrosion current drop when the load of graphene is high indicating an enhancement in corrosion protection. The same observation was noted for mixing time, where the corrosion current always drops at high mixing time. Finally, it was interesting to observe that at low load of graphene, increasing the mixing time excelled protection by attenuating the corrosion current. The interaction effect between the load of graphene and mixing time is explained in Figure 4.3, where corrosion currents are always low at high load of graphene, while the corrosion currents were high and low when a low and high mixing times were used at a low load of graphene.

The enhancement in corrosion protection efficiency can be attributed to the ability of graphene in prolonging pathways corrosive elements follow to reach metal surface and increasing the mixing time may help enhancing the dispersion of graphene and consequently advance corrosion protection property of the E/G coating.

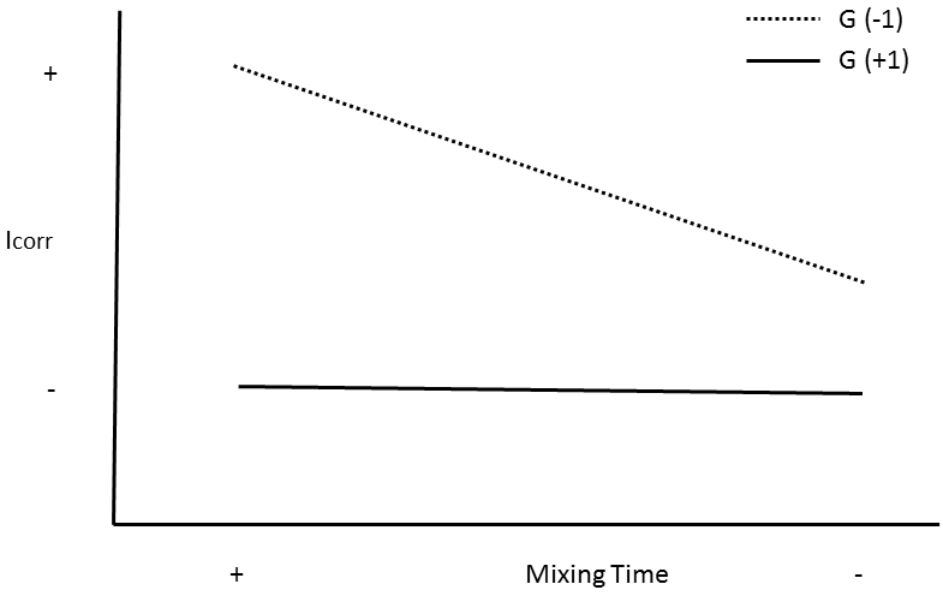

Figure 4.3: Interaction effects between load of graphene and mixing time.

4.3.3 Morphology

Dispersion of graphene in Epoxy resin was observed using SEM and TEM. Figure 4.4 (a and b), depicts the dispersion of graphene in samples I02 and I04, where the loads of graphene were high, while the mixing times were low and high, respectively. From the figures, it can be observed that in both cases graphene sheets were widely dispersed regardless of the mixing time. In contrast, graphene sheets were not always widely dispersed when a low load of graphene was incorporated in the polymeric matrix. This can be observed in Figure 4.5 (a and b), which depicts the dispersion of low loads of graphene in samples I03 and I01, where the mixing time is high and low, respectively. Here, graphene sheets were well dispersed in sample I03, where mixing time was high as presented in Figure 4.5a, while stacks of graphene sheets were observed at low mixing time in sample I01 as shown in Figure 4.5b. The observed degree of dispersion of

graphene in evaluated samples support the significance of the load of graphene, the mixing time and the interaction between the two factors as reported in previous section. The widely dispersed graphene sheets extend the pathway corrosive agents follow to reach SS304 substrates and consequently enhance the corrosion protection properties of the coatings.

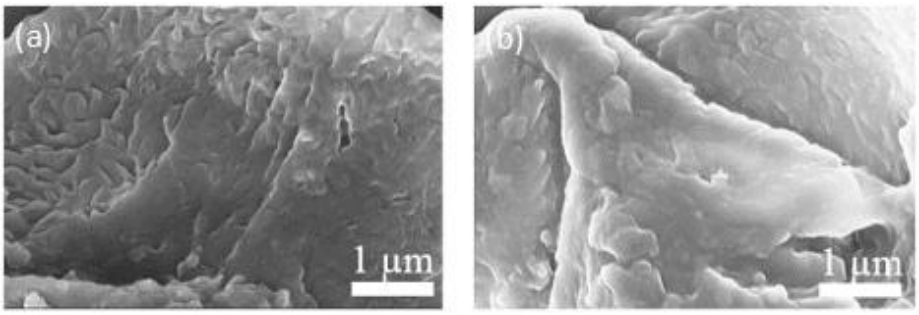

Figure 4.4: SEM images of graphene dispersion in (a) I02 and (b) I04.

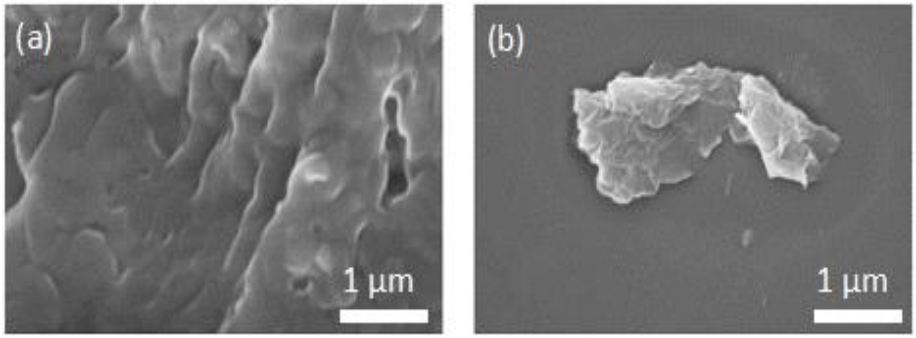

Figure 4.5: SEM images of graphene dispersion in (a) I03 and (b) I01.

TEM was also utilized to observe the dispersion of low loadings of graphene at high and low mixing times in samples I03 and I01 as depicted in Figure 4.6 (a and b), respectively. The observed thin sheets of graphene in Figure 4.6a confirms that increasing mixing time resulted in a better dispersion of graphene sheets. In contrast, the low mixing in sample I01 resulted in poor exfoliation of graphene sheets, which can be observed as thick stacks of graphene sheets in Figure 4.6b.

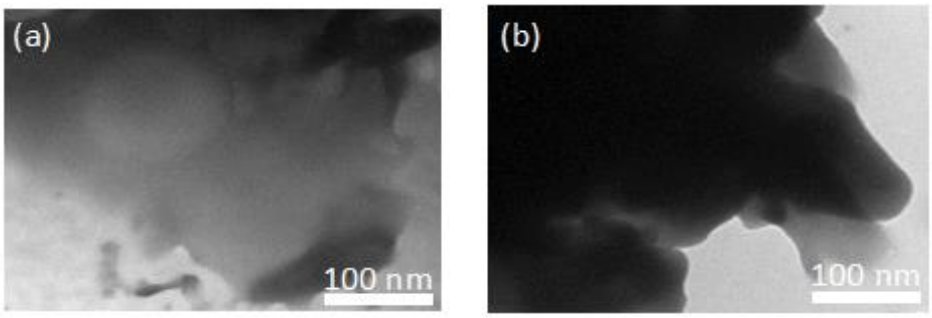

Figure 4.6: TEM images of graphene dispersion in (a) I03 and (b) I01.

4.4 Conclusion

A full factorial experimental design study was conducted to optimize corrosion protection property of Epoxy/graphene composites coatings on SS304 substrates. Influences of the preparation parameters, which include load of graphene, mixing time, curing temperature and coating's thickness on the corrosion protection properties of the coatings were evaluated at two levels using CV technique. E/G coatings were prepared by thermal curing, where in situ polymerization approach was utilized to incorporate graphene sheets in the epoxy matrix. The dispersion of graphene was captured using SEM and TEM techniques at high magnification. The study revealed that addition of graphene enhances the corrosion inhibition abilities of E/G coatings. Furthermore, it was concluded that load of graphene, mixing time and the interaction between those two parameters have significant influences on the corrosion protection properties of the E/G coatings. The enhancement in the protection properties was attributed to degree of dispersion of graphene in the matrices as presented in the SEM and TEM images, where graphene sheets may prolong the pathways corrosive agents cross to reach the metals and coatings interfaces.

Chapter 5

Corrosion Inhibition of Copper in Sodium Chloride Solution Using Polyetherimide/Graphene Composites

Abstract

In this study, Polyetherimide-Graphene composites (PEI/G) were prepared and investigated as corrosion inhibition coatings on copper substrates. Various loadings of graphene were incorporated in the Polyetherimide matrix using in situ polymerization approach and the composite coatings were cured by thermal imidization. The effect of graphene loading on corrosion inhibition and the long-term performance of the PEI/G coatings were investigated. The dispersion of graphene in the polymer matrix was examined using SEM and TEM. The study demonstrated that PEI/G nanocomposites provide advanced corrosion inhibition of copper. This conclusion was supported by the results of various electrochemical techniques such as Tafel polarization and electrochemical impedance spectroscopy (EIS). In addition to corrosion protection, the long-term performance of the coatings was confirmed by testing the adhesion of PEI/G composites to copper substrates before conducting the electrochemical tests and after 15 days of exposure to the corrosive medium.

5.1 Introduction

Corrosion is the destruction of materials by electrochemical reactions with the environment. The lack of complete prevention of such a process results in serious threats to both economy and industry. Therefore, a large number of studies have focused on different strategies to slow the kinetics and/or alternate the mechanism of corrosion. Examples of these strategies are anodic or cathodic protection [2], [3] the use of protective coatings [4], and the use of corrosion inhibitors [5]. These protection techniques have been utilized in various fields such as marine, pipeline, construction and automobile industries. However, there is a growing demand for more robust techniques with enhanced inhibition efficiency in order to boost the

life cycle of various materials for environmental and economic savings. Nanocomposites, hydrophobic and organic-inorganic hybrid coatings have already excelled in extending the life of various materials in corrosive environments [6]–[12].

Copper is extensively utilized in a wide range of technological and industrial applications due to its outstanding electrical and thermal conductivity, ductility, wear and shock resistance, and processabilty. Previous studies showed that protective copper oxides or hydroxides layers form on the copper surface under neutral or near neutral pH conditions [56]. The formation of this protective layer and the corrosion process of copper are more complex in the presence of chloride ions [15]. In an oxidative environment, the corrosion mechanism involves the dissolution of copper at local areas, referred to as the anodic sites, and electrochemical reduction of oxygen and water at the cathodic sites. The formation of the oxide or hydroxide layer will eventually slow down the rates of dissolution and reduction reactions. Indeed, several studies have illustrated that the rate of these reactions is proportional to the rate of diffusion of copper chloride ions into the chloride solution. Nevertheless, the presence of the oxides or hydroxide insoluble layer will not prevent the diffusion and reduction of corrosive agents such as oxygen [16].

Coating the metal with anti-corrosion layer not only can limit the diffusion of corrosive agents to the metal substrates protecting the metal from corrosion but also enhances the mechanical properties of the metal. Polymer based composites, which were first reported in the 1960s are perfect examples of coatings that can improve the properties of metal substrates, especially when inorganic materials are incorporated as nanofillers to form organically-inorganic nanocomposites. These inorganic nanomaterials include layered, tubular and spherical forms such as clay, carbon nanotubes and SiO2, respectively [17]–[24]. The compatibility between the polymer matrix and the inorganic nanofillers and the dispersion of the nanofillers in the matrix plays an important role in the performance of nanocomposites and therefore, enhancing the compatibility and the nanofiller dispersion in the matrix is always desired. Several polymeric materials have shown good potential as corrosion inhibitors; however, their poor adhesion to metal substrates prohibits their use for corrosion protection purposes [57], [58]. Polyetherimide (PEI) is a high-performance

polymeric material that combines various desirable properties such as outstanding thermal and chemical stability, high temperature durability, low dielectric constant, and low thermal expansion coefficient [39], [41].

Since the discovery of graphene [25], increasing number of studies has focused on incorporating graphene materials such as graphene nanosheets, graphene nanoplatelets and functionalized graphene in various polymers in order to enhance their mechanical, thermal and dielectric properties [59]–[61]. The lower density and very high aspect ratio of graphene [53] are among its main advantages over other nanofillers. These properties initiated the investigation of graphene-based materials as gas barriers and corrosion protection coatings [33], [62]–[65]. To the best of our knowledge, there is no study on use of graphene-PEI composites (PEI/G) for corrosion prevention of copper. The PEI/G coating is expected to provide protection to copper substrates through two mechanisms. First, the PEI serves as a barrier to water and oxygen permeation. The second protection mechanism is attributed to the ability of the well dispersed graphene nanosheets in PEI matrix to prolong the diffusion pathway of corrosive agents such as oxygen and water molecules. In this study, the corrosion inhibition ability of PEI/G nanocomposites is examined via electrochemical corrosion measurements in a 3.5 wt% sodium chloride aqueous solution. The long-term performance of the coatings is also investigated by carrying adhesion test after 15 days of exposure to the 3.5 wt% NaCl solution.

5.2 Experimental

5.2.1 Materials

4,4-Bisphenol A Dianhydride (BPADA. Polysciences, Inc.) was vacuum dried at 60 ^{o}C for 3 h to remove moisture prior to use. N-Methyl-2-pyrrolidinone solvent (NMP, Sigma Aldrich), m-Phenylenediamine (mPDA, Sigma Aldrich) and single layer graphene prepared by thermal exfoliation/reduction of graphite oxide, which was prepared using the modified Hummer method have been supplied by (ACS Material) and used as received. According to the supplier, the single layer graphene has a surface area of 400-1000 m2/g

and electrical resistivity of ≤ 0.3 Ω·cm. Polished multipurpose copper bars 99.9 % purity (McMASTER-CARR) were used as substrates.

5.2.2 Composite preparation, coating, and curing

PEI/G composites with graphene loading of 0.5 wt% (PEI/$G_{0.5}$), 1 wt% (PEI/G_1), and 2 wt% (PEI/G_2) were prepared using in situ polymerization approach. The overall process of composite preparation, coating and curing is detailed below and schematically presented in figure 5.1.

- ***(PEI/$G_{0.5}$):*** Single layer graphene (32.2 mg) was dispersed in 20 ml NMP by stirring for 1 h followed by bath sonication (Fisher Scientific, FS30H) for an additional hour. *m*PDA (1.1 g) was dissolved in 30 ml NMP and stirred until a clear solution is formed. The graphene suspension was added to the diamine solution and the mixture was stirred for 1 h followed by sonication for an additional hour. An equimolar amount of BPADA flakes (5.3 g) was added to the graphene-*m*PDA mixture. *m*PDA and BPADA were allowed to react overnight under N_2 purge at 60°C producing Polyamic acid (PAA), the PEI precursor. The PAA-G was homogenized for 30 min using laboratory Homogenizer (Fisher Scientific, 125) and sonication for 5 min and used to coat a polished and cleaned copper substrate. The same procedure was used to prepare (PEI/G_1) and (PEI/G_2) using 64.6 and 130.6 mg of graphene, respectively.
- ***Coating:*** the homogenized PAA-G mixture was applied to the polished and cleaned copper substrate using a brush and the thickness was controlled (65±1 µm) using a film applicator (Paul N.Gardner Company Inc.).
- ***Curing:*** the coating was heated under vacuum at 70°C for 10 h to remove most of the solvent and then subsequently heated at 100°C, 150°C and 205°C for 2 h each to complete the imidization of PEI. The coated samples were allowed to cool down to room temperature under vacuum.

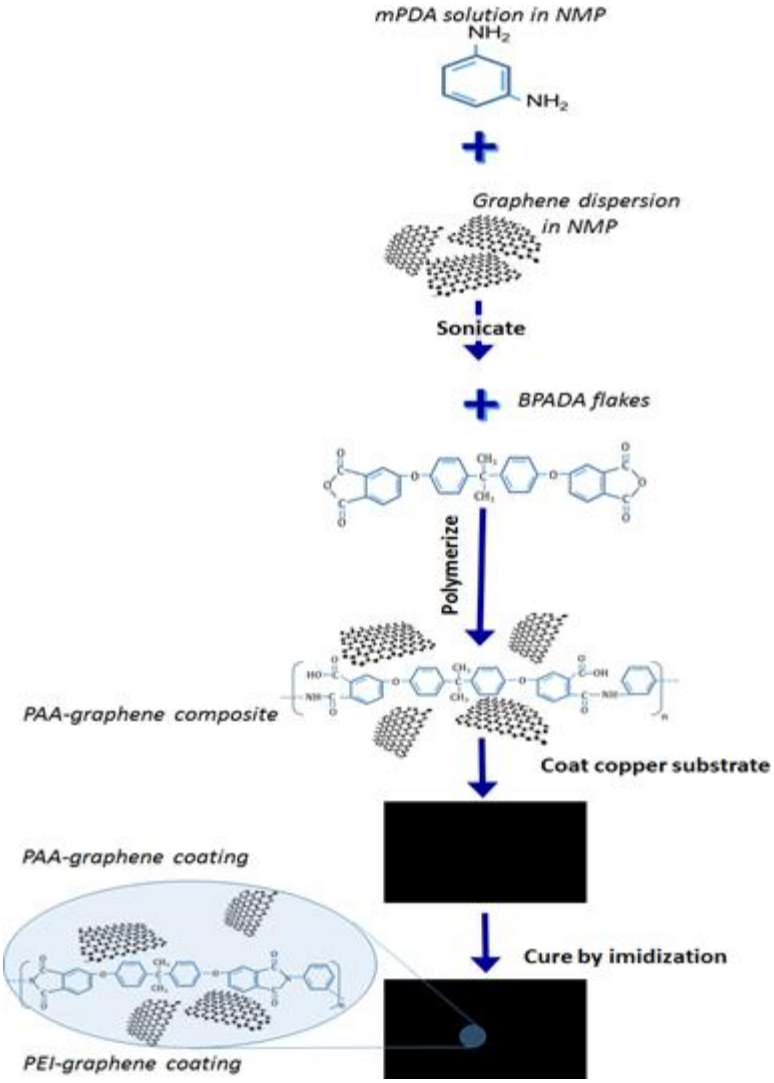

Figure 5.1: Synthesis of PEI and PEI/G composites.

5.2.3 Morphology characterization

Graphene dispersion on the PEI matrix was examined using SEM (Zeiss LEO 1550). The coated copper substrate was fixed on an SEM holder using carbon tape and it was gold coated via sputtering for 120 s. In addition, SEM was used to illustrate the conditions of the copper substrate as well as the coatings before and after conducting Tafel polarization and electrochemical impedance spectroscopy tests.

TEM (Philips CM-10 TEM) was also used to analyze the morphology of the coatings and the dispersion of graphene into the matrix. A sample from the PEI/Graphene coating was collected by scraping the coating

using a sharp knife. The collected sample was dispersed in methanol for 5 min, collected using TEM copper grid, and allowed to dry overnight under vacuum at room temperature.

5.2.4 Adhesion Test

The adhesion test was carried out according to ASTM-D3359 using adhesion- tape test kit (Paul N.Gardner Company Inc.) with 11-teeth blade with teeth spacing of 1 mm. The test was conducted twice, once after the preparation and again after 15 days of exposure to the 3.5 wt% NaCl solution in order to examine the durability of the coatings. Furthermore, the adhesion test was performed only once on PEI/G_2 due to the poor performance of the coating as will be illustrated later in the results sections.

5.2.5 Electrochemical Measurements

The electrochemical measurements were performed at 25°C using a double-jacketed corrosion cell covered with a Teflon plate containing drilled holes for the immersion of the electrodes. The measurements were carried out using a three-electrode configuration, where circular copper specimen with exposed area of 1 cm^2 was used as the working electrode (WE), two graphite rods as counter electrodes (CE) and a Silver/Silver Chloride electrode (Ag/AgCl) as the reference electrode (RE). The WE was cleaned with acetone and washed with distilled, deionized water before it was dried and installed in the Teflon sample holder. One L temperature controlled 3.5 wt% NaCl electrolyte solution was used. All electrochemical measurements were performed using VSP-300 workstation (Uniscan instruments Ltd.) and each measurement was repeated three times to check the reproducibility and the significance of the collected data. In addition, electrode potentials were allowed to stabilize for 30 min before performing the EIS followed by the potentiodynamic measurements.

At equilibrium state, the open circuit potential (OCP) was recorded as the corrosion potential (E_{corr}) in mV vs the RE. Data for Tafel plots were recorded at a rate of 10 mV/min by scanning the potential from -500 to 500 mV above the corrosion potential. The corrosion current (I_{corr}) was determined by extrapolating the straight portions of the cathodic and the anodic curves through E_{corr}. Bio-Logic EC-Lab software was

used to extract E_{corr} and I_{corr}. The same workstation was used to perform the electrochemical impedance measurements to produce Bode and Nyquist plots. The measurements were carried out using a frequency range from 100 kHz to 100 mHz. Bio-Logic EC-Lab software was used for plotting and fitting the data.

The corrosion rate (R_{corr}) in milli-inch per year (MPY) was calculated as per ASTM standard G102 using equation 5.1:

$$R_{corr} = \frac{0.13 \times I_{corr} \times EW}{A \times \rho} \tag{5.1}$$

Where EW is the equivalent weight of Copper (31.7 g), ρ is copper density (8.97 g/cm^3) and A is the surface area (1 cm^2). Tafel polarization and electrochemical impedance spectroscopy measurements were performed on bare copper as well as all coatings except PEI/G_2 due to the conditions of the coating.

5.3 Results

5.3.1 Morphology of PEI/G composites and Copper substrate

SEM is used to examine the conditions of the bare and PEI coated copper substrates before and after conducting the Tafel polarization and the EIS tests. Examining the morphology of the bare copper substrate before (Figure 5.2a) and after (Figure 5.2b) the electrochemical tests shows significant damage to the bare copper substrate during carrying the electrochemical tests. In contrast, no change is observed in the surface morphology of the PEI coated copper substrate (Figure 5.2c) after the electrochemical tests (Figure 5.2d). This proves the ability of PEI to protect the copper substrate during the electrochemical tests as no evidence of surface damage is observed.

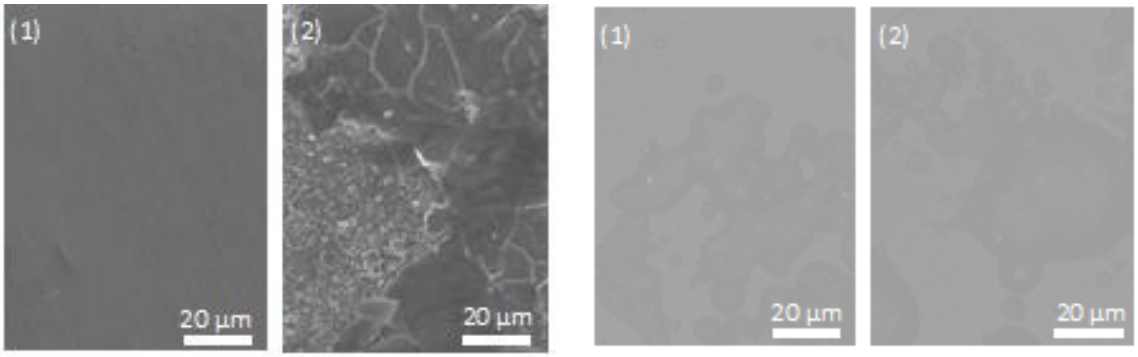

(a) (b)

Figure 5.2: SEM images for bare (a) copper substrate and (b) PEI coated copper substrate (1) before and (2) after conducting Tafel polarization and EIS tests.

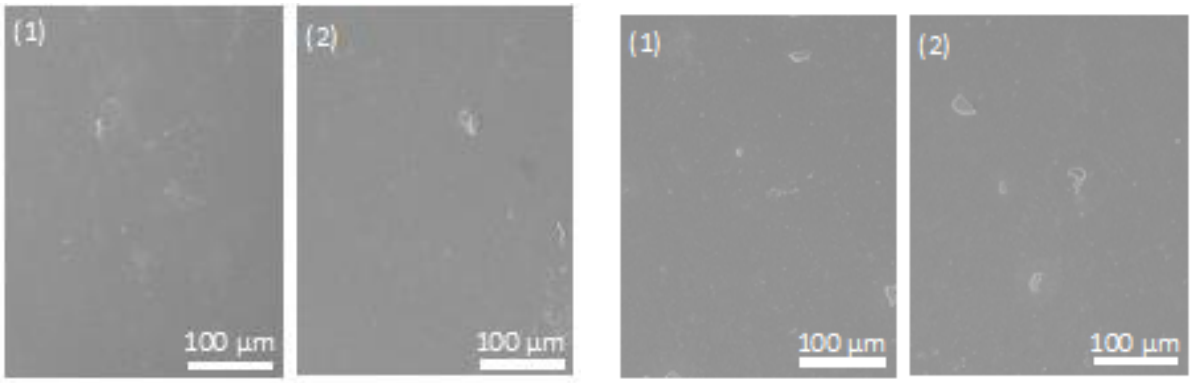

(a) (b)

Figure 5.3: SEM images for PEI/$G_{0.5}$ and PEI/G_1 (1) before and (2) after conducting Tafel polarization and EIS tests.

The surface morphology of the copper substrate coated with PEI/G is also examined by SEM before and after the electrochemical tests. Figure 5.3, illustrates the conditions of PEI/$G_{0.5}$ and PEI/G_1 coatings before (Figure 5.3a and c) and after (Figure 5.3b and d) conducting the electrochemical tests. Here too, no evidence of damage is observed on the coatings confirming the quality of these coatings as anti-corrosion coatings. Moreover, a well dispersed graphene sheets can be observed in both PEI/$G_{0.5}$ and PEI/G_1 coatings.

Furthermore, the dispersion of graphene has been examined at higher magnification as shown in Figure 5.4, where the well dispersed graphene sheets in PEI/$G_{0.5}$ and PEI/G_1 coatings were manifested in a rug-like graphene.

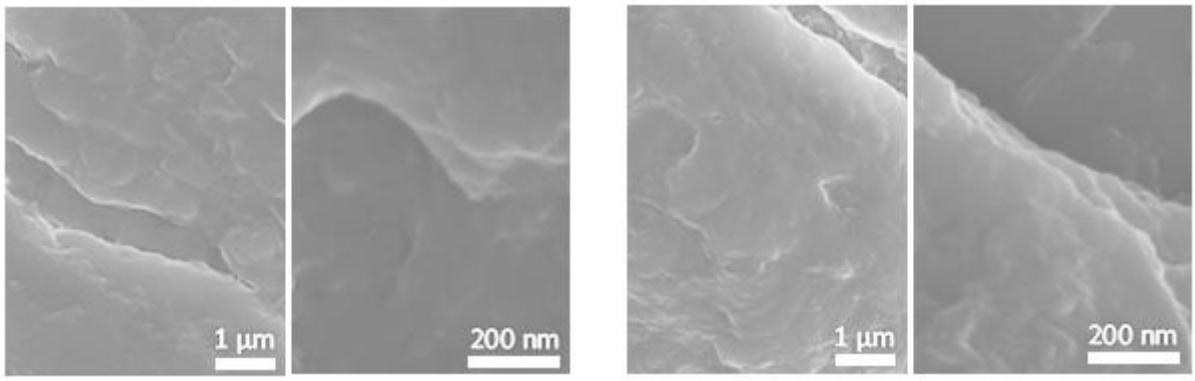

(a) (b)

Figure 5.4: SEM images for graphene dispersion in (a) PEI/$G_{0.5}$ and (b) PEI/G_1.

The dispersion of graphene in PEI was also examined using TEM as presented in Figure 5.5 for PEI/$G_{0.5}$ and PEI/G_1. From the TEM images, we clearly see the effect of graphene loading on dispersion. At low graphene loading (PEI/$G_{0.5}$), the graphene is well dispersed as indicated by the very thin sheets In contrast to the thick stack of sheets for the PEI/G_1 sample. The impact of graphene loading and the associated dispersion level on the electrochemical performance of the coating will be discussed in sections 3.3.3 and 3.3.4.

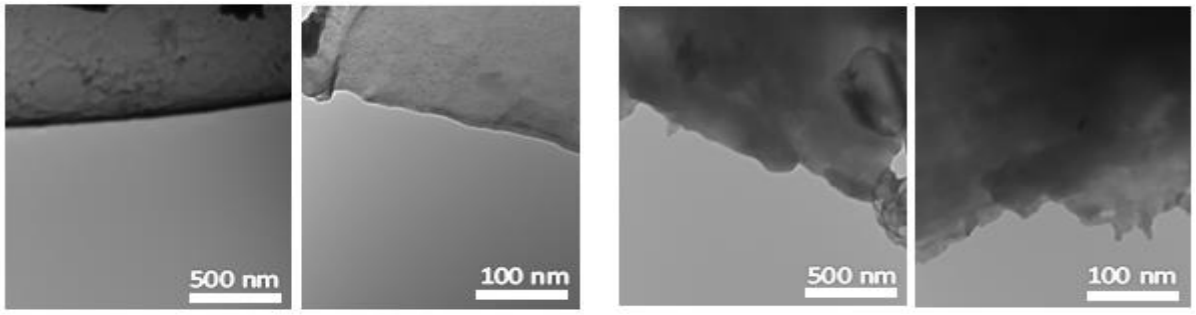

(a) (b)

Figure 5.5: TEM images for graphene dispersion in (a) PEI/$G_{0.5}$ and (b) PEI/G_1.

Finally, it was interesting to observe the disadvantage of use graphene loading much larger than the percolation loading as evident in Figure 5.6. Here, the excess load of graphene attenuated the coating flexibility and resulted in visible cracks on the coating. These cracks expose the copper substrate to the corrosive environment and therefore, no electrochemical measurements were conducted on PEI/G_2. However, adhesion test was performed on PEI/G_2 in order to illustrate the effect of the excessive graphene loading on the performance of the coating.

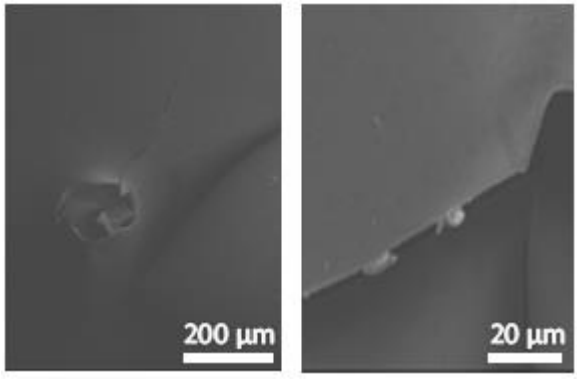

Figure 5.6: SEM images of PEI/G_2 coated copper.

5.3.2 Adhesion Test

The accumulation of corrosive agents and metal ions in void spaces at the interface between the metal substrate and the coating plays an important role in the kinetics of corrosion. Indeed, the existence of such voids is considered a primary failure mechanism for corrosion inhibition coatings. Therefore, good adhesion of the protective coating to the metal substrate is always desirable. The adhesion of PEI and PEI/G composites to copper substrate were evaluated according to the standard ASTM-3359 using adhesion tape test kit. Figure 5.7, 5.8 and 5.9, depict the adhesion test results before and after 15 days of exposure to the 3.5 wt.% NaCl solution for PEI, PEI/$G_{0.5}$ and PEI/G_1 coatings, respectively. From the shown top view SEM images, we cannot observe any peelings of the coating after the adhesion tests and all the coatings received 5B rating (0% Peeling) according to ASTM-D3359. In addition, the cross sectional SEM images demonstrate the strong adherence of PEI, PEI/$G_{0.5}$ and PEI/G_1 coatings to the copper substrates.

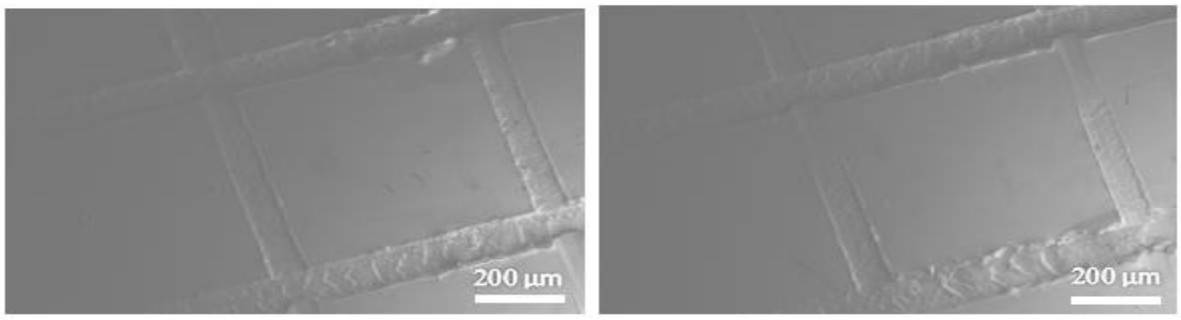

(a) (b)

Figure 5.7: SEM image of post-adhesion test copper substrates coated with PEI (a) before and (b) after 15 days of exposure to the corrosive medium.

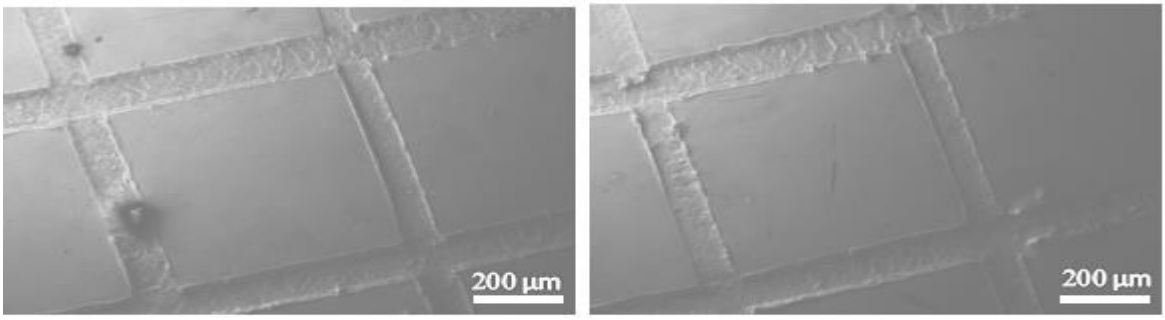

(a) (b)

Figure 5.8: SEM image of post-adhesion test copper substrates coated with PEI/$G_{0.5}$ (a) before and (b) after 15 days of exposure to the corrosive medium.

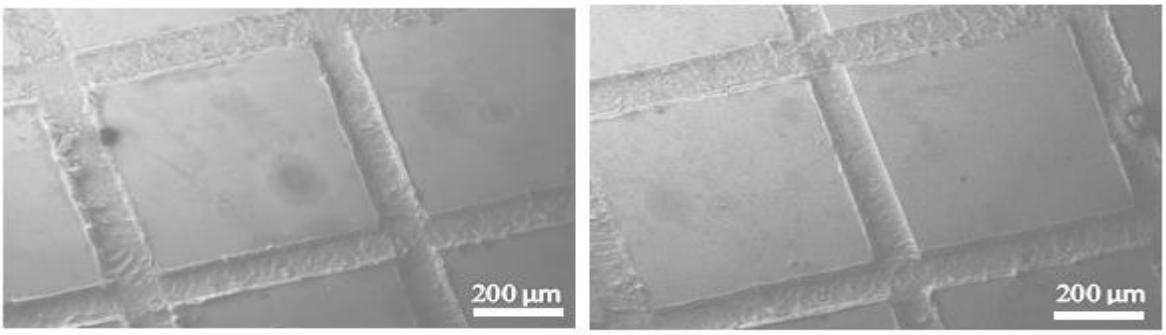

(a) (b)

Figure 5.9: SEM image of post-adhesion test copper substrates coated with PEI/G_1 (a) before and (b) after 15 days of exposure to the corrosive medium.

Figure 5.10 depicts the post adhesion test results for PEI/G_2. The figure illustrates the poor adhesion of PEI/G_2 to copper substrate, where peeling was observed on various spots and the coating received 0B rating (more than 65% peeling) according to the ASTM standard. The observed disadvantage of increasing the load of graphene can be attributed to the stacking and aggregation of graphene sheets, which attenuates the contact area between PEI/G and copper substrate. In addition, this accumulation of graphene attenuates the flexibility of the coating, considering the noble reinforcement property of graphene [66], and the combination between these two factors resulted in loss of interface adhesion.

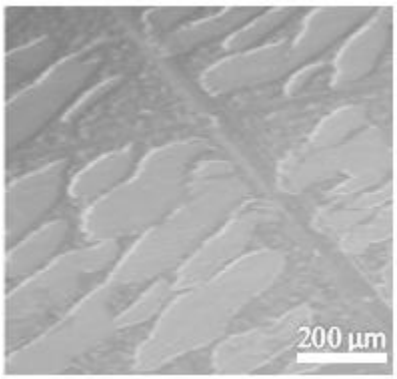

Figure 5.10: SEM image of post-adhesion test copper substrate coated with PEI/G_2 before exposure to the corrosive medium.

5.3.3 Potentiodynamic measurements

Cyclic voltammetry (CV) is a widely used approach to characterize the electrochemical properties of anti-corrosion coating. Here, a three electrode configuration has been used to collect the data. These potentiodynamic data were recorded using the EC-Lab software provided by Bio-Logic. All measurements were obtained in a 3.5% NaCl solution at 25 ^{o}C after immersing the working electrode (WE) in the electrolyte for 30 min. Figure 5.11, depicts the Tafel plots for bare copper, PEI, PEI/$G_{0.5}$ and PEI/G_1 and the corrosion parameters obtained from the Tafel plots are summarized in Table 5.1. The variation in the corrosion protection behavior of different coatings was evaluated based on the variations in the reported corrosion parameters (E_{corr}, I_{corr}, R_{corr} and R_p) obtained from the Tafel plots.

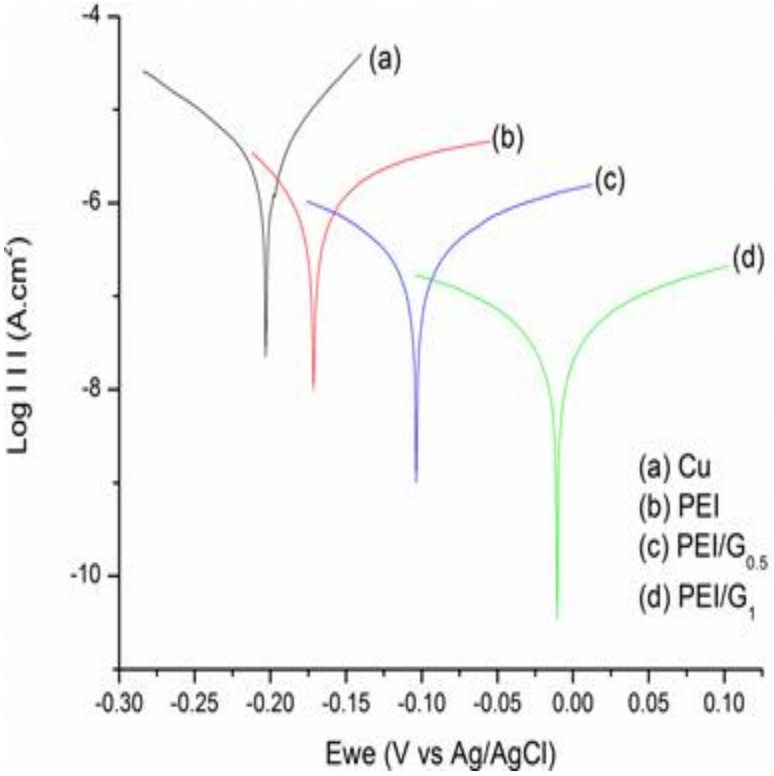

Figure 5.11: Tafel plots for (a) bare copper, (b) PEI, (c) PEI/$G_{0.5}$ and (d) PEI/G_1 coated copper electrodes in a 3.5 wt% NaCl solution at 25°C.

Table 5.1: Electrochemical corrosion parameters obtained from potentiodynamic measurements for bare copper, PEI, PEI/$G_{0.5}$ and PEI/G_1 coated copper in a 3.5 wt% NaCl solution.

Sample	E_{corr} mV vs Ag/AgCl	I_{corr} μA/cm^2	R_p Ω.cm^2	R_{corr} MPY	P_{EF} %
Cu	-202	16.25	1.33	7.46	-
PEI	-171	1.78	18	0.82	89
PEI/$G_{0.5}$	-103.6	0.439	70	0.2	97.5
PEI/G_1	-10.7	0.15	142	0.07	99.1

In general, higher values of E_{corr} and polarization resistance (R_p) in addition to lower values of I_{corr} and R_{corr} represent an enhancement in corrosion inhibition. R_p values were evaluated using the Stern-Geary equation, equation 5.2 [67].

$$R_p = \frac{b_a b_c}{2.303(b_a + b_c) I_{corr}} \tag{5.2}$$

The constants in equation 3.2 were obtained from the Tafel plots, where ba and bc are the anodic and the cathodic Tafel slops (dE/dlog I), respectively. Furthermore, the intersection between the extrapolated lines from the linear portions of the anodic and the cathodic curves determine I_{corr}. In addition to the parameters obtained from the Tafel plots, the protection efficiency (P_{EF}) is a commonly used parameter to evaluate the corrosion protection ability of coatings and P_{EF} can be calculated using equation 5.3 [68].

$$P_{EF}[\%] = (1 - \frac{I_{corr}}{I^{\circ}_{corr}}) \times 100 \tag{5.3}$$

The ability of PEI to protect the metal substrate is confirmed by the results presented in Figure 5.11 and Table 5.1, which are consistent with previously reported results [69]. In addition, these results illustrated that the performance of PEI in corrosion protection can be enhanced by the incorporation low loading of

graphene as demonstrated by a positive shift in the corrosion potential and attenuation of the corrosion current. As a result, an enhancement in the polarization resistivity was observed demonstrating the benefits of incorporating graphene in PEI matrix to fabricate anti-corrosion coatings with improved protection efficiency. Moreover, the level of the corrosion inhibition can be improved by increasing the load of graphene in the PEI matrix. This can be easily seen in Figure 5.11, where a positive shift in E_{corr} and a drop in I_{corr} are encountered for the samples coated with PEI/G_1 when compared to those coated with PEI/$G_{0.5}$.This is also confirmed by the data in Table 5.1, where the R_p value for the electrode coated with PEI/G_1 is over twice the value for the PEI/$G_{0.5}$ coated electrode. This improved performance of PEI/G_1 can be attributed to the increased tortuosity of the diffusion pathway of corrosive agents as the loading of graphene increases [70] as will be discussed in section 3.3.4. Nevertheless, the increase in the performance associated with increasing the graphene loading from 0.5 to 1 wt% is much lower than the increase associated with increasing the loading from 0 to 0.5 wt% due to the better dispersion of graphene at 0.5% loading compared to a 1% loading as discussed in section 5.3.1.

5.3.4 Electrochemical impedance measurements

In addition to CV, EIS is one of the widely used techniques to study the activity on metal substrates. This technique is used in this study in order to compare the variation in corrosion activities between bare and coated copper substrates. When an alternating current (AC) flows through a circuit, which might contain insulators, resistors or capacitors or a combination of items, the output is a complex resistance, known as impedance [71]. In EIS, an AC is fed to the corrosion system over a wide range of frequency and the impedance of the WE is reported as a complex value. The impedance behavior of the WE can be modeled using an equivalent circuit. In this study, the data fitting was performed using the EC-Lab software and all electrochemical measurements were collected after the immersion of the WE in a 3.5 wt% NaCl solution for 30 min. Figure 5.12, represents the equivalent circuit used to model the impedance raw data. In that circuit, R_s represents the solution resistance, R_p is the resistivity of the coating or the film formed on the copper substrate in the case of bare copper, CPE_1 and CPE_2 are the constant phase elements (CPEs), R_p' is

the charge transfer resistance and W is the Warburg impedance. All these elements were evaluated for each sample using the EC-Lab software and the impedance depends on the combination of these elements.

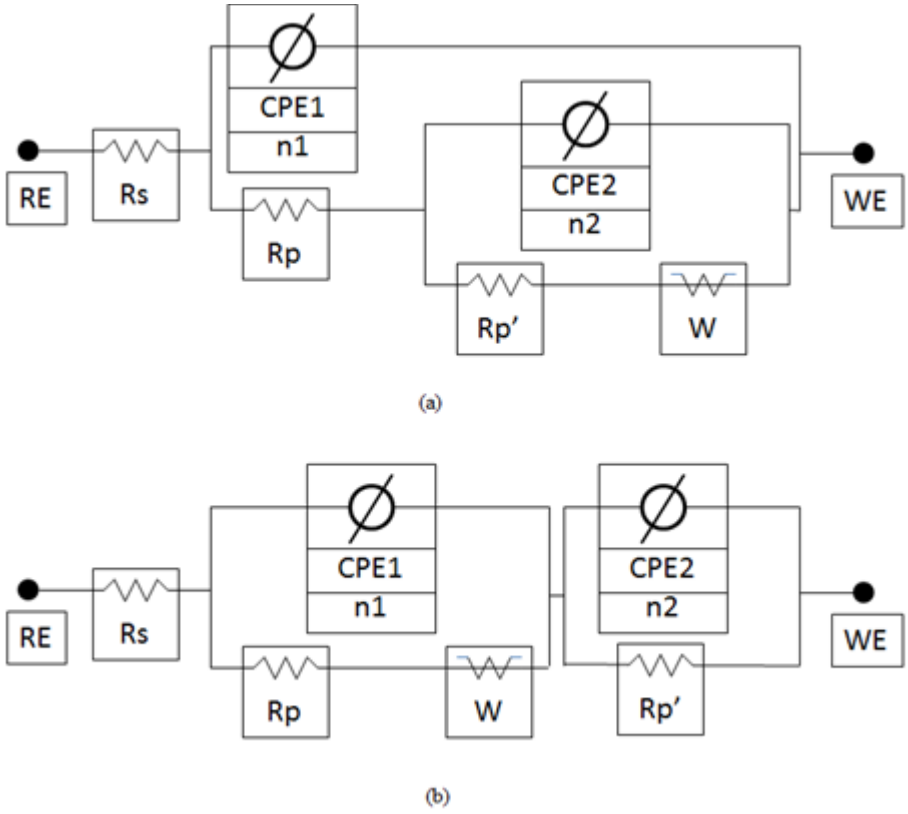

Figure 5.12: Equivalent circuits used for modeling electrochemical impedance data for (a) bare and (b) coated copper substrates in a 3.5 wt% NaCl solution.

Figure 5.13, depicts Nyquist plots, which represent the real and the imaginary part of the impedance data. Here, a typical impedance response of copper in NaCl solution is observed, where the impedance is characterized by a semi-circle followed by a sharp increase in impedance [72]. In general, a larger semi-circle represents a larger resistance and consequently a slower corrosion rate.

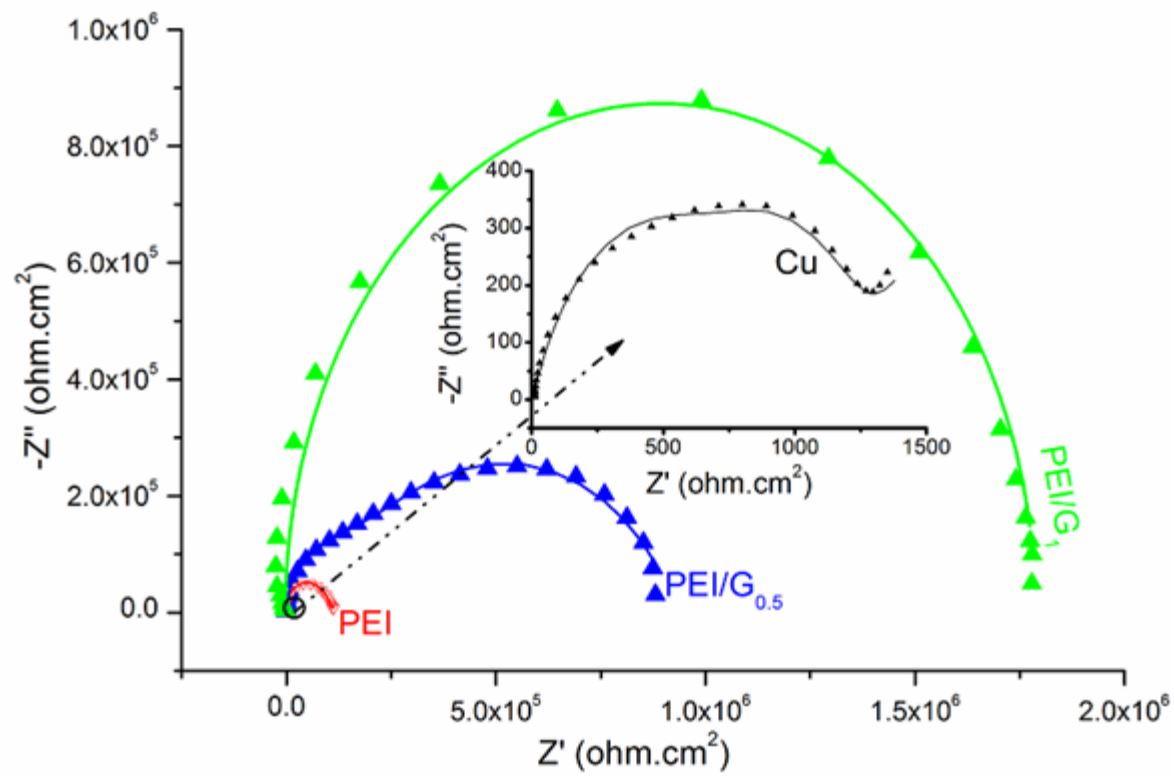

Figure 5.13: Nyquist plots for bare copper, PEI, PEI/$G_{0.5}$ and PEI/G_1 coated copper.

The ability of PEI to mitigate corrosion is clearly evident by the much larger semi-circle for PEI coated substrate compared to the bare copper substrate (inset Figure). Nevertheless, a more significant improvement in the protection of the copper substrate is observed when PEI/G composites are used as the high frequency end of the semi-circle size increases from 200x10^3*ohm.cm*^{2} for PEI to 800x10^3*ohm.cm*^{2} for PEI/$G_{0.5}$ and 1700x10^3*ohm.cm*^{2} for PEI/G_1. It is remarkable that this reduction in the corrosion with the PEI/G composite coating is achieved with graphene loading of only 0.5 and 1.0 wt%. The loading of graphene plays a significant role in the performance of the coating as the PEI/G_1 coating has superior anticorrosion properties compared to PEI/$G_{0.5}$. This is attributed to the ability of the extra graphene loading to increase the pathway for corrosive agents to reach the metal substrate.

In addition to the qualitative investigation, an equivalent circuit can be used to fabricate the electrochemical impedance behavior of the coatings and the substrates. The equivalent circuit presented in

Figure 5.12 was used for this purpose. The unique combination of the various elements in the circuit is the best representation of impedance data for copper substrates as previously reported [72], [73]. From the fitting, the values of the different elements in the equivalent circuit are presented in Table 5.2. The results presented in Table 5.2 confirm the advanced corrosion inhibition performance of PEI/G_1 over other coatings, where the charge transfer resistance R'_p of PEI/G_1 coating is 48% higher than that of the PEI/$G_{0.5}$ coating and 94% higher than PEI coating.

Table 5.2: Electrochemical corrosion parameters obtained from the equivalent circuit for EIS measurements for bare copper, PEI, PEI/$G_{0.5}$ and PEI/G_1 coated copper in a 3.5 wt% NaCl solution.

Sample	R_S	R_P	CPE_1	n_1	R'_P	CPE_2	n_2	W	P_{EF}
	Ω cm^2	Ω cm^2	$\Omega^{-1}S^{n1}cm^{-2}$		Ω cm^2	$\Omega^{-1}S^{n2}cm^{-2}$		$\Omega^{-1}S^{n1}cm^{-2}$	%
Cu	5.2	8.2×10^{2}	2.5×10^{-5}	0.74	1.4×10^{3}	1.3×10^{-3}	0.83	1.4×10^{-3}	-
PEI	5.0	5.6×10^{4}	1.3×10^{-6}	0.47	1.0×10^{5}	3.9×10^{-12}	0.99	5.2×10^{3}	98.6
PEI/$G_{0.5}$	5.4	1.8×10^{4}	1.8×10^{-10}	0.99	7.2×10^{5}	4.3×10^{-9}	0.81	1.5×10^{4}	99.8
PEI/G_1	5.8	1.5×10^{4}	1.6×10^{-8}	1.00	1.7×10^{6}	1.4×10^{-10}	1.00	2.9×10^{4}	99.9

In addition to Nyquist plots, the Bode plots are another way to present the corrosion inhibition ability of coatings. Figure 5.14, depicts the Bode plots, which represent changes in impedance vs frequency for bare copper, PEI, PEI/$G_{0.5}$ and PEI/G_1 coated copper. From the plots, the Z_{real} values at the lowest recorded frequency, which represents the corrosion resistance [74], for bare copper, PEI, PEI/$G_{0.5}$ and PEI/G_1 coated copper are 3.13, 4.1, 5.89 and 6.66 ohm.cm^2, respectively.

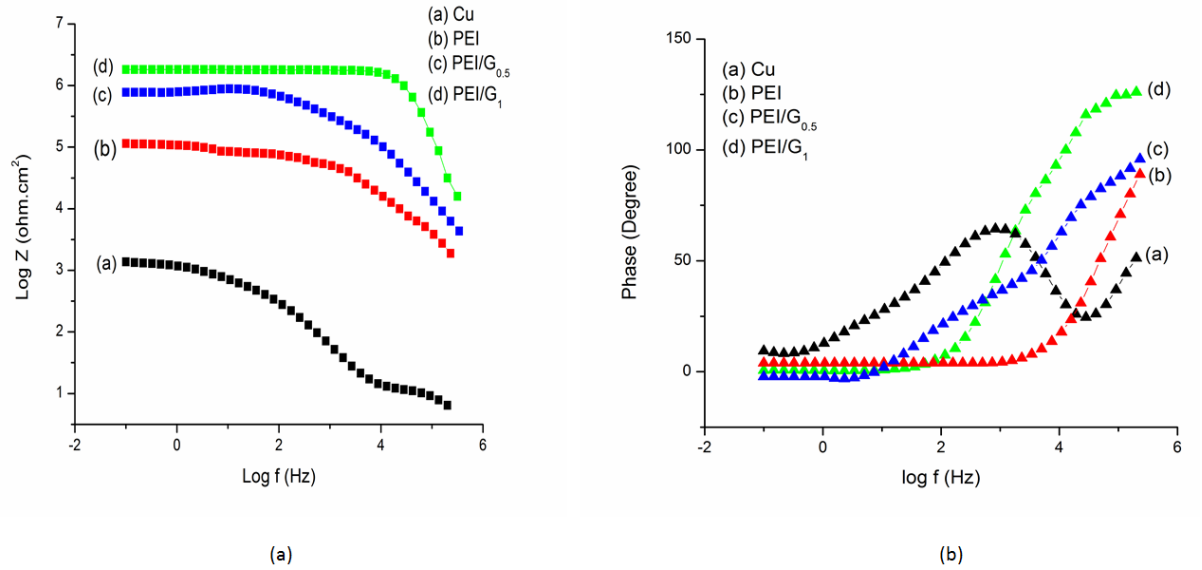

Figure 5.14: Bode plots for (a) bare copper, (b) PEI, (c) PEI/$G_{0.5}$ and (d) PEI/G_1 coated copper.

These results demonstrate that PEI and its graphene composite coatings are capable of protecting copper substrates from corrosion. In addition, the results reveal that the addition of graphene as a nanofiller enhances the corrosion inhibition. Moreover, the results confirm that the performance of PEI/G composites depends on the graphene loading. The enhancement in corrosion protection by the incorporation of graphene can be attributed to the barrier effect of dispersed graphene in the polymeric matrix. From this concept, the variation in corrosion inhibition of the PEI/$G_{0.5}$ and PEI/G_1 is attributed to the impact of graphene on the tortuosity of the diffusion pathway of the corrosive agents [70] as presented schematically in Figure 5.15.

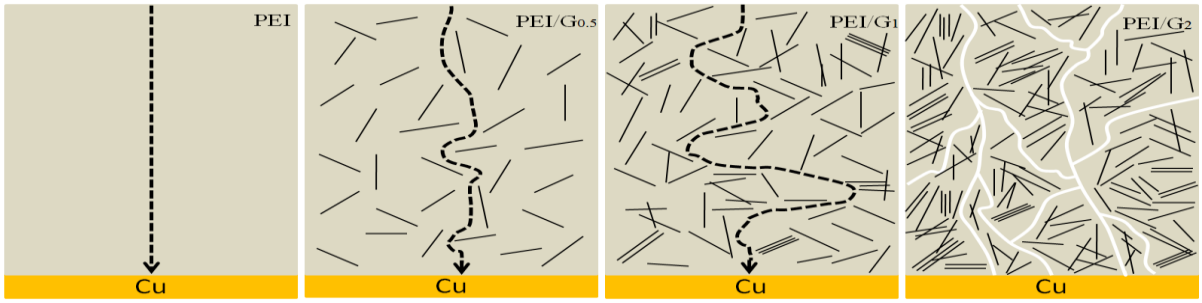

Figure 5.15: Representation of tortuous paths as corrosive agents pass through PEI and PEI/G coatings to reach the copper substrate.

5.4 Conclusion

Polyetherimide/graphene composites were prepared by thermal imidization and the graphene nanofillers were incorporated into the polymer matrix via in situ polymerization process. The dispersion of graphene in the PEI matrix was examined by SEM and TEM. In addition, the corrosion inhibition properties of the coatings with various graphene loadings were evaluated using the potentiodynamic and the EIS techniques. The study revealed that incorporation of graphene in PEI matrix enhances the corrosion prevention ability. Remarkable improvement in corrosion inhibition was observed and is attributed to the well dispersion of graphene in the polymer matrix. The well dispersed graphene acts as a protective barrier to the corrosive agents by increasing their pathways to reach the metal substrate.

Furthermore, the study concludes that graphene loading plays an important role in the corrosion inhibition and the adhesion properties of PEI. Nevertheless, an optimum graphene loading of about 1 wt% is required to avoid the poor adhesion and increased PEI stiffness at the very high loading.

Chapter 6

Enhanced Protective Properties and UV Stability of Epoxy/Graphene Nanocomposite Coating on Stainless Steel

Abstract

Epoxy-Graphene (E/G) nanocomposites with different loading of graphene were prepared via situ prepolymerization and evaluated as protective coating for Stainless Steel 304 (SS304). The prepolymer composites were spun coated on SS304 substrates and thermally cured. Transmission Electron Microscopy (TEM) and Scanning Electron Microscopy (SEM) were utilized to examine the dispersion of graphene in the epoxy matrix. Epoxy and E/G nanocomposites were characterized using X-ray diffraction (XRD) and Fourier Transform Infrared (FTIR) techniques and the thermal behavior of the prepared coatings is analyzed using Thermogravimetric analysis (TGA) and Differential scanning calorimetry (DSC). The corrosion protection properties of the prepared coatings were evaluated using Electrochemical Impedance Spectroscopy (EIS) and Cyclic Voltammetry (CV) measurements. In addition to corrosion mitigation properties, the long-term adhesion performance of the coatings was evaluated by measuring the adhesion of the coatings to the SS304 substrate after 60 days of exposure to 3.5% NaCl medium. The effects of graphene loading on the impact resistance, flexibility, and UV stability of the coating are analyzed and discussed. SEM was utilized to evaluate post adhesion and UV stability results. Our results indicate that very low graphene loading up to 0.5 wt. % significantly enhances the corrosion protection.

6.1 Introduction

Damage due to corrosion is one of the most common causes of metal component failures. The lack of mitigation protocols or methods of such electrochemical reactions may result in serious losses in both economy and industry. Although, total elimination of the corrosion process is not possible, there are different techniques that are utilized in various fields such as marine equipment, pipelines and construction

in order to attenuate the intensity and severity of corrosion. Anodic or cathodic protection [2], corrosion inhibitors [4] and protective coatings [5] are examples of these techniques. Nevertheless, an increasing number of research studies have been devoted to develop more robust techniques to extend the life cycle of metals in various environments. An effective example of such technique is the use of nanocomposites, hydrophobic and organic-inorganic hybrid materials as anti-corrosion coatings in various corrosive environments [6], [8], [10], [12].

Stainless steel already has remarkable corrosion resistance and is expected to perform satisfactorily in different environments. However, stainless steel is susceptible to pitting corrosion in chloride ions rich environments such as the marine atmospheric environment. Pitting corrosion is a galvanic corrosion process where localized active areas are formed as a result of localized inclusions or breakdown of the protective passive film of chromium oxide. The presence of corrosion agents such as chloride, water and oxygen initiates localized dissolution that penetrates through the metal thickness. This penetration may not be detected until severe damages has occurred and therefore pitting corrosion is considered insidious and more difficult to detect, evaluate and mitigate compared to other more uniform corrosions.

Therefore, additional means of corrosion protection are required to boost the life cycle of stainless steel substrates in chloride ions rich environment. Polymer based composites are perfect examples of protective coatings that can enhance various properties of the coated metal substrates including but not limited to corrosion resistance. A number of polymeric matrices have already been evaluated for corrosion protection purposes; however, the lack of interface adhesion foils the use of most of these polymeric matrices as anticorrosion coatings [57], [58]. Epoxy is an environmental friendly polymeric matrix that combines various remarkable properties such as exceptional thermal stability and low thermal expansion coefficient. These desirable properties in addition to the noble interface adhesion of epoxy with various metal substrates trigger the investigation of epoxy as an anticorrosion coating on SS304 substrates.

The properties of the polymer matrix can be further enhanced by the incorporation of nanofillers. Clay and carbon nanotubes are examples of nanofillers that are incorporated in epoxy matrix to enhance the

remarkable properties. However, the lower density, high surface area, and the very high aspect ratio attracted much attention to graphene [53] as a candidate for enhancing the corrosion protection property of epoxy. Graphene nanosheets, graphene nanoplatelets and functionalized graphene are different forms of graphene that have been utilized as fillers in various polymeric matrices to enhance their mechanical, thermal, dielectric, gas barrier, and corrosion resistance properties [32], [59], [60], [75]–[83]. The incorporation of graphene into the epoxy matrix is expected to prolong the pathway corrosive agents follow to reach the metal substrate. This graphene barrier effect is expected to limit the diffusion of ions and water molecules and consequently extends the life cycle of the coated substrates. To the best of our knowledge, there is no study that investigates the application of epoxy/graphene composites as anticorrosion coating for stainless steel Type 304.

In this study, E/G nanocomposites are developed and used as protective coating for stainless steel. The corrosion protection property of the E/G nanocomposite is evaluated by conducting electrochemical and weight loss measurements in 3.5 wt.% Sodium Chloride aqueous solution. The study also examines the effect of graphene loading on the adhesion, impact resistance and flexibility of E/G composite coatings. Furthermore, the long-term performance of the protective coatings is also examined by conducting the adhesion test after exposing the coated substrates to the 3.5 wt. % NaCl solution for 60 days. In addition, the influences of the incorporation of graphene on the thermal behavior as well as UV resistance of epoxy are evaluated.

6.2 Experimental

6.2.1 Materials

Polished SS304 sheet 99.9 % purity (3254K91, McMASTER-CARR, Ohio, USA) was used as substrates., Bisphenol A diglycidyl ether (D3415, BADGE, Sigma Aldrich, Ontario, Canada) and Poly(propylene glycol) bis(2-aminopropyl ether) (406651, B230, Sigma Aldrich, Ontario, Canada) were used as received. Graphene nanosheets (GN1P0005, ACS Material, Massachusetts, USA)

were synthesized by thermal exfoliation/reduction of graphite oxide, which was prepared using the modified Hummer method and it has a surface area of 400-1000 m^2/g and electrical resistivity of $\leq$ 0.3 Ω. cm, as per the supplier specifications.

6.2.2 Composites synthesis and coating

E/G composites with graphene loading of 0.1 wt.% ($E/G_{0.1}$), 0.5 wt.% ($E/G_{0.5}$) and 1 wt.% (E/G_1) were prepared using in situ polymerization approach. The prepolymer\graphene mixture was then spin coated on a SS304 substrate before thermal curing. Figure 6.1, schematically depicts the overall composite preparation, coating and curing process.

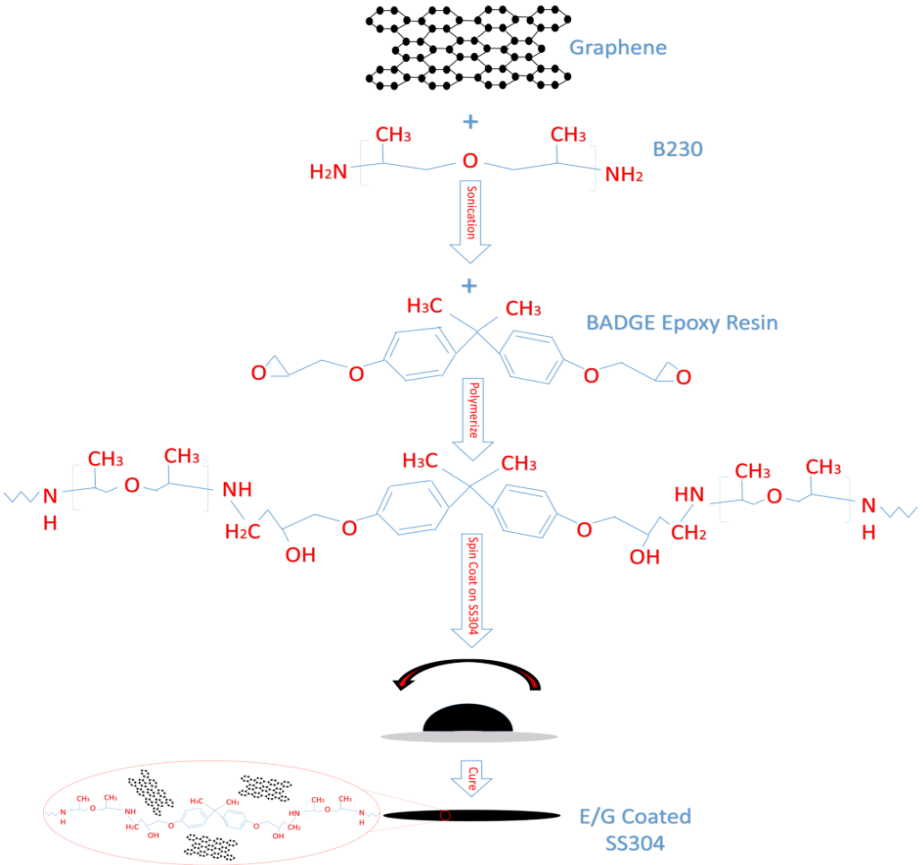

Figure 6.1: Schematic description of the process for the synthesis of E/G composites using in situ polymerization.

As an example, to prepare E/G nanocomposite with 0.1 wt.% graphene via situ prepolymerization, graphene (2.1 mg) was dispersed in 0.5 g curing agent (hardener) B230 by stirring and bath sonication (FS30H, Fisher Scientific, Ontario, Canada) for an hour each. BADGE (1.5 g) was added to the graphene suspension and the mixture was stirred for 1 h followed by sonication for an additional hour. The mixture was homogenized (125, Fisher Scientific, Ontario, Canada) for 30 min, sonicated for 5 min and spin coated (SC 100, Smart Coater, Missouri, USA) at 400 RPM for 1 min on a clean SS304 substrate. The composite was cured at 50° C for 4 h to obtain 124 ±2 µm thick $E/G_{0.1}$ coated SS304 substrate. The same procedure was followed to prepare ($E/G_{0.5}$) and (E/G_1) using 10.1 and 20.3 mg of graphene, respectively.

6.2.3 Composite characterization

The dispersion of graphene in the epoxy matrix was examined using TEM (Philips CM-10 TEM, Geneva, Switzerland). Samples for the TEM study were prepared by scraping the E/G coating with a sharp knife and the collected E/G composite was dispersed in methanol for 5 min. The sample was then fished using TEM copper grid and allowed to dry under vacuum at room temperature. FTIR (Tensor 27, Bruker, Massachusetts, USA) was used to acquire spectra of epoxy and E/G composites at room temperature. XRD diffraction patterns of epoxy and E/G composites are recorded in the range of $2\theta = 3°$ to 90° at 0.24° /min scan rate and 0.02° step size using MiniFlex 600 (Rigaku, Beijing, China).

6.2.4 Adhesion

The interfacial adhesion between the coating and the SS304 substrate was measured according to the ASTM-D3359 standard using an adhesion tape kit (PA-2000, Paul N. Gardner Company Inc., Florida, USA) with standard blade (11-teeth with teeth spacing of 1 mm). The Interface adhesion was evaluated before and after exposing the coating to the 3.5 wt.% NaCl solution for 60 days in order to examine the long-term durability of the coatings. Post-adhesion tests results were captured using SEM (Zeiss LEO 1550, New York, USA). SEM samples were placed on carbon tape attached to the SEM holder and the sample was further coated with gold via sputtering for 120 sec.

6.2.5 Gravimetric Analysis

The weight loss measurements were conducted in 500 ml glass beaker placed in a temperature controlled water bath. Coated and uncoated SS304 substrates were weighted, placed in Teflon holders with 1 cm^2 exposed surface area and immersed in a 3.5 wt.% NaCl solution for 60 days at 25° C. At the end of the exposure period, the samples were removed and washed with double distilled water before a fine brush was used to strip off the corrosion products. The samples were cleaned again by bath sonication in a double distilled water for 10 min to ensure the removal of corrosion residues, dried and weighted. All mass loss measurements were carried out in triplicate and the mean weight and the standard deviation is reported.

6.2.6 Electrochemical Measurements

Electrochemical measurements were conducted at 25°C in a double-jacketed 1 L corrosion cell covered with a drilled Teflon plate to allow electrodes immersion. A three electrode configuration was used to conduct the measurements, where a Silver/Silver Chloride (Ag/AgCl) electrode was used as the reference electrode (RE), two graphite rods as the auxiliary electrodes (AE) and a 1 cm^2 coated/uncoated SS304 substrate as the working electrode (WE). The WE was washed with acetone and double distilled water, dried and then installed in the sample holder before conducting the tests. 1 L temperature controlled 3.5 wt.% NaCl solution was used as the electrolyte. EC-Lab software (Bio-Logic) and VSP-300 workstation (Uniscan instruments Ltd., Claix, France) were used to conduct all electrochemical measurements, where each measurement was repeated three times in order to confirm the reproducibility of the collected raw data.

The potential of the WE was allowed to stabilize for 30 min before conducting the EIS followed by the potentiodynamic measurements. The EIS measurements were conducted at frequency range from 200 kHz to 100 MHz to generate Bode and Nyquist plots. Furthermore, an equivalent circuit was used to fit the raw impedance data and EC-Lab software was used to evaluate the different components of the equivalent circuits. The potentiodynamic measurements were conducted by scanning the potential of the WE from -500 mV to 500 mV at a rate of 20 mV/min to produce the Tafel plots. These plots were used to extract the

corrosion current (I_{corr}) using EC-Lab software by extrapolating the linear portion of the anodic and the cathodic curves.

6.2.7 Thermal behavior and UV degradation

The thermal stability of the nanocomposite coatings was evaluated using thermal gravimetric analysis (TGA) (TA instruments, Q500, Ontario, Canada) in the temperature range 25-800 ^{o}C, while the glass transition temperature was observed using differential scanning calorimetry (DSC) (TA instruments, Q2000, Ontario, Canada) in the temperature range 25-200 ^{o}C at 10 ^{o}C/min heating rate.

The Resistance of the prepared Epoxy and E/G coatings to UV degradation was assessed using an accelerated weathering tester (QUV, Q-LAB, Florida, USA) according to ASTM-D4587 standard. Testing specimens were continuously exposed to repeated UV cycle at 60 ± 2.5° C for 8 hours, followed by a condensation cycle at 50 ± 2.5° C for 4 hours over 30 days followed by SEM examination of the surface morphology of the epoxy and E/G coatings.

6.2.8 Flexibility and Impact resistance

Two different types of tests were carried out to illustrate the influences of graphene loading on the room temperature flexibility and impact resistance of the coatings. In the bending test, the coated substrate was bent over a conical shaped mandrel (MN-301003, Paul N. Gardner Company Inc., Florida, USA) with a diameter ranges from 3.1 to 38 mm to assess the flexibility of the coatings. The test was repeated three times and the mean diameter at which the coatings cracked were reported.

Impact resistance was performed to evaluate the resistance of the prepared coatings to rapid deformation by a falling weight. The test was conducted using a universal impact tester (IM-172RF, Paul N. Gardner Company Inc., Florida, USA) with combined 0.5-inch ball and 2-lb weight indenter according to ASTM D2794 standard. The combined weight and indenter were raised 1 inch in the testing tube and released to drop on the coated substrate and the falling weight test was repeated with 1 inch increments in height until

a crack in the coating was observed. The height at which the coating cracks was recorded and the test was repeated slightly above, slightly below and at the recorded height five times each according to the ASTM standard. The elevation at which the coating cracks in all five trials is reported as the impact resistance limit of the coating to rapid deformation.

6.3 Results

6.3.1 Characterization of E/G composites

The dispersion of graphene in the polymeric matrix for $E/G_{0.1}$ and $E/G_{0.5}$ composites was examined using SEM and TEM as shown in Figure 6.2. The TEM images, clearly illustrate the influence of graphene loading on the degree of dispersion, where graphene is well dispersed as indicated by thin sheets in the $E/G_{0.1}$ coating, while thick stack of graphene sheets were observed in $E/G_{0.5}$ coating. SEM images, depicts wide degrees of dispersion in both $E/G_{0.1}$ and $E/G_{0.5}$ composites.

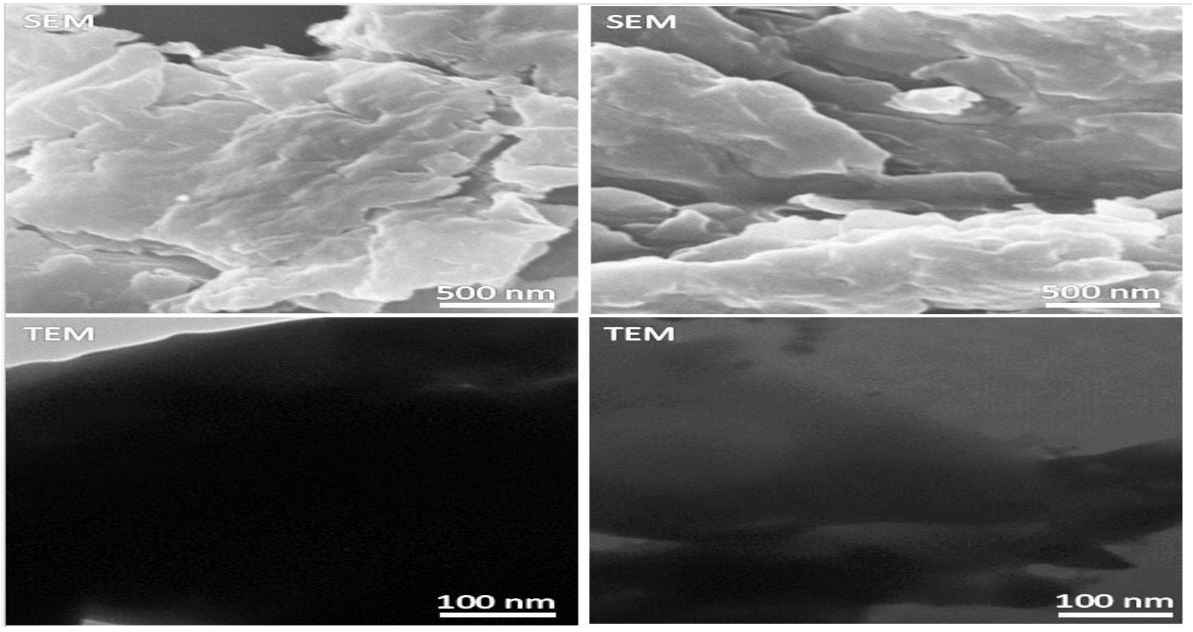

(a) (b)

Figure 6.2: TEM and SEM images for graphene dispersion in (a) $E/G_{0.5}$ and (b) $E/G_{0.1}$.

FTIR was utilized to characterize both epoxy and E/G composites as depicted in Figure 6.3. Different characteristic peaks are identified, such as the peaks at 1508 cm^{-1} and 1609 cm^{-1} (C–C skeletal stretching), 915 cm^{-1} (epoxide ring) and 3380 cm^{-1} (-OH stretching), which confirms the curing of the epoxy resin. Comparing the epoxy spectrum to the E/G composite spectra revealed that there were no clear dissimilar absorption peaks indicating no chemical linkages between graphene and the epoxy function groups. Epoxy and E/G composites were also characterized using XRD and the diffraction spectrum are depicted in Figure 6.4. All XRD patterns show broadly amorphous peak appearing around 2θ value between 10 and 30°, which ascribed to the homogeneously amorphous of epoxy. Moreover, the observed XRD patterns indicate that the degree of crystallinity of epoxy is retained after incorporation of graphene.

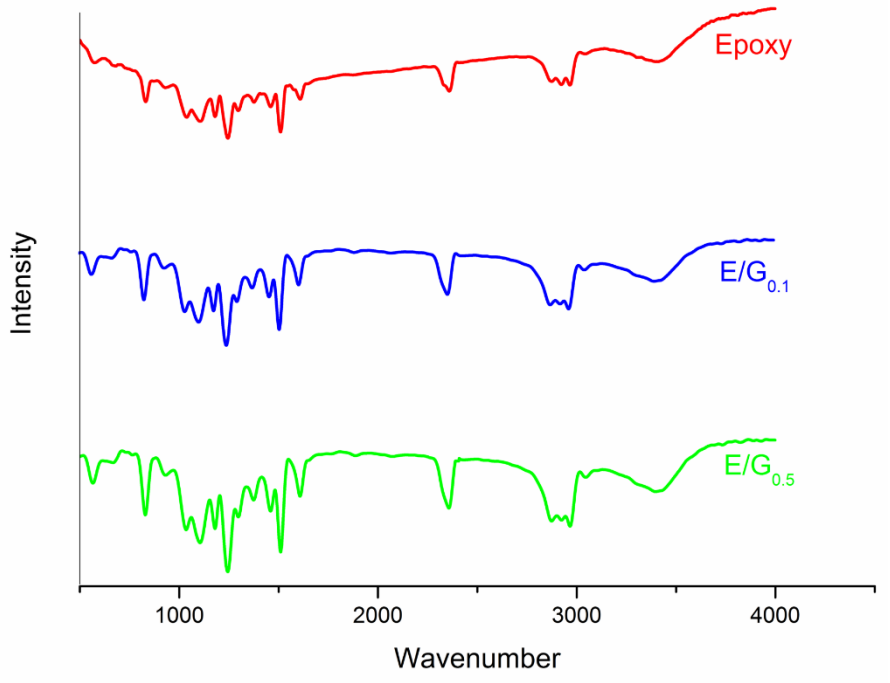

Figure 6.3: FTIR spectra of epoxy and E/G composites.

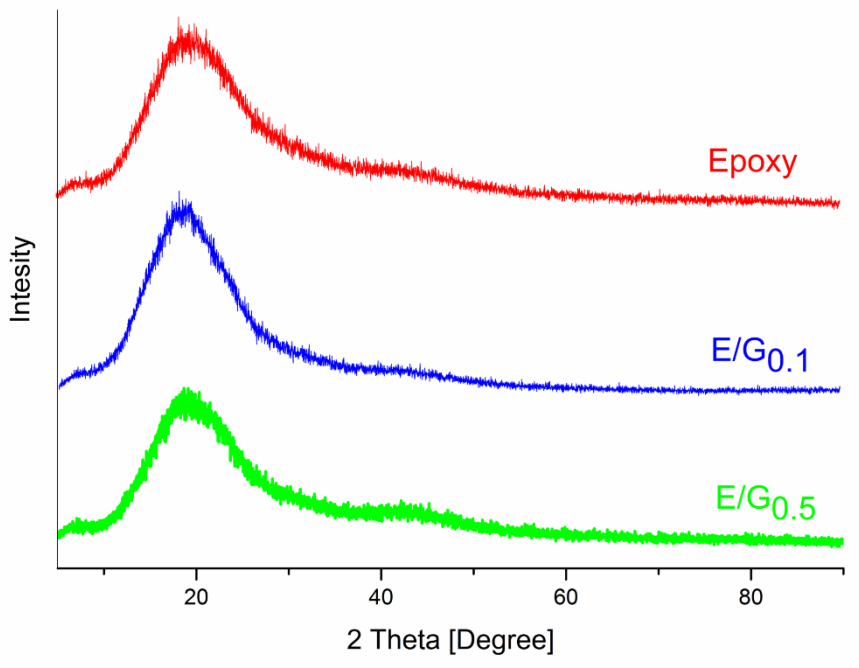

Figure 6.4: XRD patterns of epoxy and E/G composites.

6.3.2 Adhesion test

Interface adhesion between the metal substrate and the coating is a significant property that needs to be examined before the coating can be considered protective. Poor interface adhesion may result in the formation of voids between the metal substrate and the coating, where corrosive agents may accumulate and accelerate the corrosion process. Therefore, decent interface adhesion is always desired. The adhesion of E/G coatings to the SS304 substrates were examined and evaluated according to ASTM D3359 adhesion tape standard test. The test was performed on $E/G_{0.1}$ and $E/G_{0.5}$ coatings before and after 60 days of exposure to the 3.5 wt.% NaCl solution. The post adhesion test results are presented in Figure 6.5, where no peelings were observed in any of the coatings and all coatings received 5B rating (0% peeling) according to the ASTM standard.

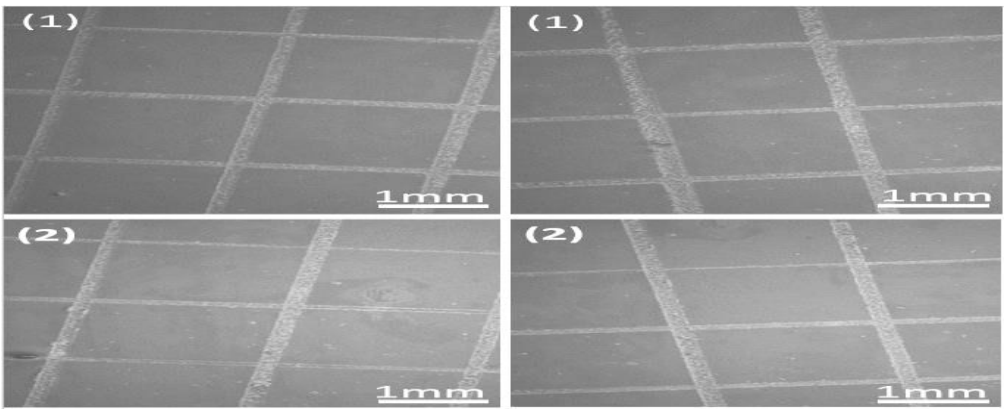

(a) (b)

Figure 6.5: SEM images of post-adhesion tests of (1) E/$G_{0.1}$ and (2) E/$G_{0.5}$ coated SS304 substrates (a) before and (b) after 60 days of exposure to the corrosive medium.

Moreover, it was interesting to observe the shortcoming of increasing the load of graphene beyond the percolation loading. The disadvantage of increasing the graphene loading is clearly depicted in Figure 6.6 a, where poor interface adhesion between the E/G_1 coating and SS304 substrate was observed and the coating receives 0B rate (more than 65% peeling) according to the ASTM standard. The observed undesirable influence of the load of graphene on the interface adhesion can be attributed to accumulation of graphene at the interface, which attenuates the contact area between epoxy resin and SS304 substrate as depicted in Figure 6.6 b, where clear gaps can be observed between E/G_1 and the SS304 substrate.

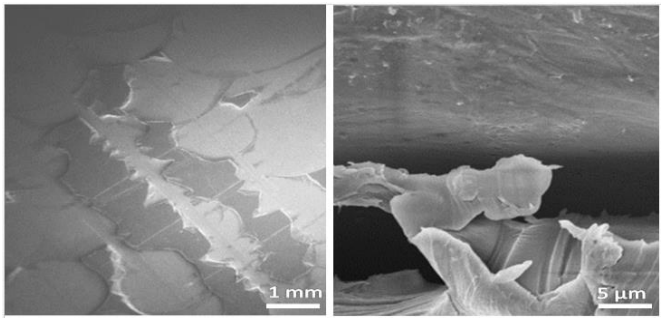

(a) (b)

Figure 6.6: SEM image of (a) post-adhesion test and (b) cross section view of E/G_1 coated SS304 substrate.

6.3.3 Weight Loss

Weight loss measurements for coated/uncoated SS304 substrate were reported after 60 days of immersion in the 3.5 wt.% NaCl solution at 25° C. These measurements were used to calculate the corrosion rate (R_{corr}) and the protection efficiency (P_{EF}) of the different coatings using (6.1) and (6.2).

$$R_{corr} = \frac{W_0 - W}{Axt} \tag{6.1}$$

$$P_{EF}[\%] = \left(1 - \frac{R_{corr}}{R^{\circ}_{corr}}\right) x100 \tag{6.2}$$

Where, A is the exposed surface area (1 cm^2), W_0 and W are the weight (mg) before and after exposure, respectively, t is the immersion time (60 days), R_{corr} and R°_{corr} are the corrosion rate of coated and bare SS304 substrates, respectively. Furthermore, standard deviation of R_{corr} ($R_{corr,\ STD}$) was computed and reported in Table 6.1 using triplicate weight loss measurements for each sample.

Table 6.1: Weight loss measurements for bare SS304, epoxy, E/$G_{0.1}$ and E/$G_{0.5}$ coated SS304 in a 3.5 wt.% NaCl solution.

Sample	W_0 mg	W mg	R_{corr} $mg.cm^{-2}.d^{-1}$	$R_{corr,\ STD}$ $mg.cm^{-2}.d^{-1}$	P_{EF} %
SS304	93.1	66.9	0.44	0.009	-
Epoxy	107	101.6	0.09	0.011	79.5
E/$G_{0.1}$	115.9	113.5	0.04	0.008	90.9
E/$G_{0.5}$	122.9	122	0.015	0.005	96.6

The data reported in Table 6.1 illustrate that coating SS304 with epoxy may prolong the life cycle of the metal substrate as indicated by the decrease in the corrosion rate. Furthermore, the results demonstrate that

the corrosion rate is attenuated and the protection efficiency of epoxy is enhanced by the incorporation of graphene. Moreover, the low values of $R_{corr, STD}$ demonstrate the excellent reproducibility of the results.

6.3.4 Electrochemical Impedance measurements

EIS is a widely used technique to investigate electrochemical activity on metal substrates. Here, EIS is utilized to examine the corrosion behavior of bare and coated SS304 substrates. In EIS, an alternating current (AC) is forced through a circuit that may contain insulators, resistors and capacitors or combinations of items resulting in a complex output resistance known as impedance. In corrosion studies, the AC is fed to the system over a range of frequency and the complex output at different frequencies are reported as the impedance of the WE. Furthermore, impedance can be modelled using equivalent circuits that contain a specific combination of different elements such as resistors and capacitors.

The impedance behavior of bare and coated SS304 substrates is measured in temperature controlled 3.5 wt.% NaCl electrolyte using the EC-Lab software after allowing the potential of the WE to stabilize for 30 min. The EC-Lab software was also used to model and fit the raw impedance data using equivalent circuits with specific combinations as shown in Figure 6.7. In the equivalent circuits, R_s and R_{ch} represent electrolyte and charge transfer resistances, respectively, while C is a double layer capacitor. The magnitudes of the various elements in the equivalent circuit and the frequency of the AC signal (ω) were utilized to fit raw impedance data using (6.3).

$$Z = Z' + jZ'' = R_s \frac{R_{ch}}{1+(R_{ch}\times C\times \omega)^2} + j\frac{{R_{ch}}^2\times C\times \omega}{1+(R_{ch}\times C\times \omega)^2} \quad (6.3)$$

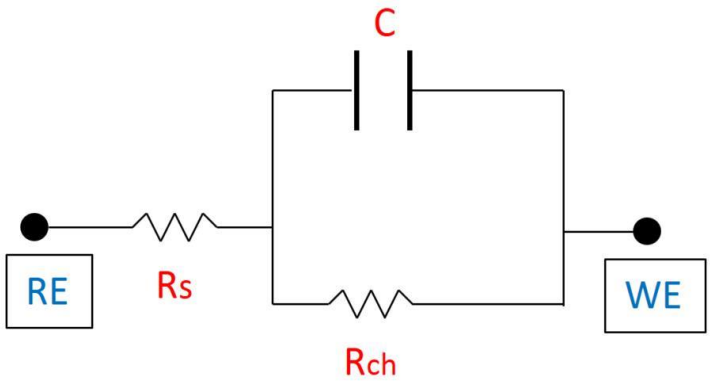

Figure 6.7: Equivalent circuits used to model the electrochemical impedance data.

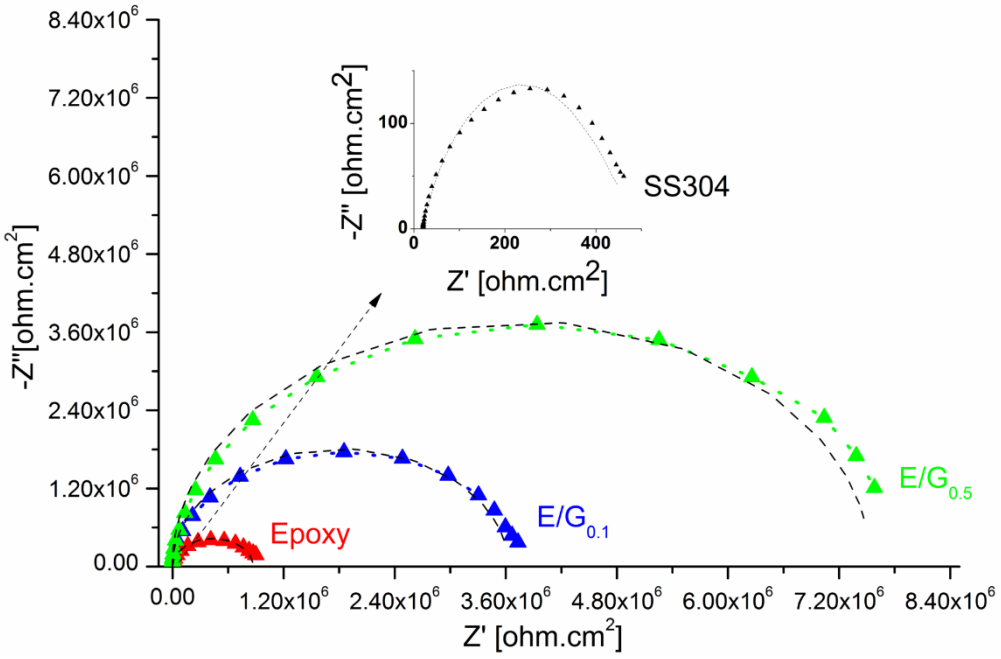

Figure 6.8: Nyquist plots for bare SS304, epoxy, E/$G_{0.1}$ and E/$G_{0.5}$ coated SS304 substrates.

Figure 6.8, depicts Nyquist plots for bare and coated SS304 substrate, where real and imaginary parts of the impedance are presented. The Nyquist plot clearly represents the corrosion protection by the epoxy coating as demonstrated by the increase in the size of the impedance semi-circle indicating an enhancement in corrosion mitigation and slower corrosion rate for the epoxy coated sample compared to the bare SS304. Nevertheless, this corrosion protection enhancement is further improved by incorporating graphene in the

epoxy matrix, where the real resistivity value at the high frequency end has increased from $1.0x10^6$ *ohm.cm²* for the epoxy coated sample to $3.8x10^6$ *ohm.cm²* for $E/G_{0.1}$ coated sample and $7.8x10^6$ *ohm.cm²* for $E/G_{0.5}$ coated sample.

In addition to the qualitative analysis, the computed values of the different elements of the equivalent circuits shown in Figure 6.7 can be used to evaluate the corrosion protection properties of the different coatings. It should be noted that the unique combinations of elements in the presented circuits resulted in the best fitting of raw impedance data. Table 6.2, represents the values of the various elements in the equivalent circuits and the repeatability of triplicate measurements is illustrated by the small values of $R_{ch, STD}$. The results clearly illustrate the ability of the epoxy coating to protect the SS304 substrate from corrosion as indicated by the increase in the charge transfer resistance. Moreover, the results illustrate the advantages of incorporating graphene as implied by the significant increase in the charge transfer resistance for $E/G_{0.1}$ and $E/G_{0.5}$.

Table 6.2: Electrochemical corrosion parameters obtained from equivalent circuit for EIS raw measurements for bare SS304, epoxy, $E/G_{0.1}$ and $E/G_{0.5}$ coated SS304 in 3.5 wt.% NaCl solution.

Sample	R_S $\Omega.cm^2$	C F	R_{ch} $\Omega.cm^2$	$R_{ch\ ,\ STD}$ $\Omega.cm^2$
SS304	18.5	$8.5x10^{-6}$	450.5	10
Epoxy	18	$1.4x10^{-10}$	$8.7x10^5$	190
$E/G_{0.1}$	18.2	$3.9x10^{-11}$	$3.63x1^6$	380
$E/G_{0.5}$	18.1	$3.9x10^{-11}$	$7.55x1^6$	260

Bode plots are another representation of the corrosion protection ability of the coating. Figure 6.9(a), depicts the Bode plots, where the real part of impedance (Z_{real}) is plotted versus frequency, while Figure

6.9(b) depicts the phase plots. Corrosion resistance can also be represented by the Z_{real} values at the lowest recorded frequencies. From Figure 6.9(a), Log Z_{real} at the lowest frequencies for bare, epoxy, $E/G_{0.1}$ and $E/G_{0.5}$ coated SS304 are 2.7, 6.0, 6.6 and 6.9 ohm.cm^2, respectively.

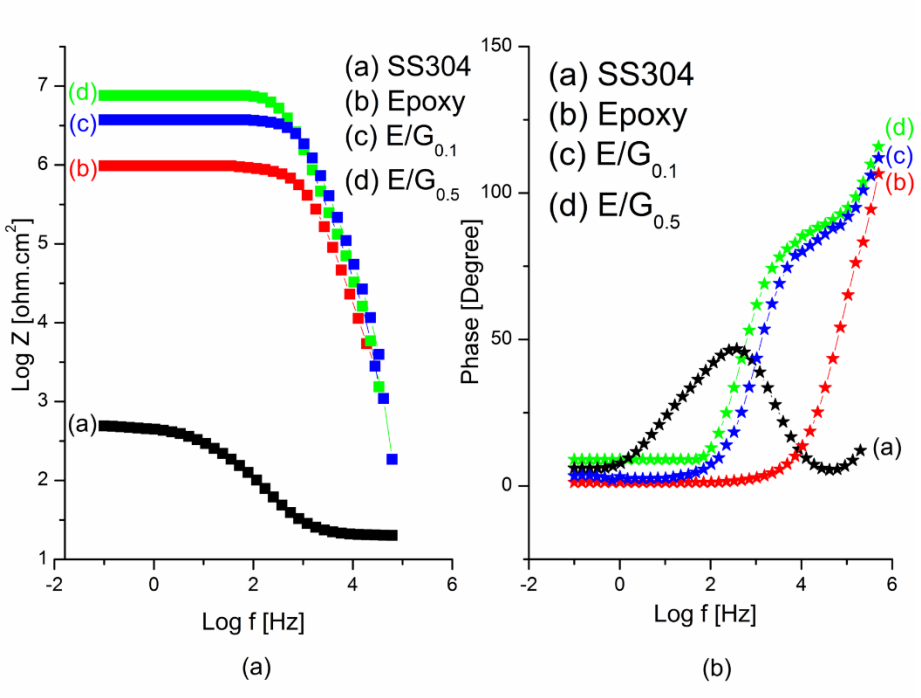

Figure 6.9: (a) Bode and (b) phase plots for bare SS304, epoxy, $E/G_{0.1}$ and $E/G_{0.5}$ coated SS304 substrates

EIS results illustrate that epoxy coatings may mitigate the corrosion process on SS304 substrate and prolong the life cycle of the metal. However, the incorporation of graphene would further enhance such a protection characteristic of the epoxy and the degree of enhancement depends on graphene loading. This variation in protection efficiencies can be attributed to the noble barrier property of graphene [78], which attenuate the corrosion rate by prolonging the tortuosity pathway for the corrosive agents to reach the SS304 substrate.

6.3.5 Potentiodynamic measurements

Cyclic Voltammetry is a widely utilized technique to characterize electrochemical behavior of metal substrates and coatings. In this study, a three-electrode configuration was used to conduct cyclic voltammetry tests on bare and coated SS304 substrates. The raw data were recorded using the EC-Lab software and all measurements were obtained in 3.5 wt. % NaCl solution at 25° C. Furthermore, the potential of the testing sample was allowed to stabilize for 30 min before conducting any experiment. Even though the potential of the working electrode was scanned from -500 mV to 500 mV, only the areas where the electrode shifted from the anodic to cathodic behavior, which is known as the Tafel plots, were presented as shown in Figure 6.10. Important parameters such as E_{corr} and I_{corr} were extracted from the Tafel plots. Furthermore, the extracted E_{corr} and I_{corr} from triplicates measurement for each sample were utilized to demonstrate the reproducibility of the results by analysis of the standard deviation of E_{corr} ($E_{corr, STD}$) and I_{corr} ($I_{corr, STD}$), which are reported in Table 6.3.

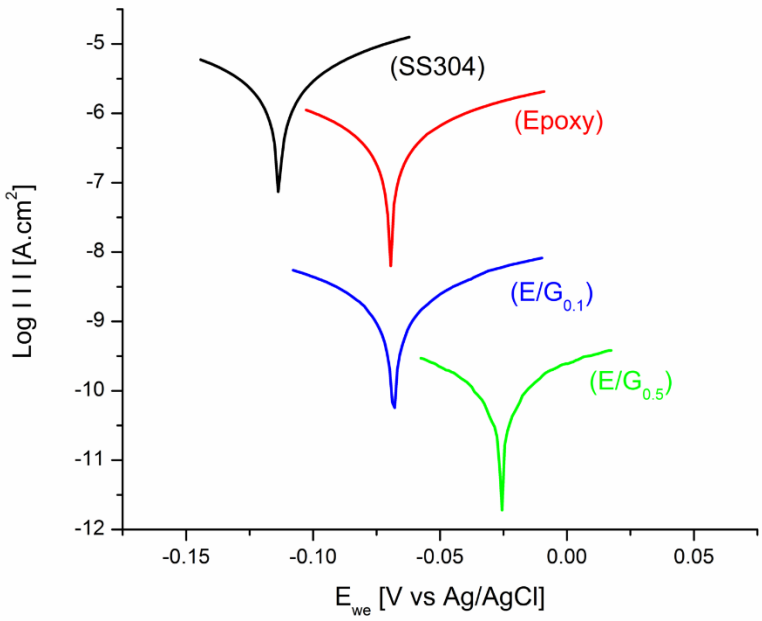

Figure 6.10: Tafel plots for bare SS304, epoxy, E/$G_{0.1}$ and E/$G_{0.5}$ coated SS304 substrates.

Table 6.3: Electrochemical corrosion parameters obtained from cyclic voltammetry measurements for bare SS304, epoxy, $E/G_{0.1}$ and $E/G_{0.5}$ coated SS304 in a 3.5 wt.% NaCl solution

Sample	E_{corr} mV	$E_{corr,\ STD}$ V	I_{corr} μA/cm^2	$I_{corr,\ STD}$ μA/cm^2	b_a	b_c	R_P Ω.cm^2	P_{EF} %
SS304	-113.5	0.009	2.4	0.002	48.2	55.3	4.6	-
Epoxy	-69.4	0.06	0.46	0.01	87	88.2	41.3	80.8
$E/G_{0.1}$	-65	0.01	0.06	0.009	82.3	74	282	97.5
$E/G_{0.5}$	-27.7	0.007	8.7×10^{-3}	0.005	61.4	54.5	1441	99.6

These extracted parameters can be used to compute the polarization resistances (R_p) of the protective coatings using (6.4), which is known as the Stern-Geary equation.

$$R_P = \frac{(b_a x b_c)}{2.303(b_a + b_c)} x I_{corr} \tag{6.4}$$

Where b_a/b_c are the anodic/cathodic Tafel slops (dE/dlog I), respectively, and extrapolating the linear portion of these curves determines I_{corr} at the intersection. Finally, I_{corr} values can be used to evaluate the protection efficiencies of the different coatings using (6.5):

$$P_{EF}[\%] = \left(1 - I_{corr}/I^{\circ}_{corr}\right)x100 \tag{6.5}$$

Where I°_{corr} and I_{corr} are corrosion currents of bare and coated SS304, respectively. The variations in corrosion and computed parameters (E_{corr}, I_{corr}, R_p), which are reported in Table 6.3 may explain the influences of the various protective coatings on the electrochemical behavior of the SS304 substrate. In general, a positive shift in E_{corr}, R_p and P_{EF} plus a drop in I_{corr}, represents an enhancement in corrosion mitigation.

The abilities of E/G coatings in mitigating corrosion on SS304 substrates were confirmed by the results presented in Figure 6.10 and Table 6.3. These results demonstrate that the corrosion protection performance

of epoxy coatings can be significantly enhanced by the incorporation of graphene as illustrated by the positive shifts in the E_{corr}, R_P and P_{EF} and the attenuation of the I_{corr}. Furthermore, it was interesting to observe that the level of enhancement in P_{EF} of E/G can be positively influenced by increasing the graphene loading as illustrated in Figure 6.10 and Table 6.3, which is in agreement with the results obtained from the gravimetric method. This enhancement in corrosion mitigation properties of E/G coatings can again be attributed to the barrier property of graphene, which prolong the pathway that corrosive agents follow to reach the metal substrate.

6.3.6 Thermal behavior and UV degradation

The incorporation of graphene in polymeric matrix has influenced the thermal stability of the resin. This can be observed as an upward shift in the glass transition temperature (T_g) as depicted in Figure 6.11. The increase in Tg has been reported for other graphene polymer nanocomposites and is attributed to the strong interface between the filler and polymer matrix, which restricts the polymer chains' mobility [84]. Moreover, incorporation of graphene increases the thermal stability of the epoxy composite as observed by the increase in onset degradation temperature (T_{onset}), which is the temperature where 5 wt.% is observed as depicted in Figure 6.12, inset has increased from 352.8 °C for the neat epoxy to 358.5 °C and 358.8 ° C for $E/G_{0.1}$ and $E/G_{0.5}$, respectively, confirming the strong interactions between graphene and epoxy polymer possibility through the amine groups on the polymer chains and the epoxy/hydroxyl groups on the reduced graphene surface.

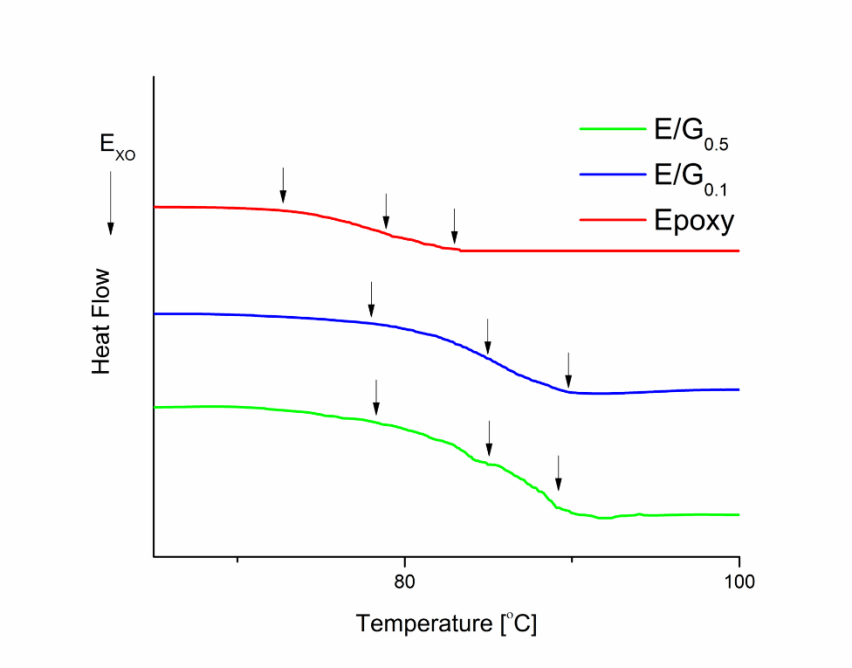

Figure 6.11: DSC thermograms of Epoxy and E/G coatings.

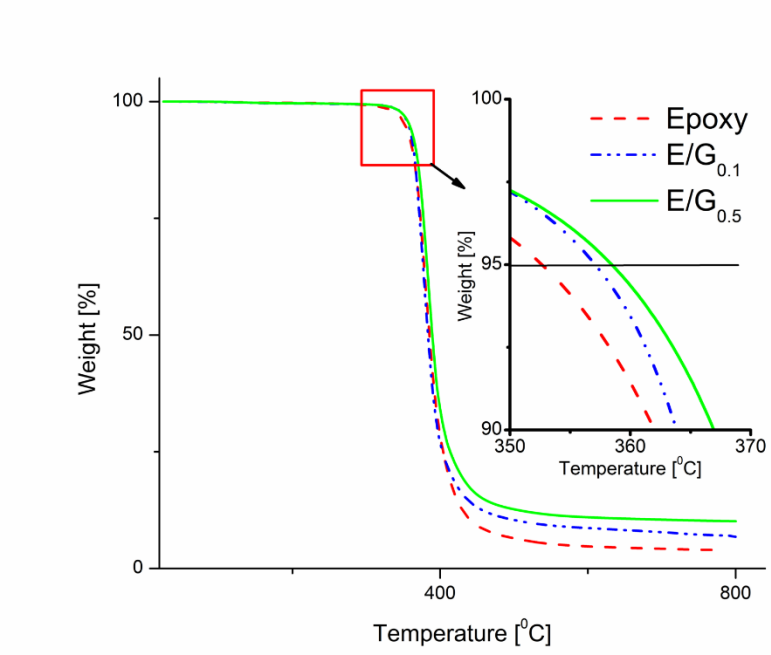

Figure 6.12: TGA thermograms of Epoxy and E/G coatings.

Epoxy polymers are known to degrade when exposed to UV radiation [85]. Therefore, the surface morphology of the prepared coatings were observed after 30 days of exposure to UV and condensation

cycles using SEM and results are depicted in Figure 6.13. Sever damages can be observed on the epoxy surface, where the damages were manifested in forms of micro-cracks and pits as illustrated in Figure 6.13.a. Surface cracking was also observed on $E/G_{0.1}$ coating as depicted in Figure 6.13.b; however, no evidence of pitting was observed. The capacity of graphene in enhancing the durability of the epoxy coating is well illustrated in Figure 6.13.c, where increasing the load of graphene to 0.5%, $E/G_{0.5}$, leads to prevention of pitting as well as significant reduction in the number of observed micro-cracks due to the enhanced UV stability induced by graphene [86].

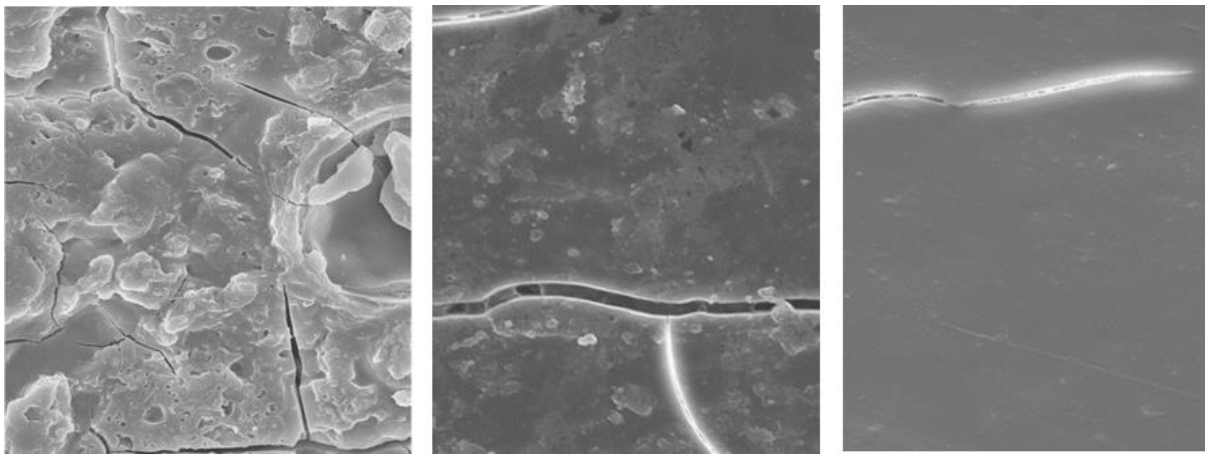

(a) (b) (c)

Figure 6.13: SEM images of post-UV degradation tests of (a) epoxy (b) $E/G_{0.1}$ and (c) $E/G_{0.5}$ coated SS304 substrates after 30 days of exposure to UV and condensation cycles.

6.3.7 Flexibility and impact resistance

Mechanical properties such as elasticity and impact resistance in addition to adhesion and corrosion mitigation are important characteristics of polymer coatings. The bending and the impact resistance tests were conducted on epoxy and E/G composites coatings in order to evaluate the impact of graphene on the flexibility and impact resistance. Figure 6.14 shows the bending and impact resistance results for different coatings, where the main bending diameters and the elevations at which the coating fails for five times are reported. These results illustrate that incorporation of graphene reduces the flexibility of the epoxy coating

and the degree of reduction increases with graphene loading, which is attributed to the increase in stiffness. In contrast, the addition of graphene enhances the impact resistance of epoxy and here too, the degree of enhancement is proportional to the graphene loading. The observed effects of graphene on the bending and the impact resistance are attributed to the increase in stiffness and toughness of the epoxy composite with graphene loading, which was also reported [82], [87]–[89], which enhances the resistance to sudden deformation and reduces the elasticity of the epoxy coating.

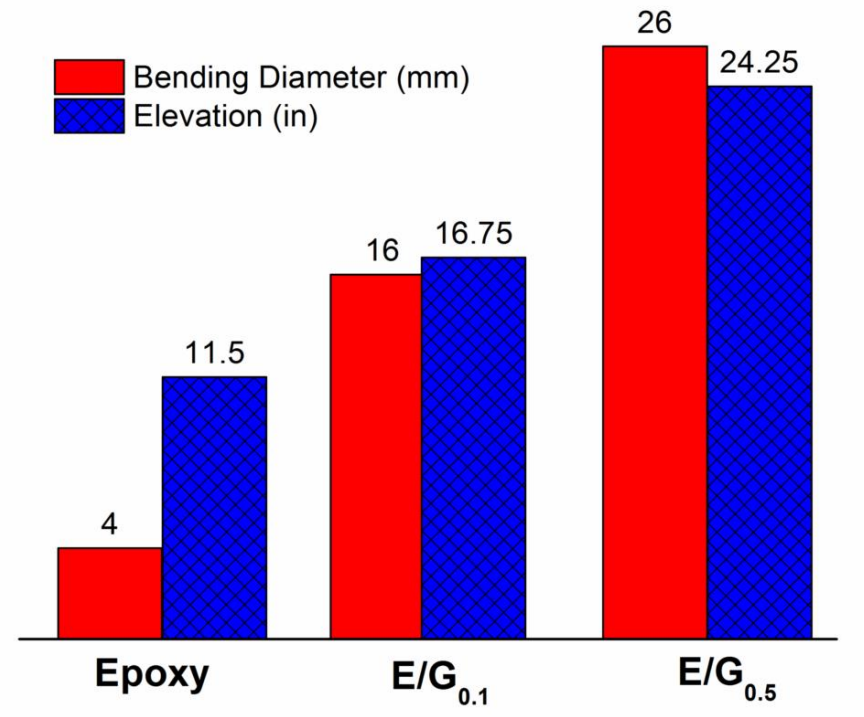

Figure 6.14: Bending and impact resistance test results for epoxy, E/$G_{0.1}$ and E/$G_{0.5}$ coatings on SS304.

6.4 Conclusion

Epoxy/graphene composites were prepared using situ prepolymerization approach, spin coated and thermally cured on SS304 substrates. We demonstrated that the corrosion protection ability of the epoxy is significantly enhanced by incorporation of graphene due to the barrier property of graphene, which shields the corrosive agents from reaching the SS304 substrate. Moreover, incorporation of graphene enhances the

mechanical properties and impact the thermal properties as well as the adhesion of the epoxy composite to the SS substrate. Graphene loading and the degree of dispersion have significant impact on the thermal, and mechanical properties as well as adhesion to the SS substrate, the corrosion protection characteristics and UV stability. Indeed, it is interesting to observe that increasing graphene loading in the epoxy matrix beyond an optimum loading of 0.5 wt.% may attenuate the interface adhesion between coating and the SS304 substrate due to aggregation of graphene and reduction of the interface area.

Chapter 7

Enhanced Advanced Electroactive Epoxy–Glass Flakes composite anticorrosive coatings on Cold-Rolled Steel

Abstract

Electroactive Epoxy-Glass Flakes composites (EE/GF) were prepared and evaluated as anticorrosion coating on Cold-Rolled Steel (CRS). EE/GF with different loadings of glass flakes were prepared via in-situ polymerization. The prepolymer composites were brush coated on CRS substrates and thermally cured. Scanning Electron Microscopy (SEM) and Transmission Electron Microscopy (TEM) were utilized to examine the dispersion of glass flakes in the electroactive epoxy matrix. The corrosion protection properties of the prepared coatings were evaluated using Electrochemical Impedance Spectroscopy (EIS) and Cyclic Voltammetry measurements. In addition to corrosion mitigation properties, the effects of the glass flakes loading on the impact resistance and UV stability of the coating are analyzed and discussed. Post interface adhesion and UV degradation morphology results were evaluated using SEM.

7.1 Introduction

One component polymeric (organic) coatings have long been used to protect substrates against versatile corrosive environments in academic and industrial fields [8]. There are two sides of protection, physically where the polymeric matrix acts as a barrier and chemically where an internal sacrificial electrode is formed, which give protection to the underlying substrate. Moreover, it has been proven that the incorporation of well-dispersed filler in the polymer matrix may effectively enhance the corrosion protection due to the increased tortuosity of diffusion pathway of corroding agents such as O_2 and H_2O molecules and destructive ions like Cl^-, H^+ and $SO2^-$ from the corrosive environment to the metallic substrate, in addition to having a high degree of polymer ordering, thermal stability, and enhanced mechanical properties compared with the

pristine polymers [90]. A filler (inorganic) could be for example, SiO_2, TiO_2, clay, graphene, glass flakes and carbon nanotubes.

As polymers could be of either electrically conducting or non-conducting nature, conducting polymers such as polyaniline, poly(n-methylaniline) and polyphenylene oxide are more widely used in comparison to their counterparts, for their applicability in more advanced and versatile fields. Lately, the preparation of such polymers as well as the evaluation of their corrosion protection effect attracts an extensive research activity, for instance, polyaniline [91], poly(n-ethylaniline) [92], as an example of the conducting polymer-filler composite, polyaniline/graphene [62], also, as an example of the non-conducting polymer-filler composite, polyetherimide/graphene [32].

Aniline oligomer-derivative electroactive polymers can also be utilized as anticorrosive coatings, by incorporating the redox catalytic (i.e., electroactivity) capability into the non-conducting polymers. For example, the preparation and electrochemical behavior of electroactive polyimide [93]–[97], electroactive polyamide [98]–[101], electroactive epoxy thermosets (EET) [101], super-hydrophobic electroactive epoxy (SEE) [102]. Also, some examples of aniline oligomer-derivative electroactive polymer-filler composite anticorrosive coatings are, electroactive epoxy/amino-SiO_2, electroactive polyimide/Clay, electroactive polyimide/SiO_2 and electroactive polyimide/TiO_2 [103]–[106]. There are academic literatures that covered the topics of epoxy/clay composites as a polymer/filler anticorrosive coating, and other work on electroactive epoxy (EE) as pristine polymer anticorrosive coating. Nevertheless, to the best of our knowledge, there has not been any effort done on preparing and characterizing electroactive epoxy/glass flakes (EE/GF) composite as an anticorrosive coating.

In this study, the preparation of EE/GF composite is presented, and the results of a series of electrochemical corrosion measurements in saline condition, UV degradation, and the adhesion to the metal substrate are analyzed. Tests are conducted on two EE/GF composite samples differing in the load of the glass flakes (10% GF, and 20% GF) and results are compared to a pristine epoxy coating.

7.2 Experimental

7.2.1 Material

Cold-Rolled Steel (CRS, McMASTER-CARR) substrates were polished, cleaned with ethanol and distilled water and dried with Kim-Tech paper before coating. Aniline (Sigma-Aldrich) was distilled prior to use. 1,4-phenylenediamine (Sigma Aldrich), trimethylolpropane tris[poly-(propylene glycol) amine terminated] ether (T-403, Sigma Aldrich), bisphenol A diglycidyl ether (BADGE, Sigma Aldrich), Glass flakes (GF, NSG) and N-Methyl-2-pyrrolidinone solvent (NMP, Sigma Aldrich) were used as received without further purification. All the reagents were reagent grade unless otherwise stated.

7.2.2 Composites preparation

A typical procedure was recently established by Wei et al. for the synthesis of the ACAT and accordingly, ACAT could be easily synthesized by oxidative coupling of 1,4-phenylenediamine and 2 equivalent aniline with ammonium persulfate as oxidant.

The electroactive epoxy resin was prepared by reacting Amino –Capped Aniline Trimer (ACAT) with T-403 and DGEBA in the presence of GF in suitable amount of NMP solvent at an epoxy equivalent weight of 0.42:0.43:1 (molar ratio of terminal amino with respect to epoxy groups is 1:1) for 30 min. under magnetically stirring at room temperature. The sample was then homogenized (125, Fisher Scientific) for 20 min. and spread on a cleaned CRS substrate. NMP solvent was extracted at 50 °C for 6 hrs. before thermally curing the coating at 120 °C for 2 hrs. and 140 °C for 0.5 hr. under vacuum. EE/GF preparation procedure is schematically presented in Figure 7.1, where 98 mg and 220 mg of GF were used to prepared 10 wt.% (EE/GF_{10}) and 20 wt.% (EE/GF_{20}) EE/GF composites protective coatings, respectively.

Figure 7.1: Scheme for the synthesis of electroactive epoxy/Glass Flake (EE/GF) composite coating.

7.2.3 Composites Characterization

The dispersion of the glass flakes in the electroactive epoxy matrix was investigated using transmission electron microscopy (TEM) (Philips CM-10 TEM) and scanning electron microscope (SEM) (Zeiss LEO 1550). SEM samples were placed on carbon tape attached to the SEM holder and samples were coated with gold via sputtering for 120 sec. Samples for the TEM study were prepared by scraping the EE/GF composite coatings with a sharp knife/blade then collected and dispersed in methanol for 5 min. The sample was then fished using TEM copper grid and allowed to dry under vacuum at room temperature. FTIR spectrometer (Tensor 27, Bruker) was used to acquire the FTIR spectra of pristine electroactive epoxy and EE/GF

composites and XRD diffraction patterns were recorded in the range of 2θ = 3° to 90° at 0.24° /min scan rate and 0.02° step size (MiniFlex 600, Rigaku).

7.2.4 Adhesion

The interface adhesion between the EE/GF composite coating and CRS metallic substrate was assessed according to the Standard Test Methods for Measuring Adhesion (ASTM-D3359). A standard blade (11-teeth with teeth spacing of 1 mm) was used to make lattice pattern cut in the film and a pressure-sensitive tape kit (Paul N. Gardner Company Inc.) was applied over cuts made. Post-adhesion tests results were captured using scanning electron microscope (SEM) (Zeiss LEO 1550).

7.2.5 Electrochemical measurements

Electrochemical measurements were conducted at room temperature in a double-jacketed 1 L corrosion cell covered with a drilled Teflon plate to allow electrodes immersion. A three electrode configuration was used to conduct the measurements, where a Silver/Silver Chloride (Ag/AgCl) electrode was used as the reference electrode (RE), two graphite rods as the auxiliary electrode (AE) and a 1 cm^2 circular piece of the sample as the working electrode (WE). The WE was washed with acetone and distilled water, dried and then installed in the sample holder before conducting the tests. The 3.5 wt.% NaCl solution was used as the electrolyte. EC-Lab software (Bio-Logic) and VSP-300 workstation (Uniscan instruments Ltd.) were used to conduct all electrochemical measurements, where each measurement was repeated three times in order to confirm the reproducibility of the collected raw data.

The potential of the WE was allowed to stabilize for 30 min. to 1 hr, before conducting electrochemical measurements. The electrochemical impedance spectroscopy (EIS) measurements were conducted at frequency range from 100 kHz to 100 mHz to generate Bode and Nyquist plots. Furthermore, an equivalent circuit was used to fit the raw impedance data and EC-Lab software was used to evaluate the different components of the equivalent circuits. At equilibrium, the potential of the working electrode was recorded as the open circuit potential (*OCP*) or the corrosion potential (E_{corr}). The potentiodynamic measurements

were conducted by scanning the potential of the WE from -500 mV to 500 mV at a rate of 20 mV/min to produce the Tafel plots. Tafel plots were used to extract the corrosion current (I_{corr}) using EC-Lab software by extrapolating the linear portion of the anodic and the cathodic curves.

7.2.6 UV stability

The Resistance of the electroactive epoxy and EE/GF coatings to UV degradation was assessed using an accelerated weathering tester (QUV, Q-LAB) according to the Standard Practice for Fluorescent UV-Condensation Exposures of Paint and Related Coatings (ASTM-D4587). Testing specimens were continuously exposed to repeated UV cycle at 60 ± 2.5 °C for 8 hrs, followed by a condensation cycle at 50 ± 2.5 °C for 4 hrs. for 30 days before evaluating surface morphology using SEM.

7.2.7 Impact resistance

Impact resistance was performed to assess the resistance of the prepared coatings to rapid deformation by a falling weight. The test was conducted using a universal impact tester (Paul N. Gardner Company Inc.) with combined 0.5-inch ball and 2-lb weight indenter according to the Standard Test Method for Resistance of Organic Coatings to the Effects of Rapid Deformation (ASTM-D2794). The combined weight and indenter were raised 1 inch in the testing tube and released to drop on the coated substrate and the falling weight test was repeated with 1 inch increments in height until a crack in the coating was observed. The height at which the coating cracks was recorded, and the test was repeated at three configurations: slightly above, slightly below and at the recorded height, five times each. The elevation at which the coating cracks in all five trials was reported as the "impact resistance limit" of the coating to rapid deformation.

7.3 Results

7.3.1 Characterization

Dispersion of GF in the EE was examined using TEM as shown in Figure 7.2. TEM images clearly illustrate the variation in the degree of dispersion with the load of GF. Images of thick stacks of GF were

captured in the EE/GF_{20} composite, while thinner and more dispersed GF where observed in the EE/GF_{10} composite. Figure 7.3 depicts cross-sectional SEM images of EE/GF composites, where wide dispersion of GF were observed in EE/GF_{10} and EE/GF_{20}.

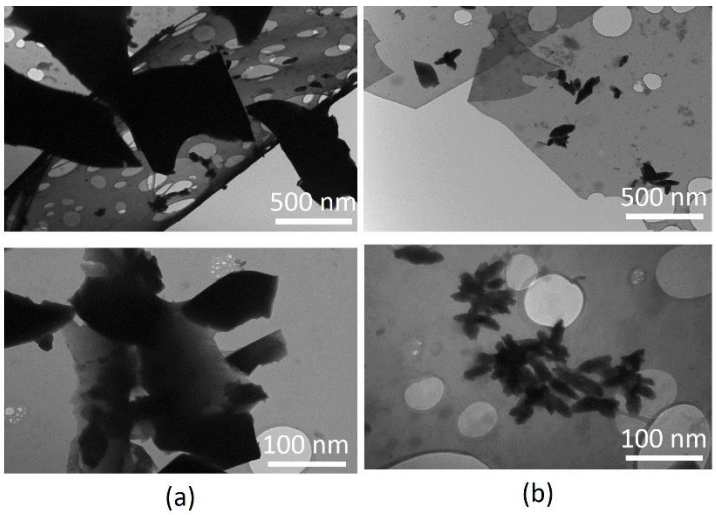

Figure 7.2: TEM images of dispersion of GF in (a) EE/GF_{20} and (b) EE/GF_{10} composites.

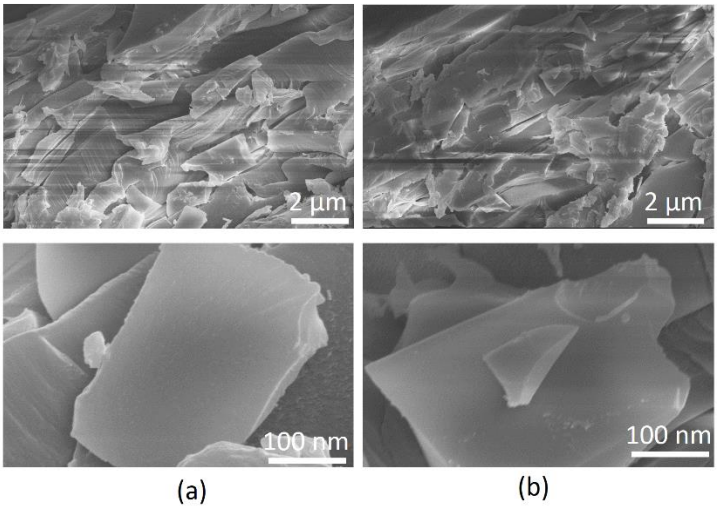

Figure 7.3: SEM images of dispersion of GF in (a) EE/GF_{20} and (b) EE/GF_{10} composites.

FTIR and X-ray diffraction (XRD) techniques were utilized to characterize EE and EE/GF composites. FTIR spectra confirm the completeness of the epoxide-ring opening curing process, where characteristic peaks such as the peaks at 3380 cm-1 (-OH stretching) were observed. Furthermore, no clear dissimilar

peaks were observed in the spectra of EE and EE/GF composites, which terminate the probability of chemical linkage between GF and EE function groups. XRD patterns display broadly peak observed at 2θ value between 10 and 30° and this broadly amorphous peak is ascribed to the homogeneously amorphous of EE. Furthermore, the intensity of XRD patterns for EE and EE/GF composites indicates that incorporation of GF in the polymer matrix retains the degree of crystallinity (please refer to supporting information for FTIR spectra and XRD patterns).

7.3.2 Adhesion

The corrosion process can be excelled by the accumulation of the various corrosive agents at the interface between the coating and the metal substrate. Therefore, a substantial adhesion between the coating and the substrate is always a desire. Here, the interface adhesion is evaluated according to the ASTM D3359 standard using the tape adhesion kit. Figure 7.4 depicts the post adhesion test results on EE and EE/GF coatings. The figure represents the noble interface adhesion between the prepared coatings and the substrates, where no peelings from the protective coatings were observed. The coatings received 5B (0% peeling) rating according to the ASTM standard. This confirms the robust interface adhesion of the protective EE and EE/GF coatings.

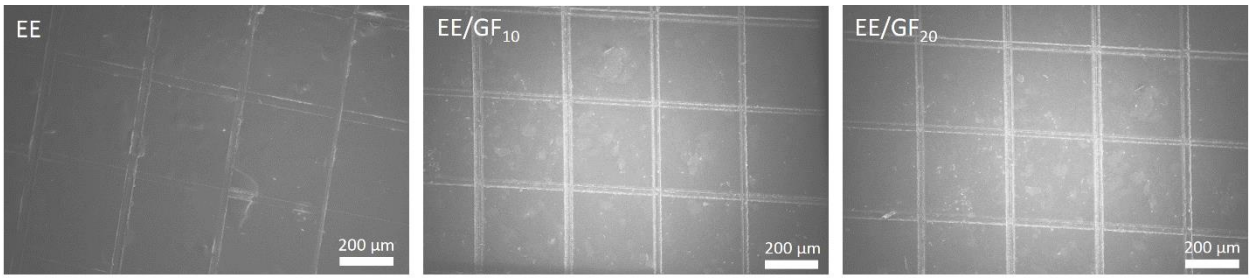

Figure 7.4: SEM images of post-adhesion tests of EE and EE/GF coated CRS substrates.

7.3.3 Impedance and cyclic voltammetry

Impedance is a complex resistance that may results from passing an alternative current through a circuit. In this study, the impedance behaviors of the bare and coated CRS substrates were investigated. Moreover,

equivalent circuits, which are depicted in Figure 7.5, were used to model the impedance behavior of the bare and coated CRS substrates. In these circuits, *CPE* is a constant phase elements and *W* is the Warburg impedance, while R_s, R_p and R_{ch} represent the electrolyte, polarization and charge transfer resistances, respectively.

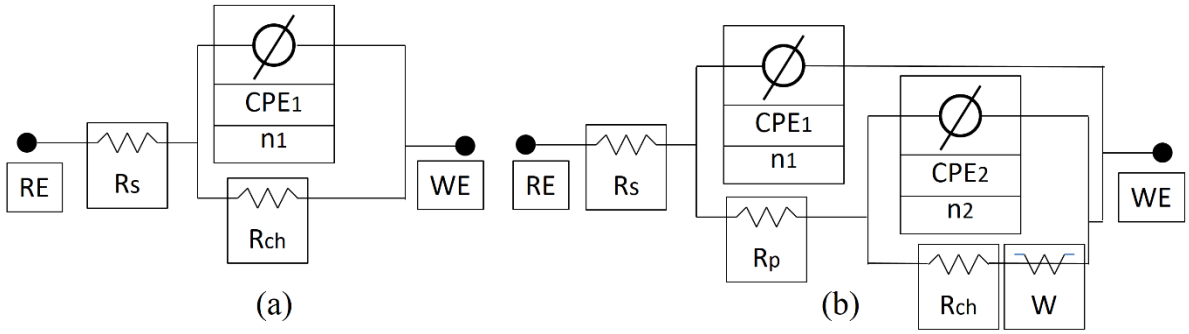

Figure 7.5: Equivalent circuits utilized to model impedance behavior of (a) Bare and EE coated CRS (b) EE/GF coated CRS substrates.

Figure 7.6 depicts the Nyquist plots for bare and coated substrates, where the plots illustrate that the incorporation of GF in the polymeric matrix influenced the single step impedance behavior of bare and EE coated substrates and resulted in the appearance of the Warburg behavior. The fitting data obtained from the equivalent circuits fit well to the raw impedance data and these fittings were used to evaluate the various elements in the equivalent circuits as reported in Table 7.1. The variations in the magnitudes of these elements may be used to evaluate the corrosion mitigation properties of EE and EE/GF protective coatings. Indeed, an increase in the charge transfer resistance reflects an enhancement in corrosion inhibition. The charge transfer resistance obtained from the fittings are 432.5, 4.09×10^5, 2.71×10^6 and 4.08×10^6 $\Omega.cm^2$ for bare, EE, EE/GF_{10} and EE/GF_{20} coated CRS, respectively.

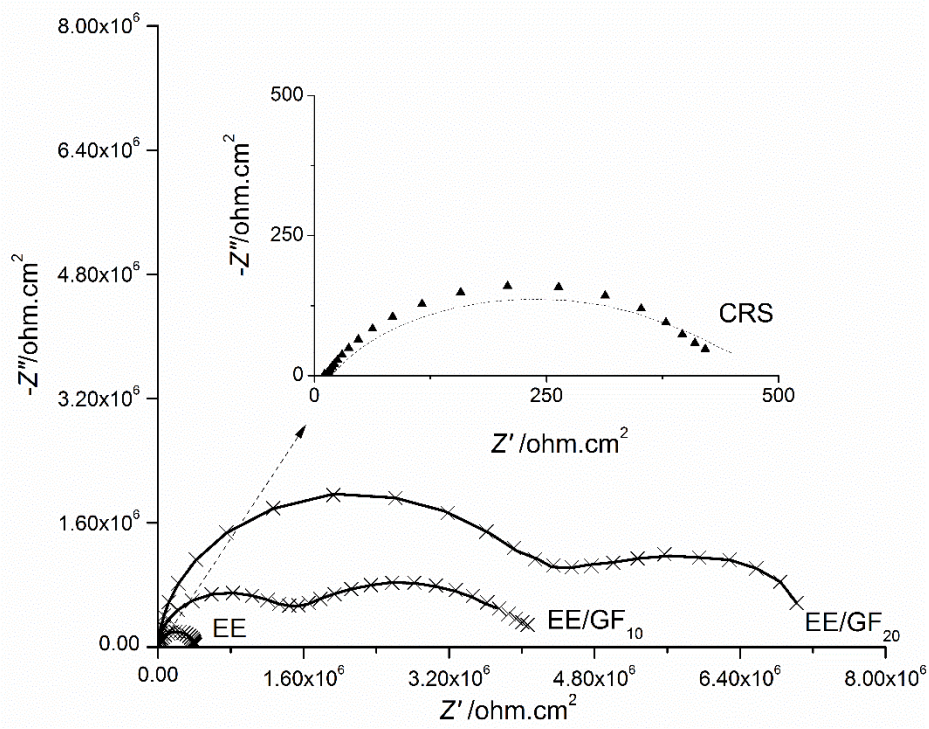

Figure 7.6: Nyquist plots for Bare, EE and EE/GF coated CRS substrates.

Table 7.1: Electrochemical corrosion parameters obtained from the equivalent circuit for EIS measurements for bare, EE, EE/GF_{10} and EE/GF_{20} coated CRS substrates in a 3.5 wt.% NaCl solution.

Sample	R_S	CPE_1	n_1	R_P	CPE_2	n_2	R_{ch}	W
	$\Omega.cm^2$	F		$\Omega.cm^2$	F		$\Omega.cm^2$	$\Omega^{-1}S^{-0.5}cm^{-2}$
CRS	13.8	$4.2x10^{-4}$	0.79	-	-	-	432.5	-
EE	13.2	$1.5x10^{-10}$	0.98	-	-	-	$4.09x10^5$	-
EE/GF_{10}	13.2	$3.06x10^{-10}$	0.96	$1.4x10^6$	$4.4x10^{-8}$	0.66	$2.71x10^6$	$7.51x10^4$
EE/GF_{20}	13.1	$2.9x10^{-10}$	0.96	$4.02x10^6$	$6.7x10^{-8}$	0.61	$4.08x10^6$	$8.09x10^5$

Bode plots may also be utilized to illustrate the corrosion protection ability of coatings. Figure 7.7 depicts the Bode plots, which represent changes in impedance with frequency for bare and coated substrates. The Z_{real} values recorded at the lowest recorded frequency may represent the corrosion resistance properties. From Figure 7.7.a, log Z_{real} for bare, EE, EE/GF_{10} and EE/GF_{20} coated substrates at the lowest frequency are 2.6, 5.7, 6.6 and 6.9 ohm.cm^2, respectively.

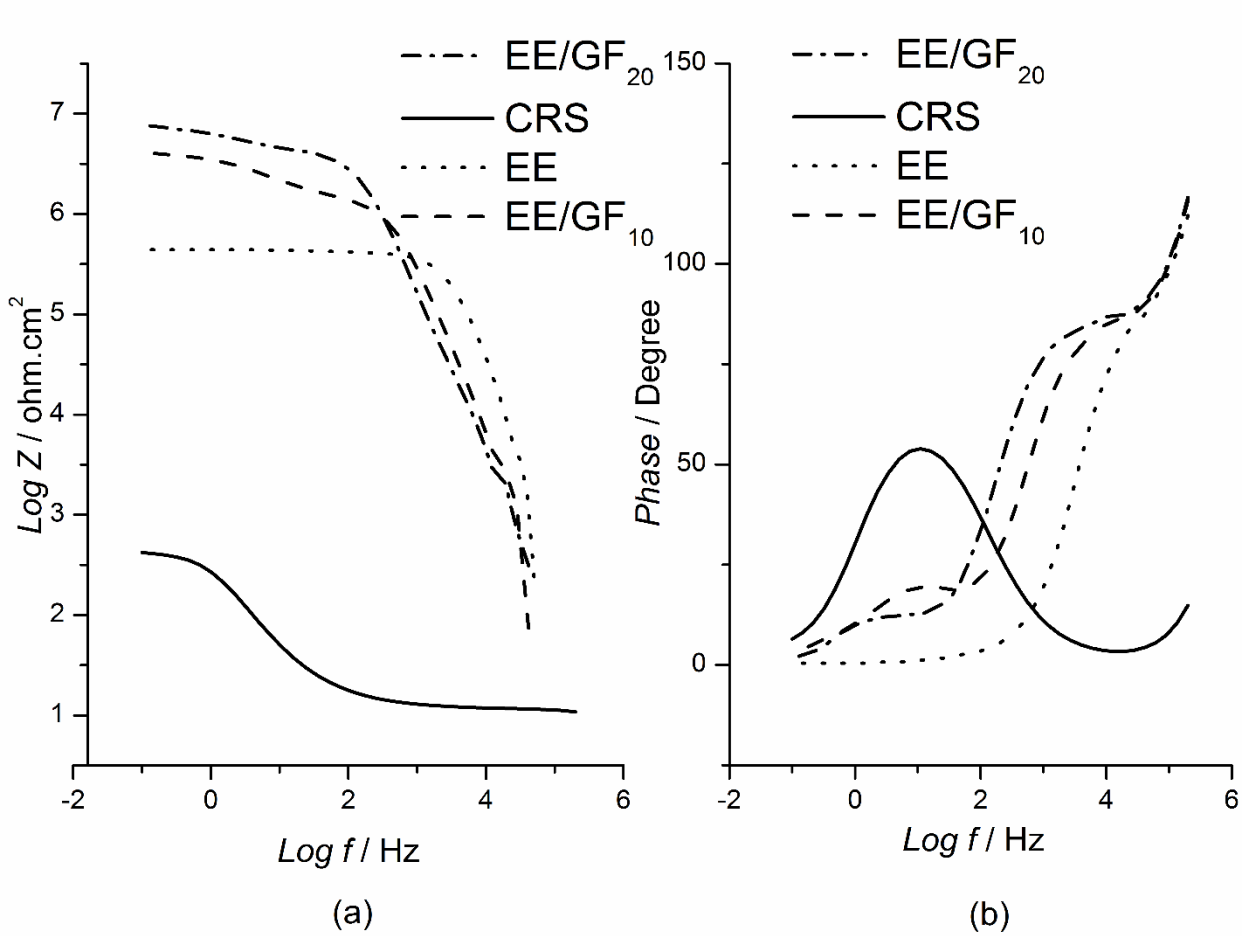

Figure 7.7: Bode and phase plots for (a) bare, (b) EE, (c) EE/GF_{10} and (d) EE/GF_{20} coated CRS.

Tafel polarization was also utilized to evaluate the electrochemical behavior of the bare and coated CRS substrate. Figure 7.8 depicts the Tafel plots for bare, EE, EE/GF_{10} and EE/GF_{20} coted substrates. These plots were used to extract valuable corrosion parameters such as corrosion potential (E_{corr}) and corrosion current (I_{corr}). The corrosion current was recorded as the intersection between the extrapolation of the linear

portions of the anodic and the cathodic curves. All extracted corrosion parameters are reported in Table 7.2, where a positive shift was observed in the corrosion potential after coating the CRS substrate with EE and a further shift was observed after incorporating the GF in the EE matrix. Furthermore, coating the CRS substrate with EE and the incorporation of GF attenuated the corrosion currents and consequently the corrosion rates, which were calculated using Eq. (7.1). Furthermore, the polarization resistance (R_p) was calculated using Eq. (7.2) and incorporating and increasing the load of GF have significantly enhanced R_p as reported in Table 7.2.

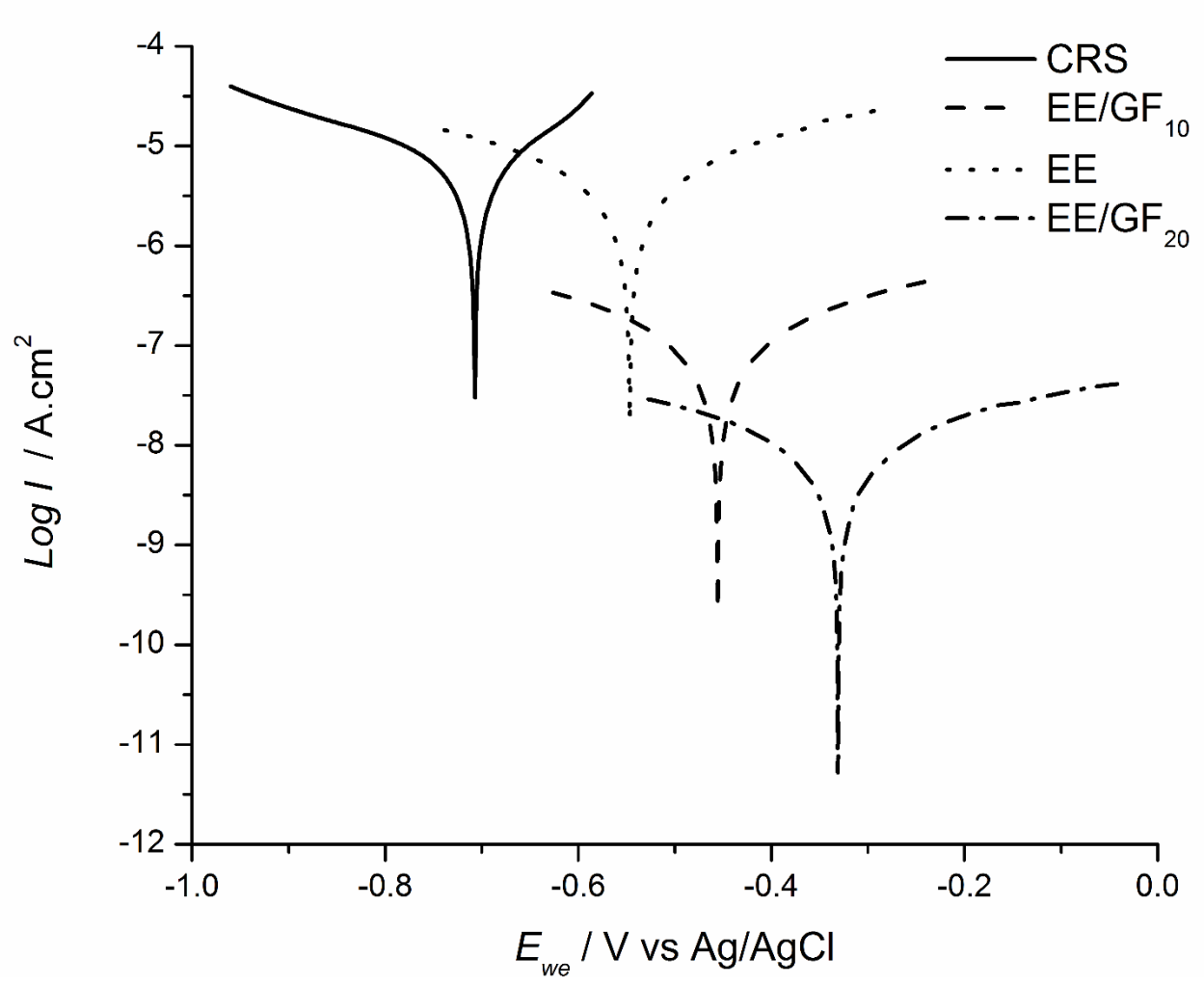

Figure 7.8: Tafel plots for bare, EE, EE/GF$_{10}$ and EE/GF$_{20}$ coated CRS.

Table 7.2: Electrochemical corrosion parameters obtained from potentiodynamic measurements for bare, EE, EE/GF_{10} and EE/GF_{20} coated CRS substrates in a 3.5 wt.% NaCl solution.

Sample	E_{corr} mV vs Ag/AgCl	I_{corr} μA.cm^{-2}	b_a	b_c	R_P Ω.cm^2	R_{corr} *MPY*	P_{EF} %
CRS	-706	2.92	68.6	84.8	5.6	1.36	-
EE	-545.8	1.07	83.7	91.0	17.7	0.5	63.4
EE/GF_{10}	-455.9	0.1	129.9	126.4	278.1	0.046	96.6
EE/GF_{20}	-329.5	0.015	206.6	210.1	3015.4	0.007	99.6

$$R_{corr}=(0.13\times I_{corr}\times EW)/(A\times\rho) \quad (7.1)$$

Where *EW* is the equivalent weight, ρ is the density and *A* is the surface area.

$$R_p=(b_a\times b_c)/(2.303\times(b_a+b_c)\times I_{corr}) \quad (7.2)$$

The reported results indicate that coating CRS with EE may slow the deterioration rate of CRS and this rate can be further attenuated by the incorporation of GF. The protection efficiency (P_{EF}) is another parameter that can be calculated using Eq. (7.3) to reflect the degree of corrosion mitigation a protective coating may deliver. The protection efficiencies for EE and EE/GF coatings were computed and reported in Table 7.2, where the P_{EF} magnitudes confirm that an enhancement in corrosion mitigation can be achieved by coating the substrate with EE and this enhancement can be further excelled by incorporating GF in the polymeric matrix.

$$P_{EF}\,[\%] = [1-I_{corr}/I^{\circ}_{corr}] \times 100 \quad (7.3)$$

Where, I^{o}_{corr} represents the corrosion current of the bare CRS substrate.

Reported results from both Tafel polarization and impedance spectroscopy measurements revealed that EE might enhance the corrosion mitigation on CRS substrate. Furthermore, incorporation of GF may further excel this corrosion inhibition property.

7.3.4 UV stability

Resistance of a protective coating to UV degradation is a crucial property that need to be assessed in addition to adhesion and corrosion mitigation in order to evaluate the durability of the coating. EE and EE/GF coatings were exposed to continuously alternating UV, condensation cycles for 30 days before the surface morphology of the coatings were observed, and evaluated using SEM. Figure 7.9 depicts post UV degradation test results for EE and EE/GF coatings. From the figure, sever damages were observed on the EE coating surface and the damages were manifested in micro-cracks. Surface cracking was also captured on EE/GF_{10} coating surface; however, it can be observed that the incorporation of GF attenuated the severity of cracking. Results illustrated in Figure 7.9 illustrate the capacity of GF in improving the durability of the EE coating, where no surface cracking were observed as the load of GF increases to 20 wt.%.

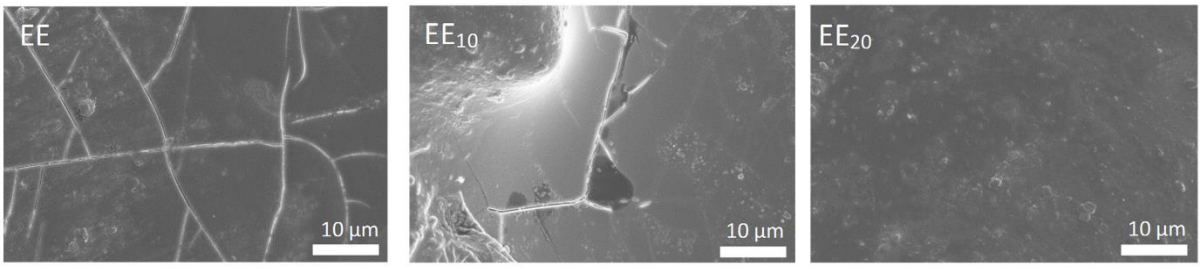

Figure 7.9: SEM images of post UV degradation test on EE, EE/GF_{10} and EE/GF_{20} coatings.

7.3.5 Impact resistance

Mechanical properties such as impact resistance is an important characterization of protective coatings in addition to interface adhesion and corrosion protection. Resistance to sudden deformation test was conducted on the prepared EE and EE/GF coatings in order to evaluate the impact of GF on the impact resistance property. Figure 7.10 depicts the impact resistance results for EE and EE/GF coatings and reports the elevations at which the coating deforms for five times. The reported results illustrate that the

incorporation of GF enhances the impact resistance property of EE and the degree of enhancement is proportional to the load of GF.

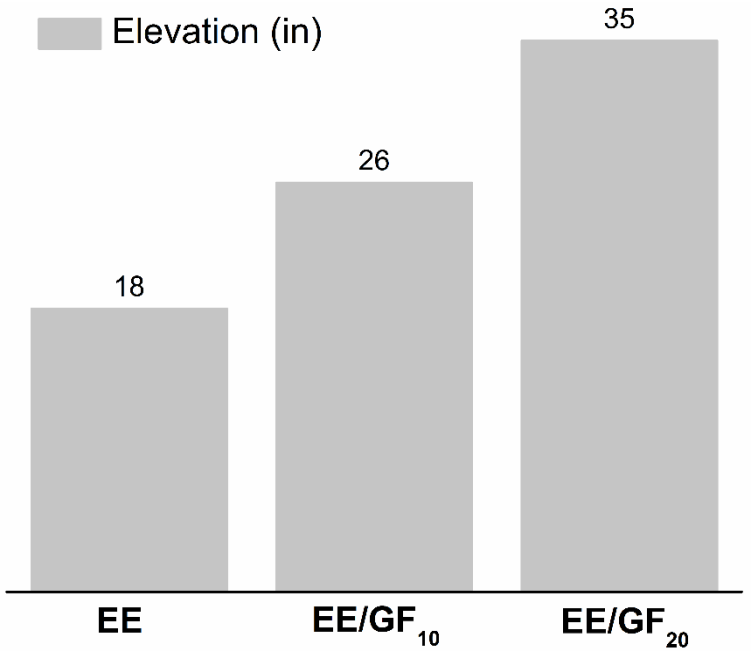

Figure 7.10: Elevation of falling weight at which EE, EE/GF_{10} and EE/GF_{20} coatings deform.

7.4 Conclusion

In this study, Electroactive Epoxy/ Glass Flake composite was synthesized using in situ polymerization and thermal curing and the prepared coatings were characterized using FTIR and XRD techniques. The dispersion of the filler was captured using SEM and TEM. The corrosion protection properties of the coatings were evaluated using Tafel polarization and EIS. Moreover, the interface adhesion between the metal substrate and the EE and EE/GF coating were evaluated as per the ASTM standard D3359. Furthermore, the durability of the prepared protective coatings were evaluated for UV degradation and impact resistances. It was reported that the incorporation of GF in the polymeric matrix might excel the corrosion protection in addition to UV stability and impact resistance properties.

Chapter 8

Role of surface functionalization on corrosion resistance and thermal stability of Epoxy/Glass Flake coating on Cold Rolled Steel

Abstract

Epoxy/Functional Glass flake (E/FGF) composites with different loadings of FGF were synthesized through in situ polymerization and examined as protective coatings on Cold Rolled Steel (CRS) substrates in a Chloride rich environment. The E/FGF composites were analyzed with X-ray diffraction (XRD) and Fourier Transform Infrared (FTIR). The influences of the functionalization of Glass flake (GF) on the dispersion of the GF/FGF in the resin was examined using Transmission Electron Microscopy (TEM), while Scanning Electron Microscopy (SEM) technique was utilized to evaluate the interface adhesion . The corrosion resistance properties of the coatings were examined using various electrochemical techniques such as Electrochemical Impedance Spectroscopy (EIS) and Cyclic Voltammetry (CV) measurements and the long term protection efficiencies of the coatings were confirmed by a 90 days gravimetric study in 3.5 wt.% NaCl solution. In addition to corrosion protection properties, thermal stabilities of the coatings were assessed using Thermogravimetric analysis (TGA) and Differential scanning calorimetry (DSC) techniques. The study demonstrates the surface modification of GF by attaching a functional Silane coupling agent with grafted amino group plays a critical role in the corrosion protection and thermal stability of the E/FGF composites coatings as revealed by substantial enhancements in corrosion resistance as well as thermal stability properties of E/GF composites can be achieved by surface functionalization of GF.

8.1 Introduction

Corrosion is a natural phenomenon that takes place in various environments causing metal components to fail at different rates based on the metal composition and environmental factors such as temperature, humidity and salinity. The lack of mitigating of such electrochemical interactions between the metal and the surroundings might raise serious threats to both economy and industry. Therefore, a growing number of research studies are dedicated to investigate the corrosion process in various mediums and to examine possible mitigation options. Indeed, total elimination of the corrosion process may not be possible especially in particular environments such as a Chloride rich mediums. Therefore, the wide utilization to metals and in particular cold rolled steel in various field including construction, pipeline and marine equipment, motivates researchers to investigate various corrosion protection techniques such as Anodic or Cathodic protection, the use of corrosion inhibitors and protective coatings [2], [4], [5] in order to extend the life span of the metal in different environments. In particular, the easiness of application, low cost and the remarkable corrosion protection efficiency of protective coatings initiates further investigation and utilization of the coating techniques for corrosion protection purposes. A growing number of research have been devoted to investigate and to further develop the coating techniques including the utilization of nanocomposites, hydrophobic and hybrid materials [6], [8], [10], [12].

There are different forms of corrosion; however, in a Chloride rich environment a metal substrate will be more susceptible to pitting corrosion. In pitting corrosion, localize active areas of the metals take part in a galvanic corrosion process and release metal ions to the surroundings resulting in localized inclusions or breakdown that might be difficult to detect. In a Chloride rich environment, the rate of the localized dissolution and penetration of the metal might be accelerated due to the presence of corrosion agents such as Oxygen, moisture and Chloride. In such form of corrosion, the level of penetration may not be detected until a severe damage has occurred and possibly leading to catastrophic failure.

Therefore, pitting corrosion can be considered insidious and unlike other forms of corrosion such as uniform corrosion, pitting corrosion is very difficult not only to detect or predict, but also to evaluate and mitigate.

Polymer composites are perfect examples of corrosion protection coatings that have already been utilized in various fields in order to extend the life span of metals. However, the lack of some essential property such as interface adhesion with metal substrates foils the use of some polymer composites based coatings for corrosion protection purposes [57], [58]. Epoxy is an example of polymers that have been widely utilized and investigated as corrosion protective coating on various metals substrates. Moreover, studies have shown that the remarkable corrosion mitigation property of epoxy can be further enhanced by the incorporation of a filler in the polymeric matrix [32], [34], [64], [79]. In particular, the advanced barrier properties of Glass flakes encourage researchers to investigate and develop corrosion resistance coatings with advances protection properties based on composites with glass flakes [45]–[48], [107]. In addition to corrosion protection, some studies have focused on the utilization of Glass flake to enhance various properties such as thermal and viscoelastic properties [44]. However, the prospect of further enhancing the corrosion mitigation performance of Glass flake composites by surface treatment and functionalization of Glass flake, to the better of our knowledge, has not been explored in the literature, which inspires the current study.

In this study, composites of epoxy resin with Glass flakes as filler were developed and evaluated as corrosion protective coating for cold rolled steel in a Chloride rich environment. The corrosion protection property of the prepared coating is examined in 3.5 wt.% NaCl solution by conducting electrochemical measurements as well as gravimetric analysis. Furthermore, the interface adhesion between the prepared coating and the Cold rolled steel metal substrate is evaluated according to ASTM standard. Besides corrosion resistance property, the study investigates the influences of the

incorporation of Glass flake in the thermal stability of the prepared protective coating. In addition to the synthesis and the evaluation of Epoxy/Glass flake composites as corrosion protective coatings, facile surface modification procedures have been developed to functionalize the surface of Glass flake and the role of the attached functional groups on the corrosion protection efficiency and the thermal stability properties of the Epoxy/Glass flake composites were analyzed.

8.2 Experimental

8.2.1 Materials

25 μm-thick Cold Rolled Steel (CRS) sheet (McMaster-Carr) was used as the substrate. It were polished, washed with acetone and DDI water and cleaned with KIMTECH wipes before coating. Bisphenol A diglycidyl ether (BADGE, sigma Aldrich) and Poly(propylene glycol) bis(2-aminopropyl ether) (B230 ,Sigma Aldrich) were the Epoxy resin and hardener. (3-Aminopropyl) triethoxysilane (3AS, sigma Aldrich) was utilized to modify the surface functionality of GF, GF were supplied by NSG Group as micro-pigment with average thickness of 1-3 μm.

8.2.2 Functionalization of GF

To prepare the FGF, the desired amount of GF is added to 10 ml of 1M Ammonium hydroxide solution. The solution was stirred in ice bath at 5 ^{o}C for 30 min then 3 ml of 3AS was added slowly under continued stirring for another 30 min at 5° C followed by 6 hrs stirring at room temperature. FGF were collected by vacuum filtration and the collected particles were washed with 40 ml ethanol to remove excess 3AS before the particles were finally washed with double distilled water until neutral pH was observed.

8.2.3 Composites preparation

E/GF and E/FGF composites were prepared by in situ polymerization approach by dispersing the desired amount of the filler in 1.5 g BADGE under stirring for 1 hr, followed by sonication (add bath brand and watt) for an additional hour. 0.5 g of B230 was then added to the Epoxy/filler mixture and the mixture was stirred for 30 min and homogenized (125, Fisher Scientific) for another 30 min at room temperature. Composites were prepared with various filler loading using 225 mg, 500 mg and 860 mg of FGF to prepare about 2 g of E/FGF_{10}, E/FGF_{20} and E/FGF_{30}, respectively. For comparison purpose, similar synthesis procedures and the same loadings of GF were utilized to prepared E/GF_{10}, E/GF_{20} and E/GF_{30} composites.

The composites were spin coated (SC 100, Smart Coater) on clean CRS substrates at 500 RPM for 2 min and cured at 50 ^{o}C for 4 hr to prepare CRS coated substrates with 30 ±2 μm thick coatings. The preparation procedures are schematically depicted in Figure 8.1.

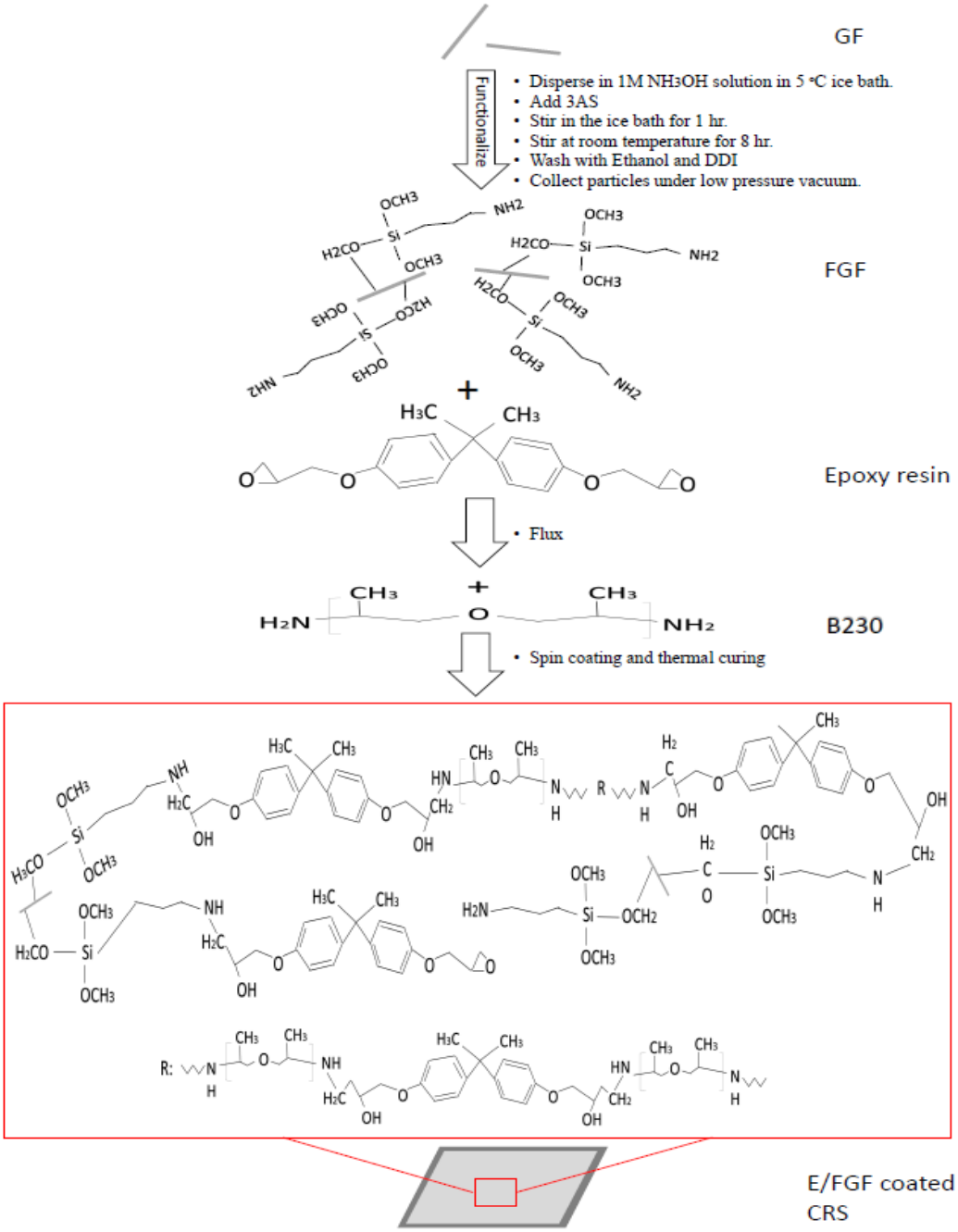

Figure 8.1: Schematic description of the preparation of E/GF and E/FGF composites using in situ polymerization.

8.3 Characterization

FTIR (Tensor 27, Bruker) was used to record the IR spectra Epoxy, E/GF and E/FGF composites in the range of 400 to 4000. XRD (Rigaku) was used to record diffraction patterns of Epoxy, E/GF and E/FGF composites in the range of $2\theta = 3°$ to 90° at 0.24° /min scan rate and 0.02° step size.

The filler dispersion in the polymeric matrix was examined using TEM (Philips CM-10 TEM). To prepare the TEM samples, the composites coating were scrapped with a sharp knife and the collected samples were dispersed in methanol and sonicated for 5 min. the samples were fished on TEM copper grids and allowed to dry over night at room temperature.

Adhesion of the composites to CRS substrates were examined and evaluated according to ASTM-D3359 standard using Adhesion tape kit (PA-2000, Paul N. Gardner Company Inc.) with 11 teeth and 1 mm teeth spacing blade and the post adhesion surface morphology were captured using SEM (Zeiss LEO 1550). Samples for SEM imaging were attached to SEM holder using carbon tape and gold coated via sputtering for 120 sec. Further corrosion testing via weight loss and electrochemical measurements as well thermal stability were only conducted on composites coatings that display novel interface adhesion with the metal substrates.

Gravimetric analysis were conducted in order to confirm the long term protection performances of the prepared coatings. The weight loss measurements were carried out in a 500 ml of 3.5 wt.% NaCl solution at $25^{o}C \pm 2$. Coated and uncoated CRS substrates were cleaned with double distilled water, dried with KIMTECH paper, weighted and placed in a Teflon holder with 1 cm^2 exposed area before the samples were immersed separately in 3.5 wt.% NaCl solutions for 90 days. After exposing the coated and uncoated samples for the Chloride rich environment for 90 days, samples were removed from the Teflon holders, washed with double distilled water and corrosion products were stripped using

a fine brush. Finally, the samples were immersed in double distilled water sonication bath for 10 min to remove any corrosion residues before the samples were dried and weighted. Gravimetric analysis were carried out in triplicate and the mean weight loss in reported in addition to the standard deviation.

Electrochemical properties of the prepared coated/uncoated substrates were evaluated using a temperature controlled 1 L corrosion cell at 25 ^{o}C, where 3.5 wt% NaCl was used as the electrolyte, graphite rods as the counter electrodes and Silver/Silver Chloride (Ag/AgCl) as the reference electrode. Testing sample, which will be referred to as the working electrode was washed with acetone and double distilled water and placed in a Teflon sample holder with 1 cm^2 exposed surface area. Electrochemical measurements were conducted using VSP-300 workstation (Uniscan instruments Ltd.) and EC-Lab software (Bio-Logic). The open circuit potential was allowed to stabilize for 30 min before conduction electrochemical measurements. Impedance study was performed at frequency range from 200 kHz to 100 mHz and the measurements were repeated three times in order to examine the repeatability of the recorded impedance data. Furthermore, an equivalent circuit with various components was utilized to fit the raw impedance data and the values of the various components were used to evaluate the impedance behavior of the testing samples. Following the non-destructive impedance test, CV measurements were carried out by scanning the potential of the testing samples from -500 mV to 500 mV around the open circuit potential at 20 mV/min.

Thermal stabilities of the prepared composites were evaluated by thermal gravimetric analysis (TGA) (TA instruments, Q500), where the thermal degradation of the prepared composites was observed over temperature range 30-800 ^{o}C at 10 ^{o}C/min heating rate. In addition, the shift in glass transition temperature (T_g) of the prepared composites with the load and surface modification of GF was examined with Differential Scanning Calorimetry (DSC) (TA instruments, Q2000) over temperature range from 30-100 ^{o}C at 10 ^{o}C/min.

8.4 Results and Discussion

8.4.1 Characterization of GF and FGF

The prepared functionalized filler and composites were characterized using FTIR and XRD. The FTIR spectra and the XRD diffraction patterns of GF and FGF are depicted in Figures 8.2 and 8.3. FTIR spectra of GF and FGF depicted in Figure 8.2 display typical absorption bands of Silica [20], which is the main component of composition of GF. These absorption bands include peaks at 452 and 1048 cm^{-1} (Si-O), peak at 794 cm^{-1} (Si-O-Si) and the moisture (H_2O) peak at 1430 cm^{-1}. After functionalization of GF with the silane coupling agents, new absorption bands were observed in the FTIR spectra of FGF as depicted in Figure 8.2. For instance, the appearance of the absorption peak at 1457 cm^{-1} corresponds to NH_2 group attached to the 3AS coupling agent [108]. In addition, the appearance of broad peak at 1100-1126 cm^{-1} corresponds to Si-O-C, which bridges the grafted NH_2 functional group to the GF [108]. Furthermore, the broadening of the absorption peaks at 1100-1126 cm^{-1} can be attributed to various types of molecular vibrations of the Si-O-C (Rocking; Scissoring; Wagging; Twisting).

The XRD patterns of GF and FGF are presented in Figure 8.3, where typical XRD patterns of Silica based materials [109] such as GF were observed, where a broad diffraction peaks around 2θ values from 15-40 were detected for both GF and FGF. The reported XRD patterns and in particular the similarity in the amplitude of the diffraction peaks for both GF and FGF illustrates that the surface treatment of GF by attaching the Saline coupling agent 3AS had no influences on the structure of GF.

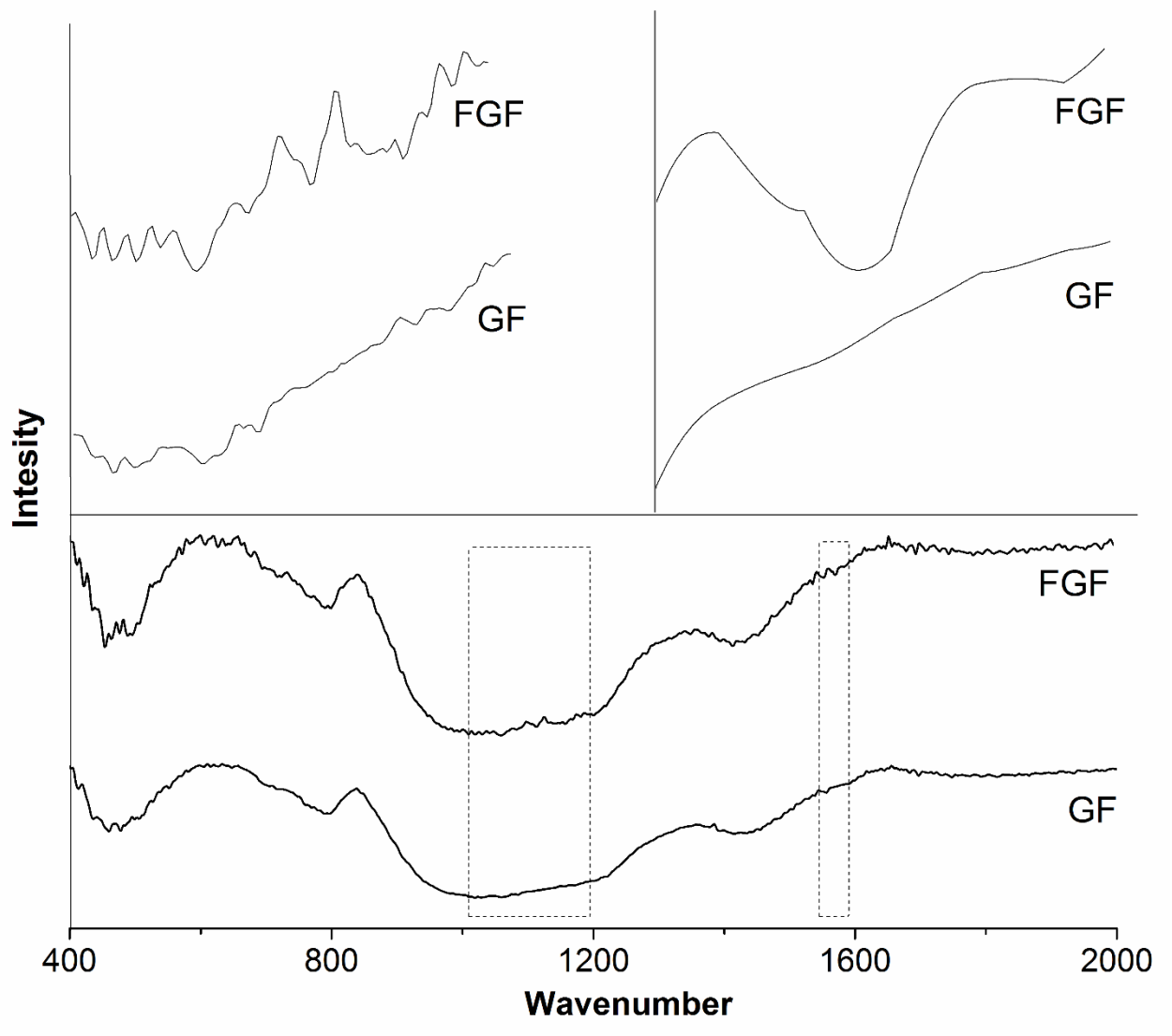

Figure 8.2: FTIR spectra of GF and FGF.

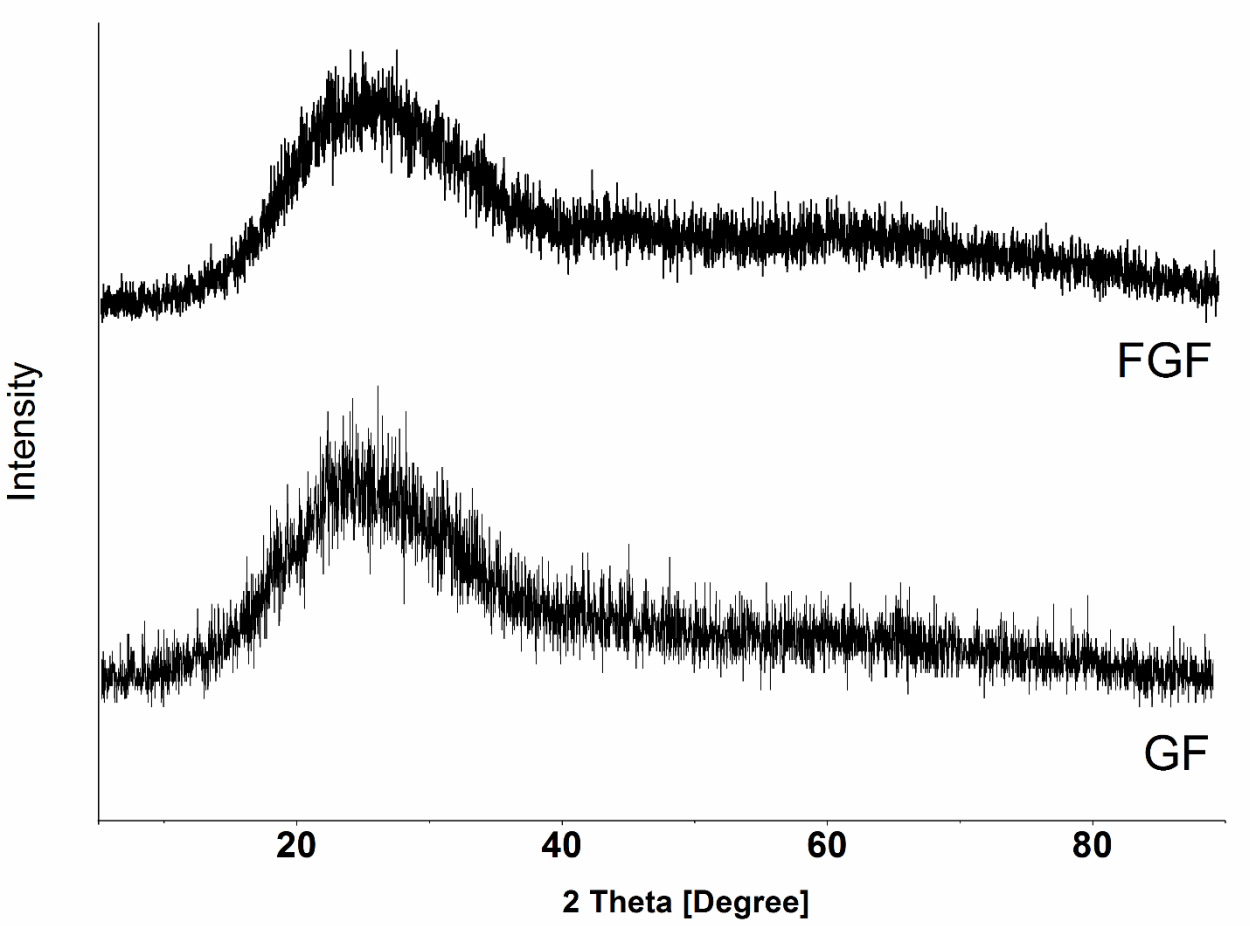

Figure 8.3: XRD patterns of GF and FGF.

8.4.2 Composites and coatings Characterization

The FTIR spectra of epoxy, E/GF and E/FGF composites are shown in Figure 8.4, where various characteristic peaks were identified such as peaks at 1508 cm^{-1} and 1609 cm^{-1} (C–C skeletal stretching), 915 cm^{-1} (epoxide ring) and the appearance of the (-OH stretching) peak at 3380 cm^{-1}, which confirms the thorough curing of epoxy. In addition, no clear dissimilar absorption peaks were identified between epoxy, E/GF and E/FGF composites.

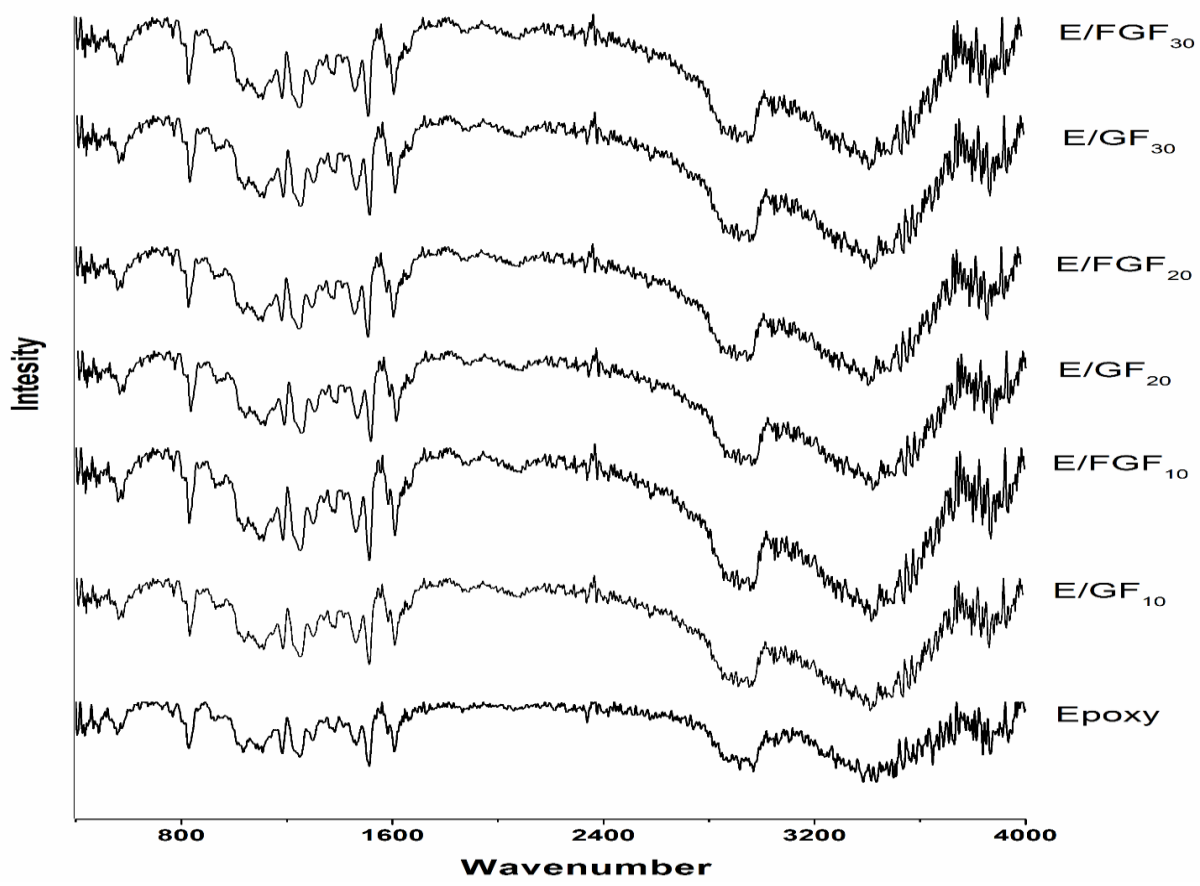

Figure 8.4: FTIR spectra of epoxy, E/GF and E/FGF composites.

The XRD diffraction patterns of epoxy, E/GF and E/FGF are presented in Figure 8.5, where broad amorphous peak appears around 2θ of 10 to 30° for all the samples. This is ascribed to the homogeneously amorphous morphology of epoxy. Furthermore, the XRD patterns shown in Figure 8.5 demonstrate that the degree of crystallinity of epoxy was not altered by the incorporation of GF/FGF.

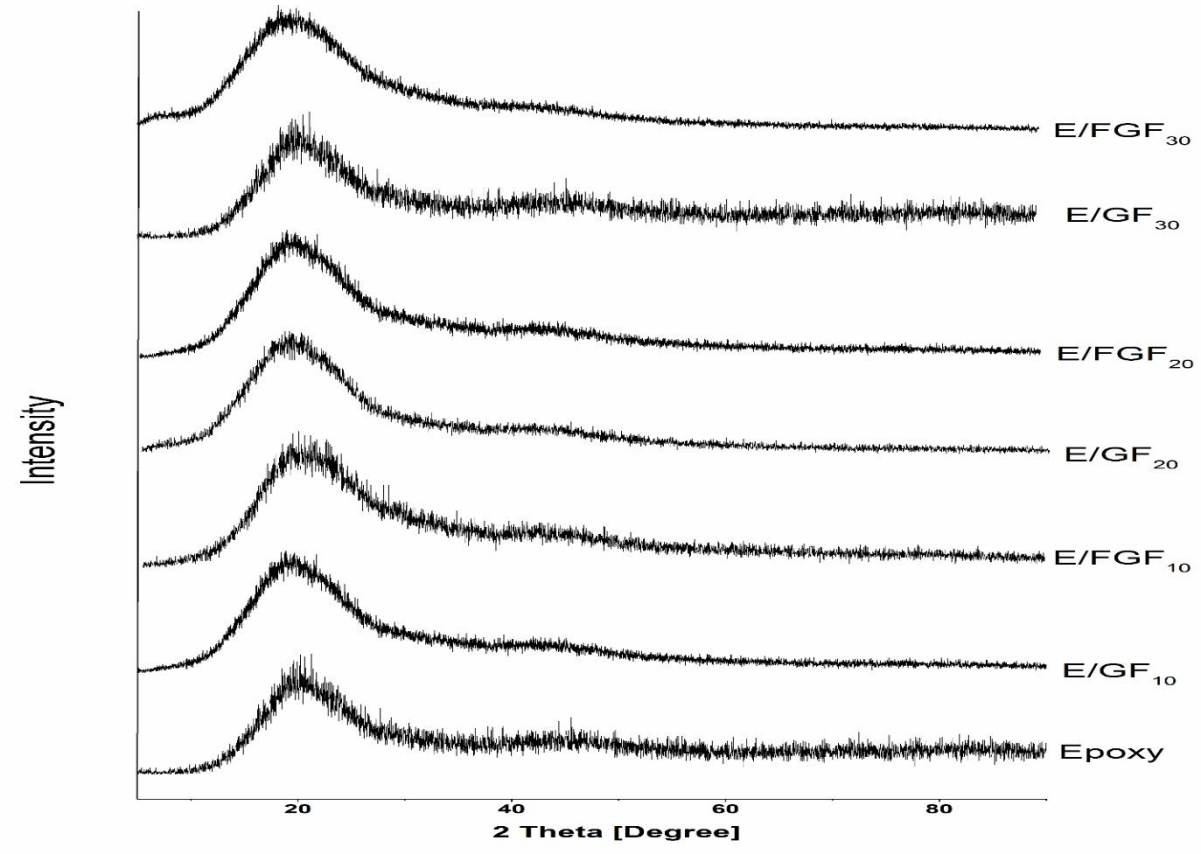

Figure 8.5: XRD patterns of epoxy, E/GF and E/FGF composites.

8.4.3 Adhesion Test

The interface adhesion is a crucial property for protective coatings and therefore must be well examined before progressing with electrochemical evaluations. Indeed, defects in interface adhesion disqualify the coating from being utilized for protection purposes. The interface adhesion between the prepared protective E, E/GF and E/FGF composites coatings were assessed according to ASTM-D3359, however; post adhesion test for the epoxy coating is not presented for brevity. Figure 8.6, depicts the post adhesion results for $E/GF_{10,20}$ and $E/FGF_{10,20}$ coatings where no peelings were observed and the coatings received 5B rating (0% peeling) as per the ASTM standard.

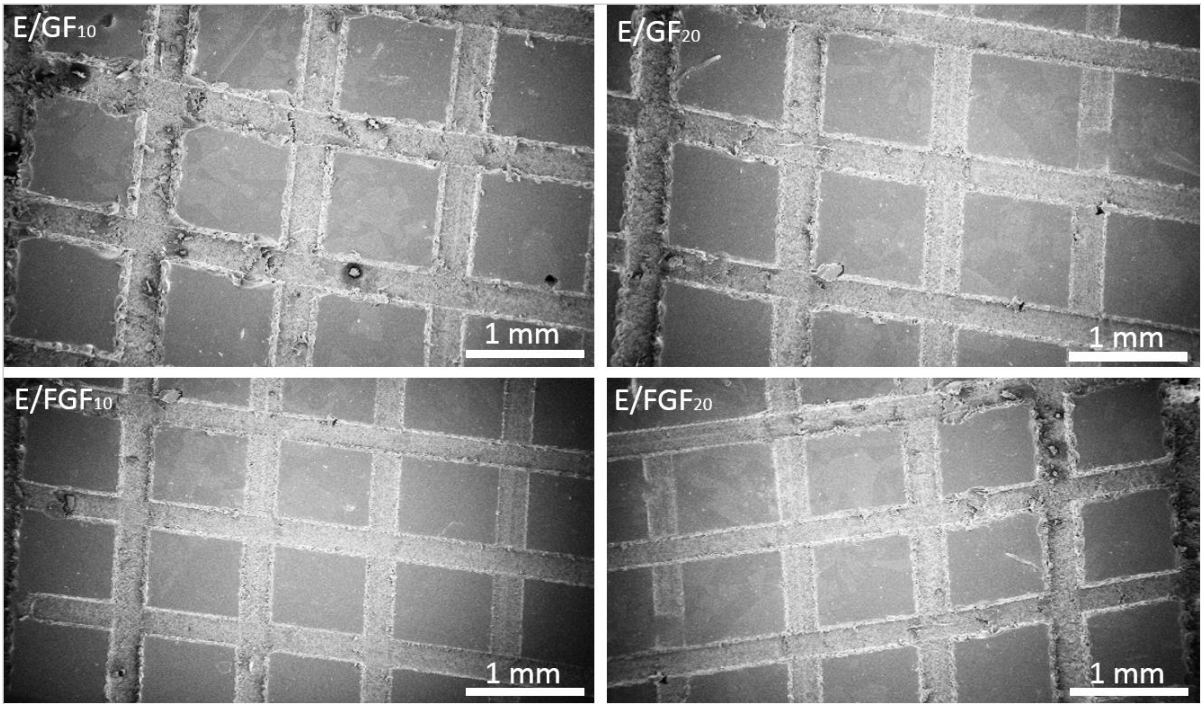

Figure 8.6: SEM images of post-adhesion tests of E/GF$_{10,20}$ and E/FGF$_{10,20}$ coated CRS substrates.

Furthermore, it was interesting to the shortcoming of incorporating higher load of GF or FGF in the polymeric matrix. This is clearly evident in Figure 8.7, where both E/GF$_{30}$ and E/FGF$_{30}$ protective coatings lose interface adhesion with underneath CRS substrates and therefore, adhesion tests were not conducted on E/GF$_{30}$ and E/FGF$_{30}$. The poor interface adhesion between E/GF$_{30}$ and E/FGF$_{30}$ coatings and CRS substrates can be attributed to the accumulation (aggregation) of GF or FGF particles at the coating and metal substrates interfaces resulting in formation of void spaces at the interfaces as depicted in Figure 8.7.

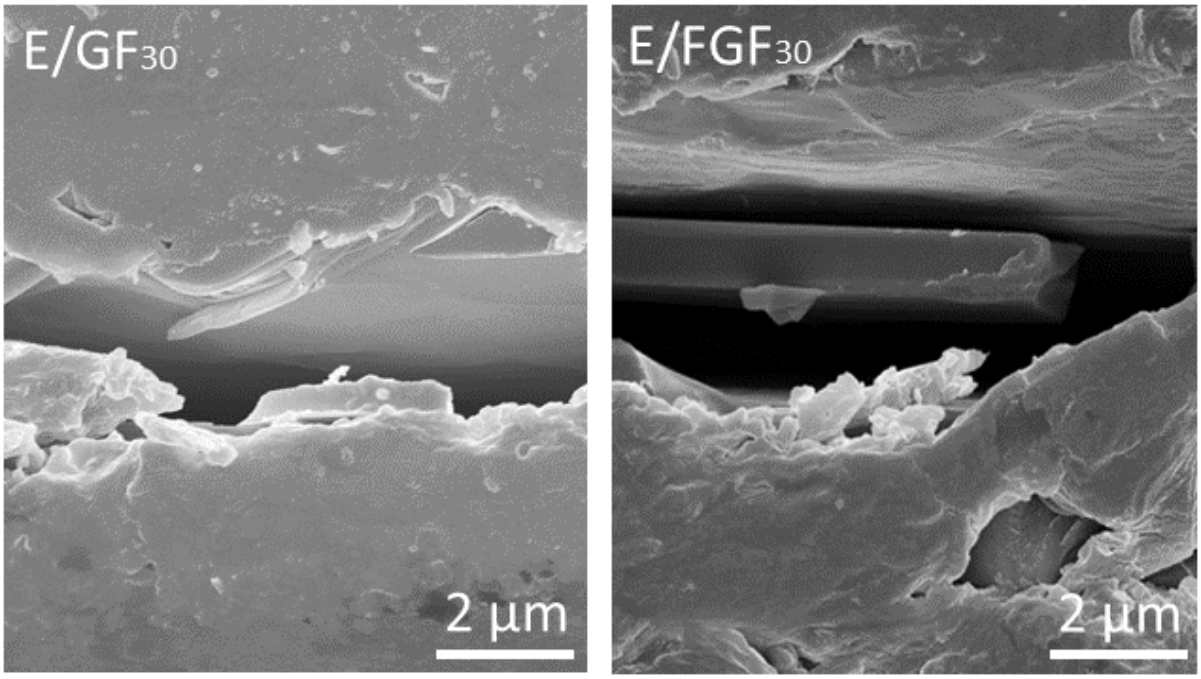

Figure 8.7: SEM cross section view of the interface between (a) E/GF$_{30}$, (b) E/FGF$_{30}$ coatings and CRS substrates.

8.4.4 Dispersion

The dispersion of the GF/FGF particles in the polymeric matrix was captured with TEM and depicted in Figure 8.8. The role of the surface modification of the GF by attaching the Amino based functional group in the dispersion of the filler is clearly observed in the presented TEM images, where well dispersed FGF particles were detected in both E/FGF$_{10}$ and E/FGF$_{20}$ composites. Whereas, TEM images for E/GF$_{10}$ and E/GF$_{20}$ composites show accumulations of GF particles in the resin as depicted in the figure. The enhanced degree of dispersion after the functionalization of GF can be attributed to the improved interaction and compatibility between FGF and epoxy as the attached amino group to the FGF could crosslink with the epoxy group of the resin.

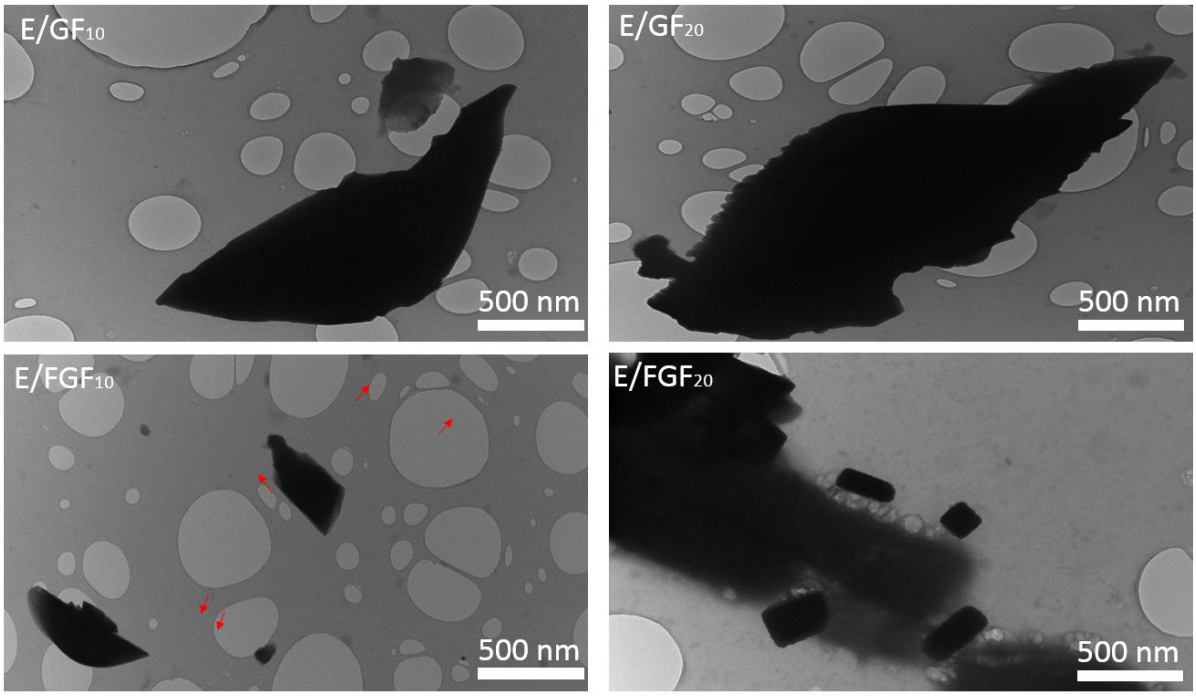

Figure 8.8: TEM images for GF and FGF dispersion in E/GF$_{10}$, E/GF$_{20}$, E/FGF$_{10}$, and E/FGF$_{20}$.

8.4.5 Impedance measurements

Impedance is very relevant characteristic for corrosion protection coatings that is widely utilized to evaluate the electrochemical activity on coated metal substrates. Impedance is a complex resistance generally observed when passing an alternating current (AC) through an electrical circuit composed of various elements such as insulators, resistors and capacitors. In corrosion studies, AC is fed through the corrosion cell over a range of frequency and the complex output is reported as the impedance of the bare or coated testing samples. Furthermore, an equivalent circuit can be used to fit the raw impedance data and evaluate the magnitude of the various components of the circuit. The variation in the magnitudes of these components can be utilized to evaluate the corrosion protection performance of different protective coatings.

In this study, the impedance behaviours of bare and coated CRS substrates are examined to evaluate the corrosion resistance properties of the prepared coatings. The impedance behaviour was examined after allowing the potential of the test samples to stabilize for 30 min in 3.5 wt.% NaCl electrolyte solution at room temperature. The raw impedance data fitted to equivalent circuit with combination of components using the EC-Lab software and equation (8.1).

$$Z = Z' + jZ'' = R_s \frac{R_{ch}}{1+(R_{ch}\times C\times \omega)^2} + j\frac{{R_{ch}}^2\times C\times \omega}{1+(R_{ch}\times C\times \omega)^2} \quad (1)$$

Where (ω) represents the frequency of the AC signal

The circuit that provides the best fitting of the raw impedance data and equation (8.1) is presented in Figure 8.9. In this circuit, C represents a double layer capacitor, R_s represent the electrolyte solution resistance, and R_{ch} represent the charge transfer resistance.

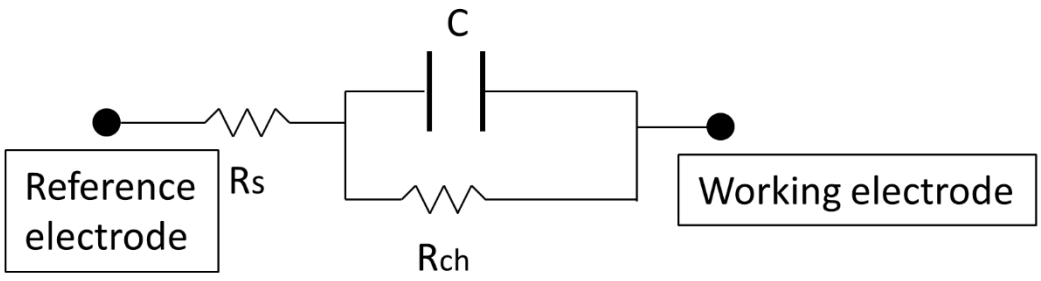

Figure 8.9: Equivalent circuits used to model the electrochemical impedance data

The raw and fitting impedance results are presented in the Nyquist plots shown in Figure 8.10. In Nyquist plot, an increase in the size of the semi-circle of raw impedance data generally represents an enhancement in the corrosion resistance. The results depicted in the Nyquist plots demonstrates the excellent corrosion protection property of the epoxy coating and the potential to significantly make this performance superior by incorporation of GF and FGF in the polymeric epoxy matrix. Furthermore, The Nyquist plots clearly illustrate the importance of functionalizing the GF as higher enhancement in

the corrosion resistance was observed for E/FGF compared to E/GF coatings with exact loadings of filler. In addition to the qualitative analysis, fitting the data computed from the equivalent circuit depicted in Figure 8.9 and equation (8.1) can be used to provide quantitative analysis by examining the variation in the magnitudes of the various elements of the equivalent circuit and these results can be used to evaluate the variation in the corrosion protection properties of the protective coatings. In particular, an increase in the charge transfer resistance indicates an enhancement in the corrosion resistance of a coating. Table 8.1 provides the magnitudes of the various elements of the equivalent circuit for all coatings. Here too, the increase in R_{ch} illustrates the corrosion protection properties of epoxy and the possibility of enhancing this protection property by the incorporation of GF. Nerveless, such an enhancement in the corrosion resistance property can be further improved by surface modification of GF.

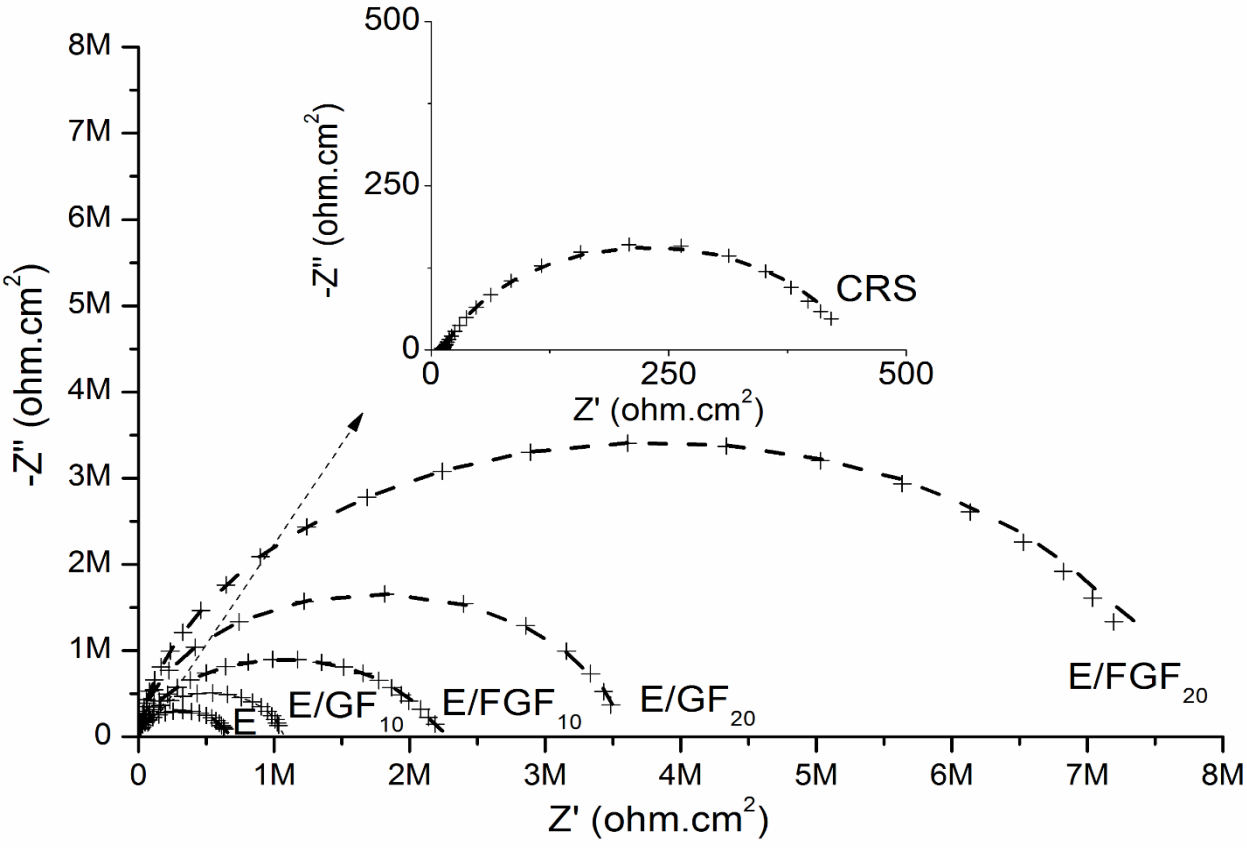

Figure 8.10: Nyquist plots for bare CRS, Epoxy, E/GF$_{10}$, E/GF$_{20}$, E/FGF$_{10}$ and E/FGF$_{20}$ coated CRS substrates.

Table 8.1: The electrochemical corrosion parameters obtained from equivalent circuit for EIS measurements for bare CRS, Epoxy, E/GF$_{10}$, E/GF$_{20}$, E/FGF$_{10}$ and E/FGF$_{20}$ coated CRS in a 3.5 wt.% NaCl solution.

Sample	R_S	C	R_{ch}	$R_{ch,ST}$
	$\Omega.cm^2$	F	$\Omega.cm^2$	$_D$ $\Omega.cm^2$
CRS	18.1	4..3x10^{-4}	433.7	2

Epoxy	18.3	$6.9x10^{-11}$	$6.70x10^{5}$	20
E/GF_{10}	18.4	$9.0x10^{-11}$	$1.06x1^{6}$	450
E/FGF_{10}	18.3	$1.9x10^{-10}$	$2.20x1^{6}$	330
E/GF_{20}	18.1	6.2×10^{-11}	$3.58x1^{6}$	210
E/FGF_{20}	18.2	9.5×10^{-11}	$7.60x1^{6}$	180

In addition to the qualitative and quantitative analysis of the Nyquist plots, the real part of the raw impedance data (Z_{real}) can be plotted versus the frequency in a Bode plot as depicted in Figure 8.11.a in order to examine the corrosion protection properties of the prepared coatings. An increase in the magnitudes of Z_{real} at the lowest recorded frequency represents an enhancement in the corrosion resistance of a coating and from the figure, Z_{real} values at the lowest frequency for bare CRS, epoxy, E/GF_{10}, E/GF_{20}, E/FGF_{10} and E/FGF_{20} coated CRS substrates are 2.62, 5.83, 6.02, 6.59, 6.36 and 6.90 $M\Omega.cm^2$, respectively.

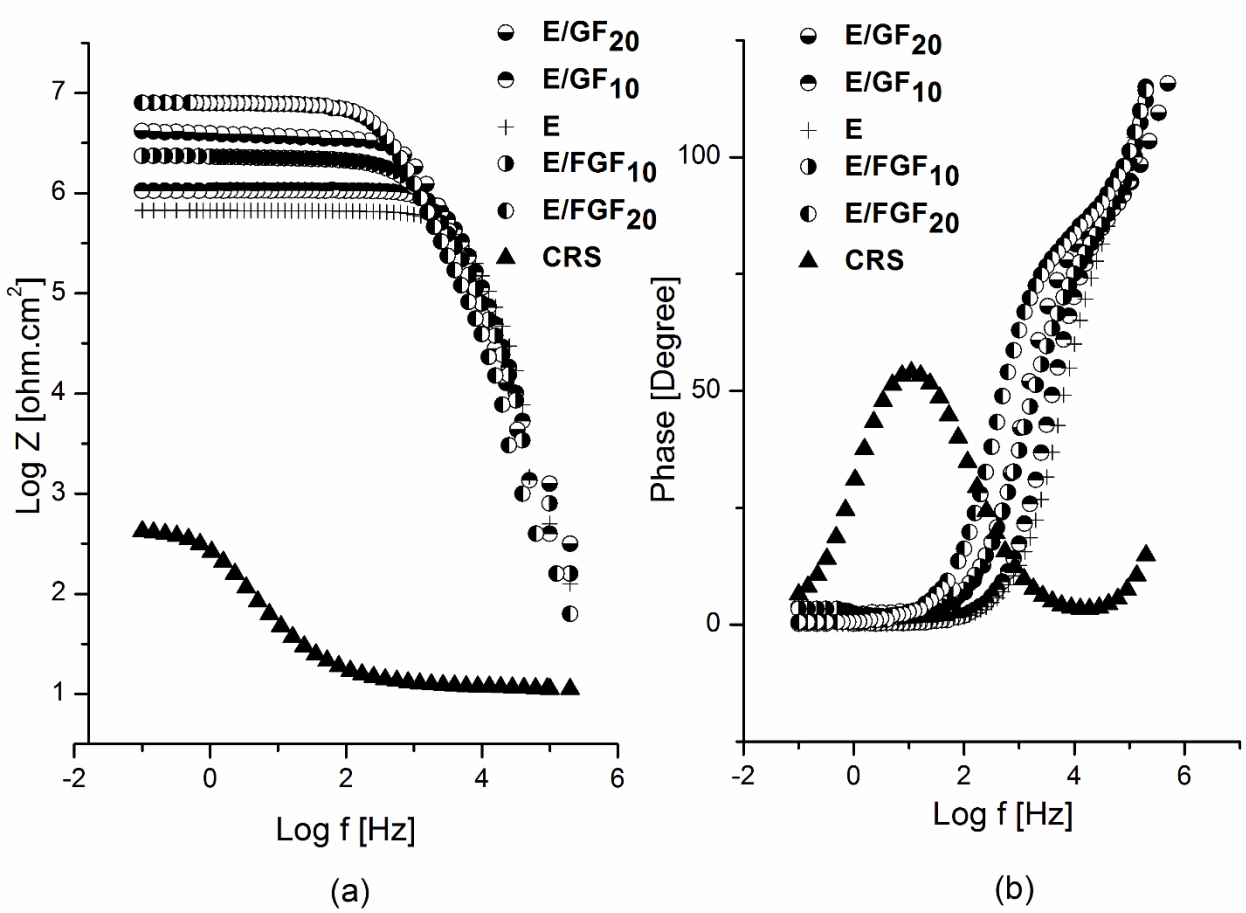

Figure 8.11: (a) Bode and (b) phase plots for bare CRS, Epoxy, E/GF$_{10}$, E/GF$_{20}$, E/FGF$_{10}$ and E/FGF$_{20}$ coated CRS substrates.

The reported impedance results illustrate possibility of protecting CRS substrates from corrosion in Chloride rich environment. Furthermore, the incorporation of GF in the resin may further enhance the corrosion protection property of epoxy. This enhancement in corrosion protection can be attributed to the barrier property of GF, which extend the pathways corrosion elements such as Oxygen and moisture travel to reach the underneath metal substrate. Moreover, the presented results demonstrate that the corrosion protection properties of E/GF coatings can be further excelled by attaching an Amino based functional group to the GF functionalization of GF may deliver significant enhancement in corrosion

resistance properties. The observed gain of surface treatment of GF in corrosion resistances properties can be attributed to role of functional group in enhancing the compatibility and dispersion of the filler in the polymeric matrix, which further add to the tortuosity of pathways corrosion agents follow to reach coated substrates.

8.4.6 Potentiodynamic measurements

Cyclic voltammetry is another electrochemical technique that is widely used to study the electrochemical behavior of bare and coated metal substrates. A three electrodes configuration was used to study the electrochemical behavior of bare and coated CRS in a temperature controlled 3.5 wt.% NaCl at 25 ^{o}C. After allowing the potential of the bare or coated CRS samples to stabilized for 30 mins, the observed potential of the sample was recorded as the open circuit potential and CV study was carried out by scanning the potential of the bare/coated CRS from -0.5 V to 0.5 V above the open circuit potential. The area where the electrochemical behavior of the testing sample shifts from anodic to cathodic behavior, which is known as the Tafel plot was reported as depicted in Figure 8.12. The reported results in Tafel plots can be used to extract significant parameters such as corrosion current (I_{corr}) and corrosion potential (E_{corr}) that may allow assessing the corrosion protection properties of the prepared protective coatings. Furthermore, the extracted I_{corr} can be further utilized with equation (8.2), which is known as the Stern-Geary equation to compute the polarization resistances (R_p) of the coatings. In addition, the reported I_{coor} for bare and coated CRS substrates can be used to compute the corrosion protection efficiency of the coatings (P_{EF}) using (8.3).

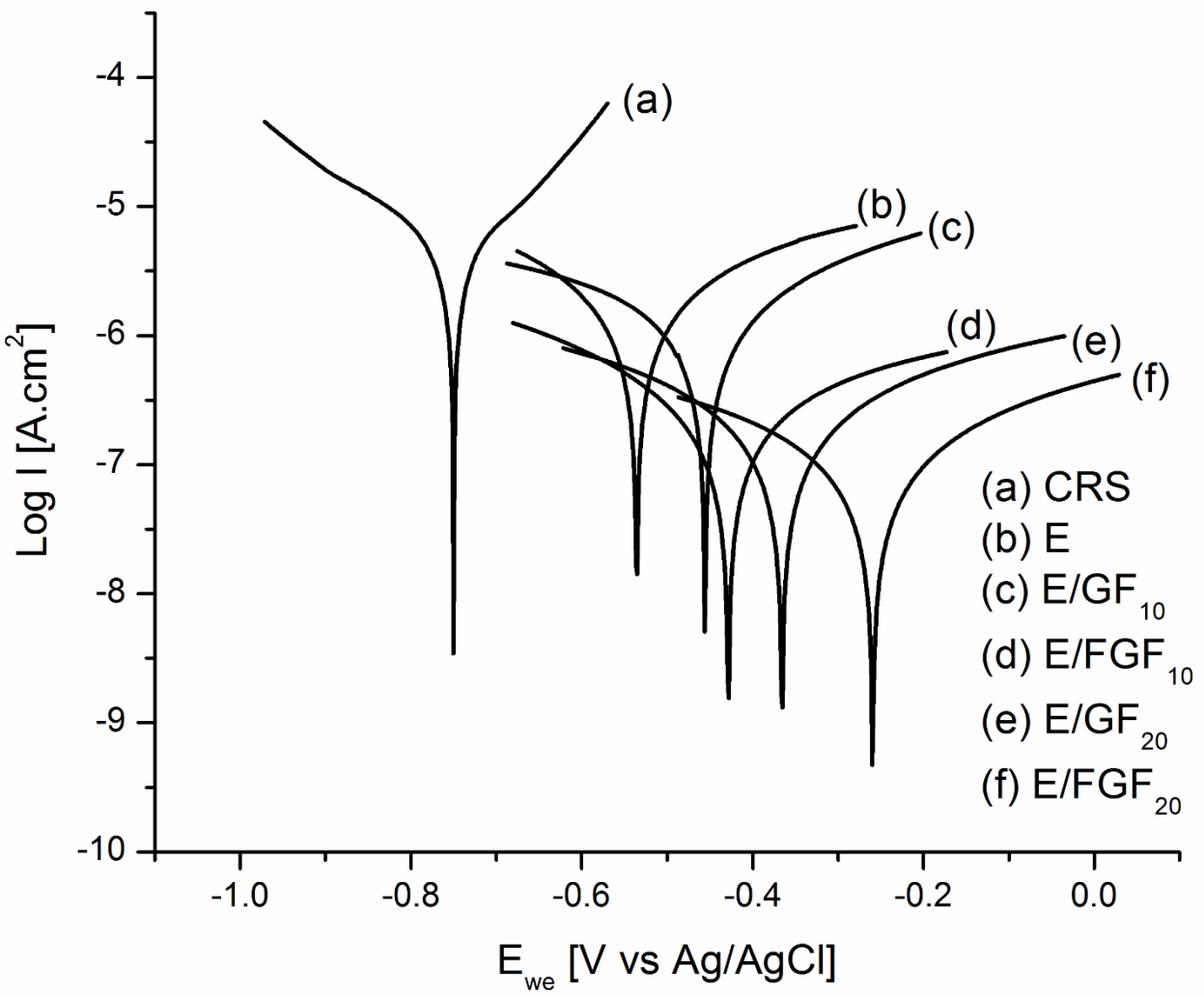

Figure 8.12: Tafel plots for bare CRS, Epoxy, E/GF$_{10}$, E/GF$_{20}$, E/FGF$_{10}$ and E/FGF$_{20}$ coated CRS substrates.

$$R_P = \frac{(b_a x b_c)}{2.303 \times (b_a + b_c) \times I_{corr}} \tag{8.2}$$

$$P_{EF}[\%] = \left(1 - I_{corr}/I^{\circ}_{corr}\right) x100 \tag{8.3}$$

Where, b_a/b_c represent the slops of the linear portion of the anodic/cathodic sides of Tafel plots, respectively. In addition, I°_{corr} and I_{corr} are corrosion currents of bare and coated CRS, respectively.

The magnitudes of the computed parameters (E_{corr}, I_{corr}, R_p and P_{EF}), which are reported in Table 8.2 may explain how the prepared coatings influence the corrosion behavior of the coated CRS substrates as well as the influences of the incorporation and the functionalization of GF. In general, a positive shift in E_{corr} and drops in I_{corr} represent an enhancement in corrosion protection and these shifts in E_{corr} and I_{corr} may deliver enhancements in R_p as well as P_{EF}.

Table 8.2: Electrochemical corrosion parameters obtained from cyclic voltammetry measurements for bare CRS, Epoxy, E/GF_{10}, E/GF_{20}, E/FGF_{10} and E/FGF_{20} coated CRS in a 3.5 wt.% NaCl solution.

Sample	E_{corr} *mV vs Ag/AgCl*	$E_{corr,STD}$ *V vs Ag/AgCl*	I_{corr} µA/cm^2	$I_{corr,STD}$ µA/cm	b_a	b_c	R_P Ω.cm^2	P_{EF} %
CRS	-750	0.009	5.4	0.002	171.3	242.6	8.07	-
Epoxy	-537	2.5	0.55	0.001	293.4	396.5	133.3	89.8
E/GF_{10}	-456.5	30.8	0.3	0.02	256.1	358.2	216.4	94.4
E/GF_{20}	-366	28.5	0.121	0.01	309.9	302.6	549.4	97.7
E/FGF_{10}	-428	5.6	0.144	0.008	236.8	175.2	303.6	97.3
E/FGF_{20}	-260.4	6.2	0.072	0.005	295.3	291.2	12732.7	99.8

Results reported in Figure 8.12 and Table 8.2 demonstrate the possibility of enhancing the life span of CRS substrates by coating and the prospect to prompt the corrosion protection property of coating

by incorporating a filler in the polymeric matrix such as GF. Furthermore, the reported results illustrate the advantage of increasing the load of the filler in the resin, which provide further corrosion protection to the coated metal substrates. Moreover, it was interesting to observe the substantial influences of functionalization of GF on the protection performance of the prepared coatings. Functionalizing the GF facilitates significant enhancement in the corrosion protection properties of the coatings without manipulating the load of GF, which may attenuate the interface adhesion between the coating and the CRS substrates as reported in the adhesion section. Here too, the enhancement in corrosion protection property after the incorporation of GF can be attributed to the barrier property of GF and the role of functionalization in improving the dispersion of GF in Epoxy can be accountable for the excelled corrosion resistances of E/FGF_{10} and E/FGF_{20} over E/GF_{10} and E/GF_{20}.

8.4.7 Long term corrosion protection

Bare and coated CRS substrates were exposed with surface area of 1 cm^2 to 3.5 wt.% NaCl solutions at 25° C for 90 days to evaluate the long term corrosion prevention properties of the prepared coatings. Weight loss measurements were used to compute the corrosion rate (R_{corr}) as well as the protection efficiency (P_{EF}) for each coating using equation (8.4) and (8.5).

$$R_{corr} = \frac{W_0 - W}{\mathrm{A}xt} \tag{8.4}$$

$$P_{EF}[\%] = \left(1 - \frac{R_{corr}}{R^{\circ}_{corr}}\right) x100 \tag{8.5}$$

Where, A is the coated/uncoated exposed surface area (1 cm^2), W_0 and W are the weight of the sample (mg) before and after exposure period, respectively, t is immersion time (90 days) and R_{corr} and R°_{corr} represent the corrosion rate of the coated and bare CRS substrates, respectively. Furthermore,

triplicate measurements for each sample were used to calculate the average and standard deviation ($R_{corr, STD}$) of R_{corr} as reported in Table 8.3.

Table 8.3: Weight loss measurements for bare CRS, Epoxy, E/GF$_{10}$, E/GF$_{20}$, E/FGF$_{10}$ and E/FGF$_{20}$ coated CRS in a 3.5 wt.% NaCl solution.

Sample	W_0 mg	W mg	R_{corr} mg.cm^{-2}.d^{-1}	$R_{corr,STD}$ mg.cm^{-2}.d^{-1}	P_{EF} %
CRS	81	52	0.45	0.003	-
Epoxy	115.1	112.3	0.3	0.006	93.1
E/GF$_{10}$	120.4	118.9	0.017	0.01	96.3
E/GF$_{20}$	121.2	120.6	0.006	0.02	98.5
E/FGF$_{10}$	115.3	114.4	0.01	0.007	97.8
E/FGF$_{20}$	120.1	119.9	0.002	0.004	99.5

The weight loss analysis demonstrates that coating CRS with epoxy would prolong the life span of the metal substrate and the incorporation of GF would further enhance this corrosion protection property of epoxy. Furthermore, the results reported in Table 8.3 reveals that the corrosion resistance efficiency of E/GF composites could be further excelled by functionalizing the GF.

8.4.8 Thermal stability

Thermal gravimetric analysis (TGA) was used to assess the thermal stability of the prepared E/GF and E/FGF composites in order to illustrate the role of surface functionalization of GF as well as the load of the GF/FGF on the thermal degradation. Figure 8.13, shows the thermograms for E/GF and E/FGF composites over temperature range 30-800 ^{o}C. The TGA results clearly demonstrate the influences of the incorporation of GF on the nonoxidative degradation of the epoxy. The incorporation of GF and FGF and increasing their loading clearly enhances the thermal stability of the epoxy as demonstrated by the increase in the degradation temperature (T_{onset}), which is taken as the temperature where 5% of the materials is degraded. For example, T_{onset} of epoxy was 352.6 ^{o} C and has increased to 356.4^{o} C for E/GF_{10} and to 357.2 ^{o} C for E/GF_{20}. Moreover, the TGA data depicted in Figure 8.13, evidently presents the positive influences of FGF on the thermal stability and T_{onset} of the prepared E/FGF, where at FGF leads to higher shift in the T_{onset} compared to that caused by GF of the same loading as the T_{onset} was increased to 358.5^{o} C for E/FGF_{10} and to 360.6 ^{o}C for E/FGF_{20} as reported in Table 8.4. The positive impacts of the incorporation of GF in the thermal stability of the coating can be attributed to the enhanced interface interaction between the resin and the FGF. In addition to T_{onset}, the temperature at which the materials degrade by 50% ($T_{50\%}$) were also reported in Table 8.4 and it was interesting to observe that the incorporation of GF in Epoxy caused minor drop in $T_{50\%,}$ while the functionalization of GF positively shifts $T_{50\%.}$ These influences of GF/FGF in $T_{50\%}$ can be attributed to excelled interactions between Epoxy FGF, while the poor interaction with GF causes some of the fluffy GF particles to get alienated from E/GF_{10} and E/GF_{20} composites.

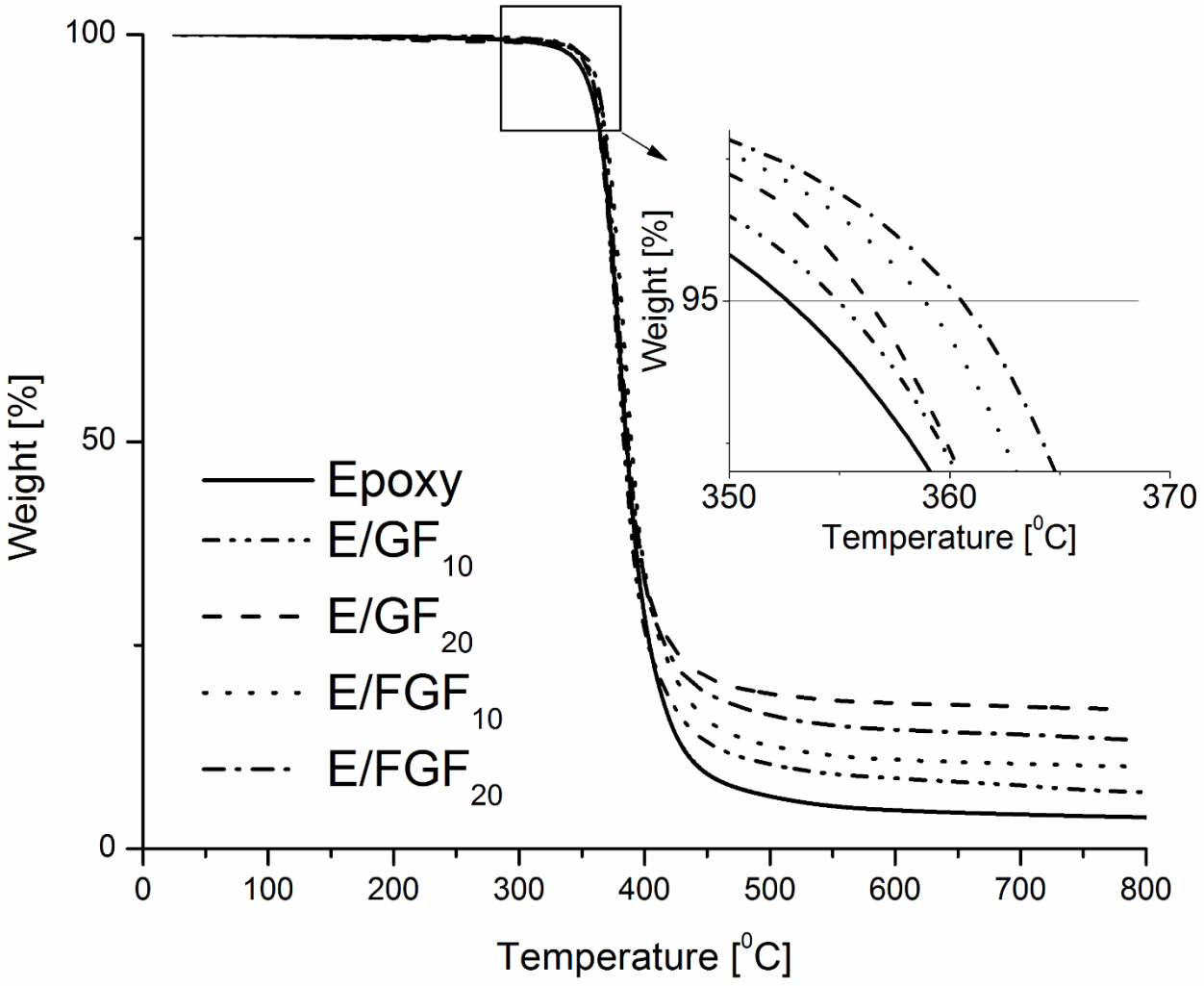

Figure 8.13: TGA thermo-grams of Epoxy, E/GF$_{10}$, E/GF$_{20}$, E/FGF$_{10}$ and E/FGF$_{20}$ coatings.

The impact of the incorporation of GF and FGF on the second order phase transition, glass transition (Tg), for the epoxy was examined by DSC. The DSC thermograms for the epoxy and the composite samples shown in Figure 8.14 clearly demonstrate the impact of the incorporation of GF and the utilization of FGF as observed by an upward shift in the glass transition temperature. This upward shift in T_g is attributed to the restricted epoxy polymer chain's mobility by the GF and the FGF. Moreover, the high Tg shift observed for the E/FGF composites in comparison to the E/FG composites is attributed

to the to the stronger interface interaction and potential cross linking between the epoxy group in the resin and the amino group on the FGF as reported in Table 8.4.

Table 8.4: Thermal analysis results for Epoxy, E/GF$_{10}$, E/GF$_{20}$, E/FGF$_{10}$ and E/FGF$_{20}$ composites

Sample	*Initial weight* mg	T_{onset} °C	$T_{50\%}$ °C	*Residue* %	T_g °C
Epoxy	25.48	352.6	385.6	3.85	79.6
E/GF$_{10}$	30.14	356.4	383.5	6.76	81.3
E/GF$_{20}$	38.99	357.2	385.5	17.07	86.78
E/FGF$_{10}$	31.47	358.5	387.1	10.11	87.95
E/FGF$_{20}$	34.79	360.6	389.4	13.34	89.1

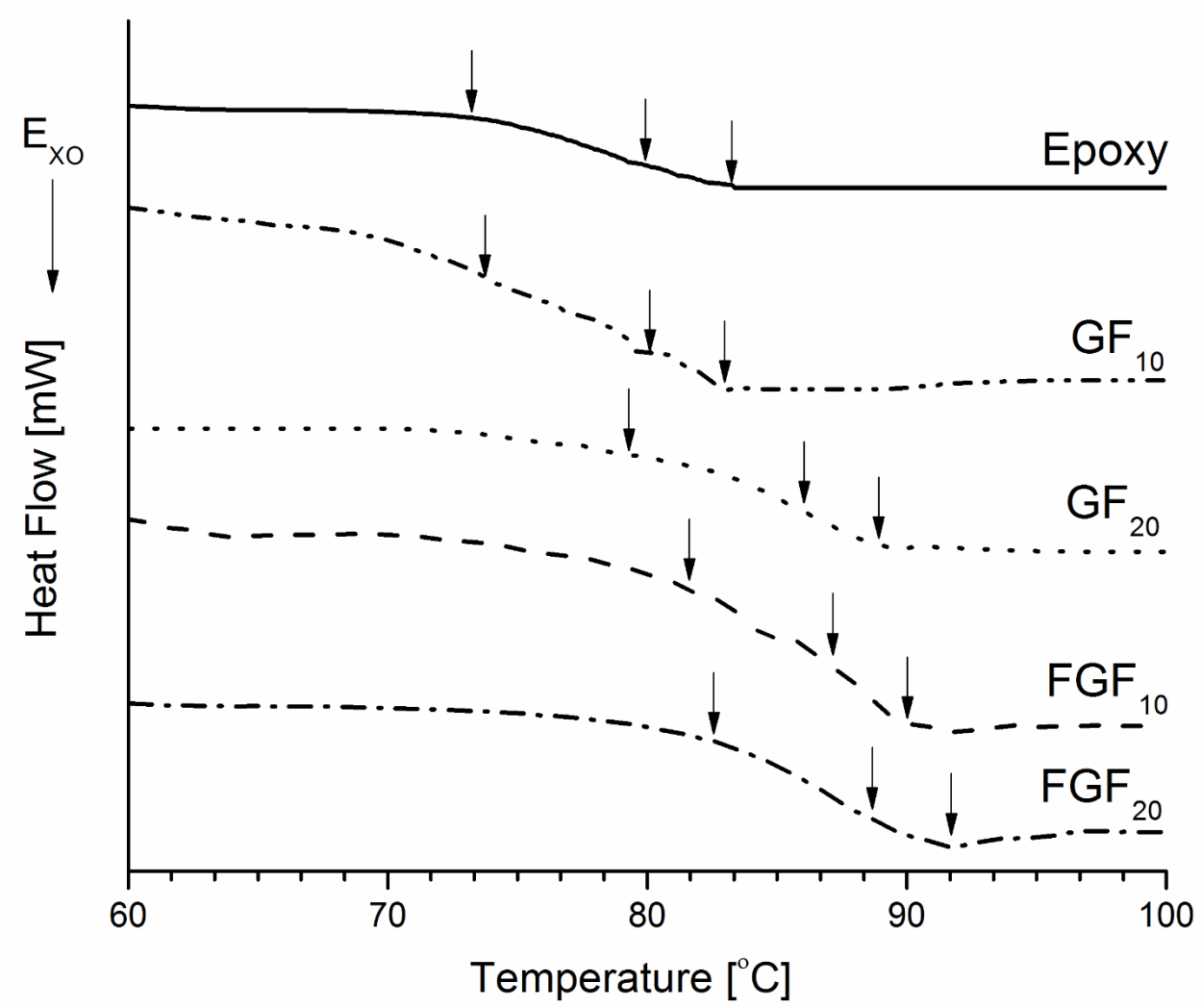

Figure 8.14: DSC thermo-grams of Epoxy, E/GF_{10}, E/GF_{20}, E/FGF_{10} and E/FGF_{20} coatings

8.5 Conclusions

Protective coating of Epoxy/Glass flake and Epoxy/Functional Glass flake composites were spin coated on CRS substrates and thermally cured and their corrosion protection of CRS in Na+ rich aqueous environment was analyzed gravimetrically as well as using impedance and electrochemical analysis. Our results clearly demonstrate incorporation of GF in Epoxy significantly enhance the

corrosion protection and the thermal stability properties of Epoxy and the level of such enhancements can be further excelled by increasing the load of GF up to 20%. Furthermore, epoxy composite containing GF functionalization with aminosilane groups leads to much more significant enhancement in the corrosion protection and the thermal stability of the coating compared to the composites containing GF. The improvements in the corrosion protection and the thermal stability of E/FGF can be attributed to the enhanced dispersion of the filler in the polymeric matrix and the stronger surface interaction between the host resin and the functionalized filler as demonstrated by the significant shift in Tg and T_{onset}.

Moreover, the long term performances of the prepared composites were examined and confirmed by conducting gravimetric analysis over 90 days exposure period to 3.5 wt.% NaCl solution in a controlled temperature environment. Finally, it was interesting to observe that increasing the loading of GF and FGF above 20% may attenuates the interface adhesion between the coatings and the underneath CRS substrates.

Chapter 9

Amino functionalized Graphene oxide/Epoxy nanocomposite coatings with advanced protection properties

Abstract

Advanced anticorrosion coating with superior corrosion resistance, thermal stability and impact resistance properties is developed based on epoxy nanocomposite with amino functionalized graphene oxide (FGO) and used as protective coating for Cold rolled steel (CRS) substrates in a Chloride rich environment. The performance of the epoxy-FGO nanocomposite (E/FGO) prepared via situ pre-polymerization is superior not only to the epoxy coating but also to epoxy-graphene oxide (E/GO) coating with the same loading and prepared in similar manner as the E/FGO. The dispersion of GO and FGO in the Epoxy composite matrix is examined using TEM, XRD and FTIR are used to characterize the synthesized nanocomposites. The corrosion resistance properties of the prepared coatings are examined using Electrochemical Impedance Spectroscopy (EIS) and Potentiodynamic measurements in 3.5 wt. % Sodium Chloride (NaCl) solution. In addition to the electrochemical measurements, the long-term corrosion protection properties of the nanocomposite coatings are evaluated by gravimetric analysis over 90 days exposure period to the 3.5 wt.% NaCl solution. The interface adhesion between the prepared coatings and the CRS substrates are examined as per ASTM-D3359 and SEM is used to evaluate the adhesion. The thermal stability and thermal transition of the nanocomposite coatings are analyzed using TGA and DSC. The impact resistance of the prepared coatings is measured according to ASTM-D2794.

9.1 Introduction

Corrosion is the deterioration of metal driven by electrochemical reactions between the metal and the environment and the severity and rate of corrosion are governed by various factors including the nature of the metal and the surrounding environment. The failure to mitigate corrosion may cause serious threats to both industry and the economy. Therefore, a growing number of studies have been devoted to exploring the possibility of complete prevention or mitigation of corrosion using different strategies, including anodic/cathodic protection, use of corrosion inhibitors and protective coatings[2], [3], [5]. Coating is one of the eminent approaches utilized in various areas of applications for corrosion protection purposes. Organic coatings, in particular, have been widely utilized to mitigate the deterioration of metals by acting as a physical barrier between metal substrates and the surrounding corrosion environments. However, pores in organic coatings may network and create channels that allow corrosion species such as chloride, oxygen and moisture to diffuse to the interface between the protective coating and the metal substrate. The migration of the corrosion elements through the protective coating may attenuate the protection performance of the coating and accelerate adhesion loss, coating blistering and metal corrosion.

A growing number of studies have focused on the possibility of enhancing the corrosion resistance properties of organic coating particularly by incorporating additives or corrosion resistance pigments. For example, Jiang *et. al.* revealed that the corrosion protection performance in addition to the adhesion of epoxy can be enhanced by incorporating active (amino-propyltrimethoxy) and non-active (bis-1,2-[triethoxysilyl]ethane) silane precursors [110], [111]. Other studies revealed that the utilization of TiO_2 doped poly-pyrrole coating could result in significant enhancements in the corrosion resistance of Aluminum substrates [112], while the life span of Magnesium alloy can be extended by applying hydroxyapatite and octacalcium phosphate coatings [113]. In addition to the simple incorporation of

fillers in polymeric matrices, studies have focused on the utilization of nano-materials to excel the corrosion performance of protective coatings. For instance, Pour-Ali *et al.* investigated epoxy/polyaniline–camphorsulfonate nanocomposite as a corrosion protection coating on steel in Chloride rich environment and the investigation illustrated the possibility of enhancing the corrosion protection properties by the application of the coating [114].

There are different types of filler that have been investigated for corrosion protection purposes [115]–[121]. However, a growing number of studies have focused on graphene and graphene derivatives as fillers in various polymer composite coatings in order to enhance various properties including corrosion resistances [32], [34], [62], [78], [79]. In addition to the utilization of protective composite coatings, several studies have investigated the chemical vapor deposition (CVD) method for deposition of graphene on various metal substrates and reported that deposited graphene coating may excel the corrosion resistance of the underneath metal substrates by acting as a passive layer that shields the transportation of ions and electrons between metals and surroundings [36], [55], [122]–[126]. The excellent performance of graphene coating is attributed to the lower density, high surface area, and high aspect ratio of graphene compared to other fillers such as clay [53].

In addition to the simple incorporation of pristine graphene in polymer composites or CVD coating with graphene, many researchers have focused on the functionalization of graphene and the influences of such functionalization on various properties including corrosion resistance. For instance, a recent study revealed that the corrosion protection of epoxy and graphene oxide (GO) composites coatings can be enhanced the attaching titanium dioxide on the GO surface using 3-aminopropyltriethoxysilane as coupling agents [42]. Another study investigated the incorporation of fluorographene particles into polyvinyl butyral composite coatings for corrosion protection purposes. The study revealed that shielding property of may remarkably enhance the corrosion resistance of the coating by blocking the

diffusion paths of corrosive elements and moisture [43]. Recently, the influences of the incorporation of functionalized GO in epoxy composites, through the wet transfer of amino functionalized GO, on the corrosion resistance property of epoxy coating were investigated. The study demonstrated that significant enhancement in the corrosion mitigation property of epoxy can be achieved by improving both ionic resistance and barrier properties.

In this study, amino functional group was grafted on the surface of GO to synthesize FGO that is used to make epoxy nanocomposite, which is used as protective coatings on CRS substrates. The pristine GO and FGO were characterized using FTIR and XRD techniques, while the dispersion of the fillers in the polymeric matrix was examined using TEM. The study reports the influences of the GO surface modification on various properties including corrosion and impact resistance as well as thermal stability and thermal transition. The long-term corrosion protection ability of the prepared E/FGO was evaluated by gravimetric analysis in 3.5% NaCl solution. Moreover, electrochemical techniques such as EIS and potentiodynamic measurements were utilized to examine the corrosion resistance properties of the epoxy, epoxy-GO, and epoxy FGO nanocomposites in 3.5% NaCl solution. The thermal stability of the prepared coatings was investigated using DSC and TGA. Furthermore, the impact resistance of the prepared coatings was measured according to ASTM D2794 standard.

9.2 Experimental

9.2.1 Materials

Polished CRS sheet (McMASTER-CARR) was used as substrates, Bisphenol A diglycidyl ether (BADGE, Sigma Aldrich,), N-Methyl-2-pyrrolidinone solvent (NMP, Sigma Aldrich), m-Phenylenediamine (mPDA, Sigma Aldrich) and GO with average diameters of 1-5 μm and average

thickness of 0.8 - 1.2, which was synthesized by the modified Hummer method and thermally treated to improve dispersion, was supplied by ACS Material and used as received.

9.2.2 Composite Synthesis

Graphene functionalization: the functionalization of GO with amine groups was carried as follows: 2.1 mg GO were dispersed in NMP via bath sonication (FS30H, Fisher Scientific) overnight. 0.5 g of mPDA was added to the GO suspension and mixed under reflux for 6 h at 90◦ C to prepare the FGO suspension. NMP solvent were removed at 90◦ C under vacuum and the dry FGO is collected and washed three times with ethanol and double distilled water to remove any residual mPDA and dried under vacuum overnight.

Composite preparation: 2.1 FGO is dispersed in 1.5 g of BADGE under reflux for 1 h and bath sonicated for an additional hour. 0.5 g curing agent (hardener) B230 was added to the FGO/BADGE suspension and the mixture was mixed under reflux for 1 h, homogenized (125, Fisher Scientific) for 30 min and bath sonicated for additional 30 min.

9.2.3 Coating and curing

The CRS substrate was polished with different grades of sand papers, cleaned with acetone and double distilled water and dried with KimTech wipes before applying the prepolymer/FGO mixture. The prepolymer/FGO mixture was spin coated (SC 100, Smart Coater) at 400 RPM for 1 min on a clean metal substrate and cured at 50 ˚C under vacuum for 4h to produce 120 ±2 µm E/FGO coated CRS substrate.

The functionalization process of GO and the composite synthesis procedure are schematically depicted in Figure 9.1. Similar procedures were followed to prepare Epoxy and E/GO composites,

where 0.5 g B230 and 1.5 g BADGE were mixed without/with the incorporation of 2.1 mg of GO to prepared 120 ±2 µm Epoxy and E/GO coated CRS substrates.

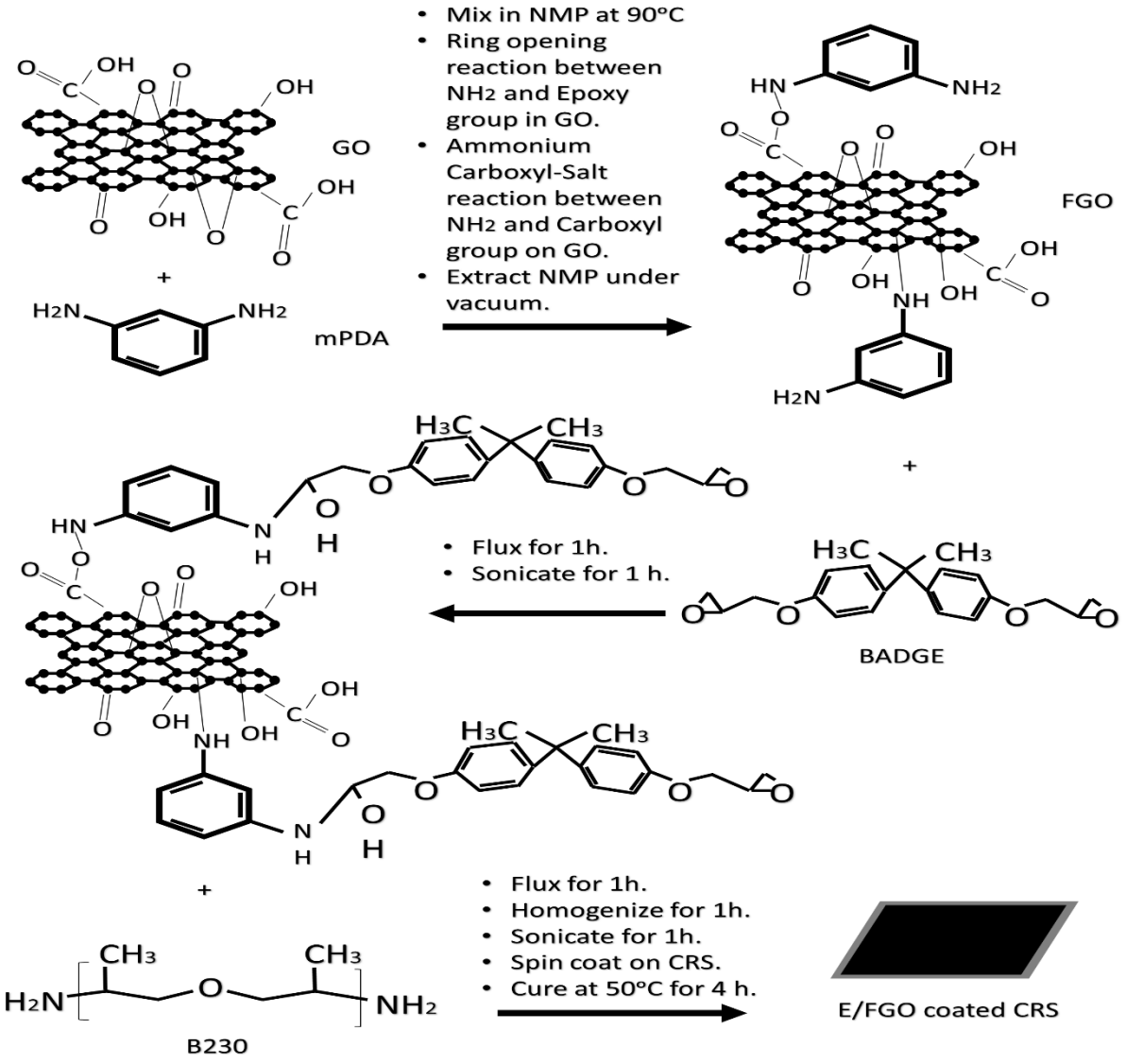

Figure 9.1: Schematic description of the process for the functionalization of GO and synthesis of E/FGO composites using in situ polymerization.

9.2.4 Composite and Coating Characterization

The functionalization of GO sheets was examined using FTIR (Tensor 27, Bruker) and XRD (MiniFlex 600, Rigaku). FTIR spectra of GO, FGO, Epoxy, E/GO and E/FGO composites were recorded from 400 to 4000 cm^{-1} and the XRD diffraction patterns were recorded in a range of $2\theta = 3$ to 90° at 0.02° step size and 0.24° /min scan rate.

The dispersion of the FGO and GO in the composites was examined using TEM (Philips CM-10 TEM). TEM samples were prepared by scrapping the prepared composite coatings with a sharp knife before dispersing the collected samples in methanol using a sonication bath for 30 min. Copper grids were used to collect the dispersed composites samples from methanol and the collected samples on the grids were allowed to dry under vacuum at room temperature overnight.

The interface adhesion between the prepared coatings and the CRS substrates were examined and evaluated according to ASTM D3359. To evaluate the long-term durability of the coatings, the interface adhesion was evaluated after exposing the prepared protective coatings to 3.5% NaCl solution for 90 days. The adhesion test was conducted using tape kit (PA-2000, Paul N. Gardner Company Inc.) with a standard blade (11-teeth with teeth spacing of 1 mm). The state of the coating post adhesion was observed using SEM (Zeiss LEO 1550). The samples were fixed on SEM holder using carbon tape and gold coated via sputtering for 120 sec. The post-adhesion SEM images were evaluated according to ASTM D3359.

9.2.5 Coating Testing

Gravimetric analysis was conducted for 90 days in 3.5% NaCl solution at room temperature to examine the long-term corrosion protection properties of the prepared coatings. The bare and coated samples were washed with acetone and double distilled water and dried using KimTech wipes before

the initial weights were recorded and the samples were placed in Teflon holders with 1 cm^2 exposed area. At the end of the exposure period, the samples were again washed with double distilled water and cleaned with a fine brush to remove any corrosion residues. After that, the samples were dried under vacuum at room temperature overnight before recording the final weight. Mass loss measurements were conducted on triplicates to examine the reproducibility of the results and the mean and standard deviation data are reported.

Electrochemical measurements were conducted at 22°C in a temperature controlled double jacketed 1 L corrosion cell using a three-electrode configuration in 3.5% NaCl solution as electrolyte. Silver/Silver Chloride electrode was used as the reference electrode (RE), two graphite rods as the auxiliary electrodes and sample of the prepared composite coating in a Teflon holder with 1 cm^2 exposed surface area as the working electrode (WE). After immersing the samples in the electrolyte, the potential of the working electrode was allowed to stabilize for 30 min before conducting the electrochemical measurements using potentiostat (VSP-300, Uniscan instruments ltd.). All electrochemical measurements were conducted in triplicates to evaluate the reproducibility of raw electrochemical data. The nondestructive EIS measurements were carried out first followed by the potentiodynamic measurements. EIS tests were conducted over frequency range from 200 KHz to 200 mHz and the collected raw impedance data were used to generate the Bode and Nyquist plots. In addition, equivalent circuits with specific combinations were utilized to generate a matching fitting for the raw impedance data and the variation in the scales of the different components of the equivalent circuits were used to compare the corrosion resistance performance of the different coatings. Following EIS tests, the potentiodynamic measurements were conducted to generate the Tafel plots and extract imperative corrosion parameters. Starting from the potential of the working electrode, the potential was scanned from -0.5 V to 0.5 V around the potential of the working electrode at a rate of 20 mV/min.

Thermal stability of the prepared composites was evaluated by conducting a thermal degradation analysis using thermal gravimetric analysis (TGA) (TA instruments, Q500) in the temperature range of 25 to 800° C. In addition to the thermal degradation analysis, the glass transition temperatures (T_g) of the composites were measured using differential scanning calorimetry (DSC) (TA instruments, Q2000) by heating the sample from 25 to 100° C at 10° C/min heating rate.

Impact resistance is the resistance of the material to deformation by sudden impact of a falling weight, was examined and evaluated according to ASTM D2794 using universal impact tester (IM-172RF, Paul N. Gardner Company Inc.) with a combined 0.5 in. ball and 2 Ib. weight indenter. The influence of the incorporation of GO and FGO in the epoxy resin on the impact resistance is analyzed. The impact resistance of the prepared composites was evaluated by rising the falling combined weight 1 inch in the testing tube and allowing the weight to drop on the composite surface. The falling procedure were repeated with 1 inch increment in height until the first sign of cracks were observed on the surface of the composite. Following the ASTM standard, the height at which the cracks were observed was recorded and the falling test was repeated five times at the recoded height, 1 inch above, and 1inch below the recorded height and the height at which the composite cracks all the times was reported as the impact resistance limit of the composite to sudden deformation.

9.3 Results and Discussion

9.3.1 Composites characterization

FTIR and XRD techniques were utilized to evaluate the surface modification of GO with the grafted Amino group from the Diamine. Figure 9.2 depicts FTIR spectra for GO and FGO. From the figure, peaks that correspond to typical groups attached to GO sheets, which are epoxide, carboxyl and hydroxyl were observed at 1226, 1602 and 3410 cm^{-1}, respectively. Moreover, the FTIR spectra for GO

illustrates the weak adsorption peak for O-H at 3410 cm^{-1}, which can be attributed to the thermal reduction of GO to enhance the exfoliation of the GO sheets. The bonding between the diamine and the GO sheets may occur as a ring opening reaction between the amino group in the diamine and the epoxide group on the surface of GO. Another possible reaction is the interaction between the amino group in the diamine and the carboxyl group on the edge of GO sheets to form Ammonium carboxylate or salt. FTIR spectra of FGO confirms the bonding between the diamine and GO sheets. For instance, the strong adsorption peak around 3000 cm^{-1}, represents C-H stretching, which is an indication of the existence of aromatic diamine in FGO. In addition, the new adsorption peak at 1500 cm^{-1}, confirms the C-N bonding resulted from the ring opening reaction between the Diamine and the epoxide group on the basal plan of GO. Finally, the attenuation in the intensity of the epoxide adsorption peak at 1226 cm^{-1} confirm the reduction in the density of the epoxide group on the basal plan of GO and this in addition to the increased density of the hydroxyl group at 3410 cm^{-1} can be attributed to the ring opening reaction. XRD was also utilized to examine the bonding between diamine and GO sheets as depicted in Figure 9.3. XRD patterns of GO and FGO confirms the influences of the bonding between the diamine and the GO sheets on the crystal structure and the d-spacing, where the d-spacing increased from 7.96 Å for GO sheets to 22.41 Å for FGO based on Bragg's law.

FTIR and XRD were also utilized to confirm the completion of the curing process of the Epoxy composites. The FTIR spectra depicted in Figure 9.4, clearly show some characteristic peaks such as the peaks at 3380 cm^{-1} (-OH stretching), which confirm the curing of the Epoxy resin in addition to the peaks at 1508 cm^{-1} and 1609 cm^{-1} (C–C skeletal stretching), 915 cm^{-1} (epoxide ring). XRD depicted in Figure 9.5, represent a typical XRD patterns for Epoxy composites, where a broad amorphous peak around 2θ value 10° - 30°, which attributes to the homogeneously amorphous of Epoxy. Furthermore,

the amplitudes of the diffraction peaks for E/GO and E/FGO indicate that the degree of crystallinity of Epoxy is reserved after the incorporation of GO and FGO in the polymeric matrices.

Dispersion of GO and FGO filler in the E/GO and E/FGO composites was observed and captured using TEM as depicted in Figure 9.6. The TEM images illustrates the influences of the surface modification of GO, which can be observed as significant improvement in dispersion and exfoliation of the filler in the Epoxy composites. GO sheets were manifests in thick stacks of GO layers, whereas the attachment of the grafted amino group on the surface of FGO enhances the degree of dispersion and thin sheets of FGO are observed in the E/FGO composites. The impact of GO functionalization on the degree of dispersion and exfoliation can be attributed to enhanced surface interaction between the amino group on FGO and the Epoxy group in the resin.

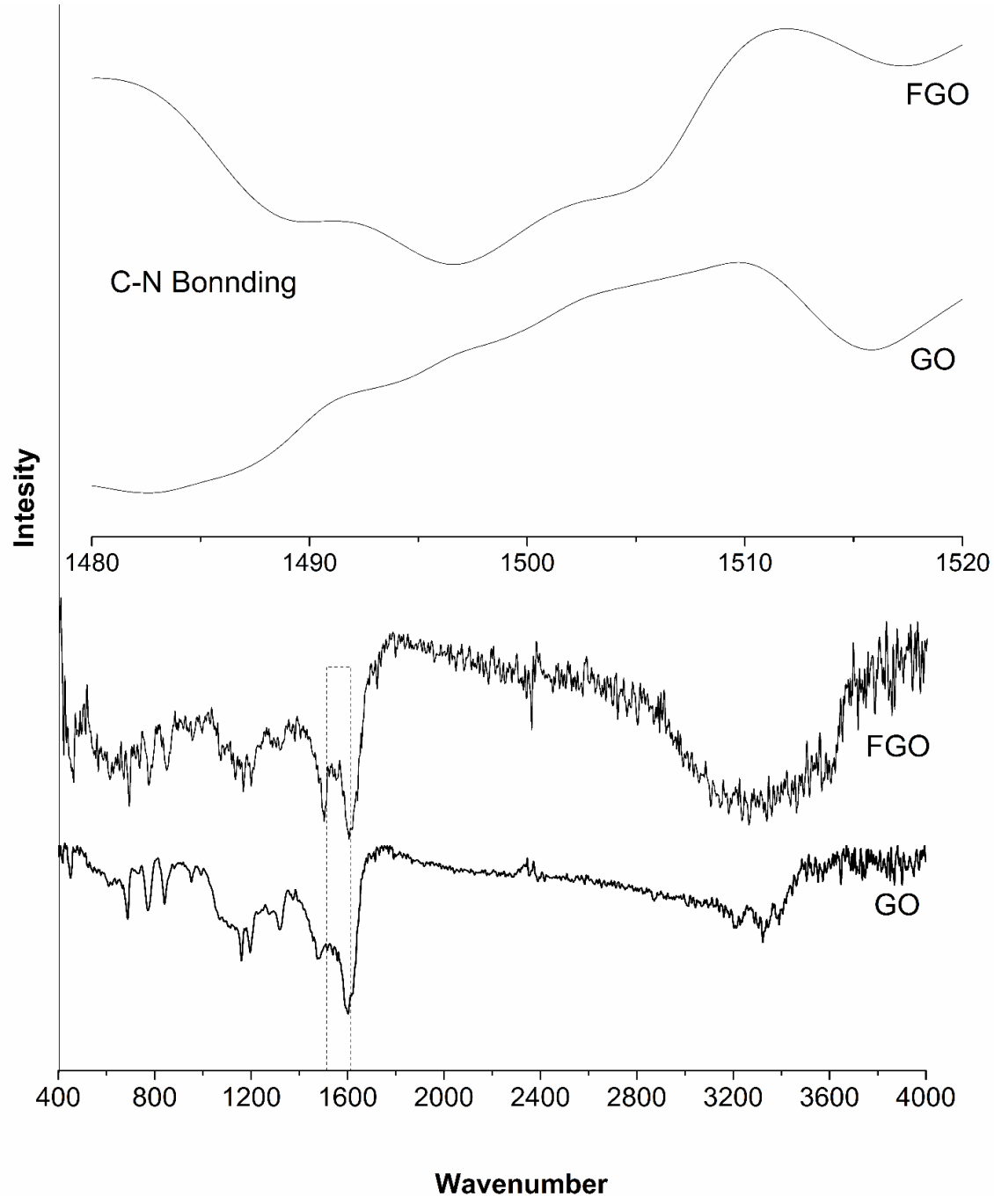

Figure 9.2: FTIR spectra of GO and FGO composites.

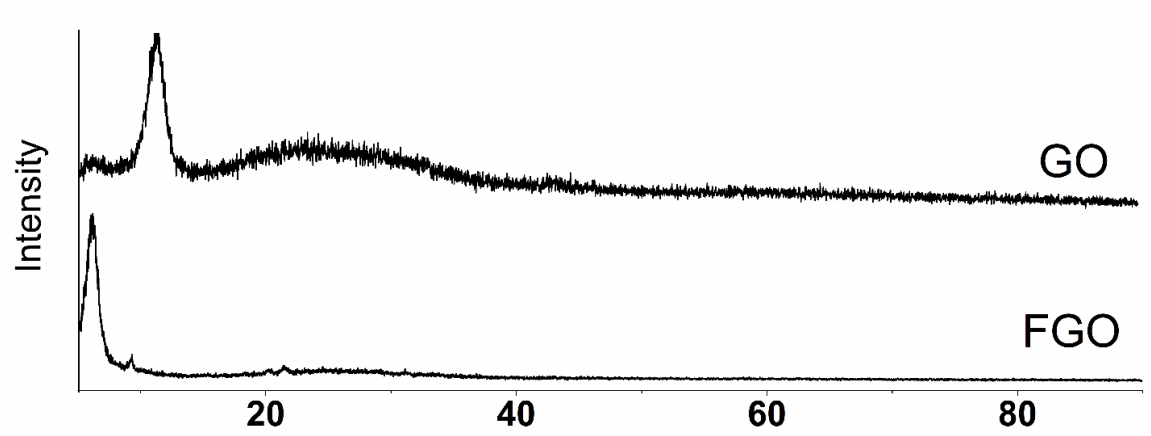

Figure 9.3: XRD patterns of GO and FGO composites

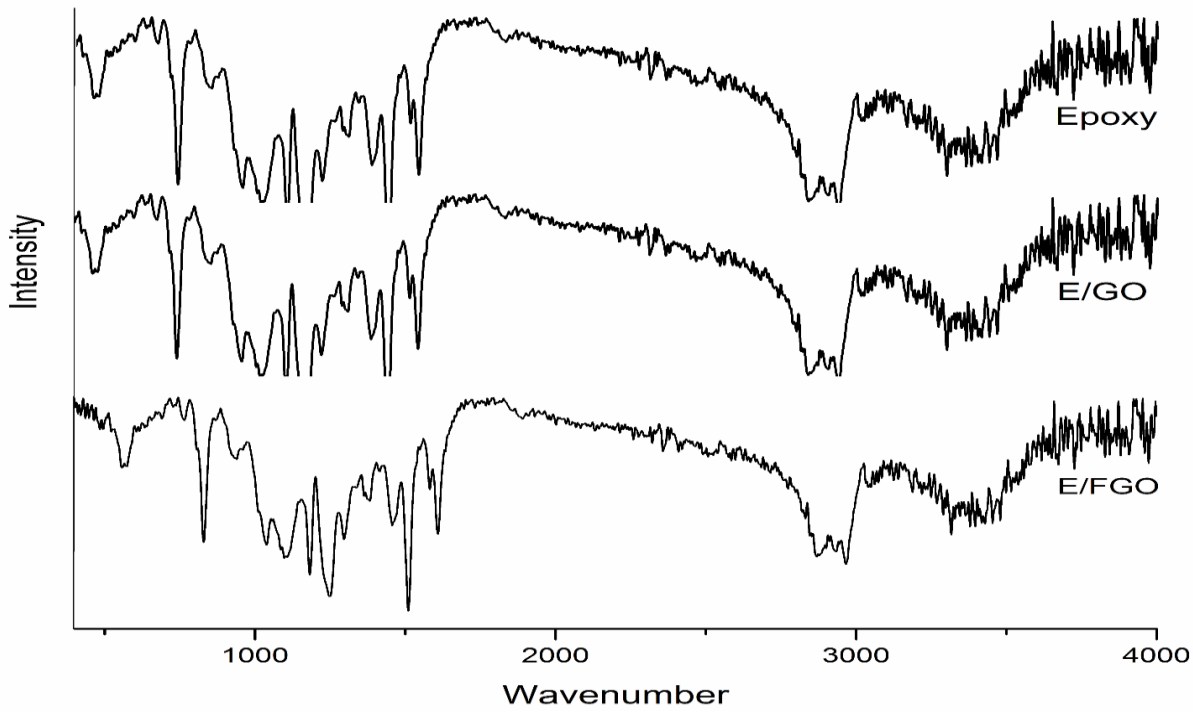

Figure 9.4: FTIR spectra of Epoxy, E/GO and E/FGO composites.

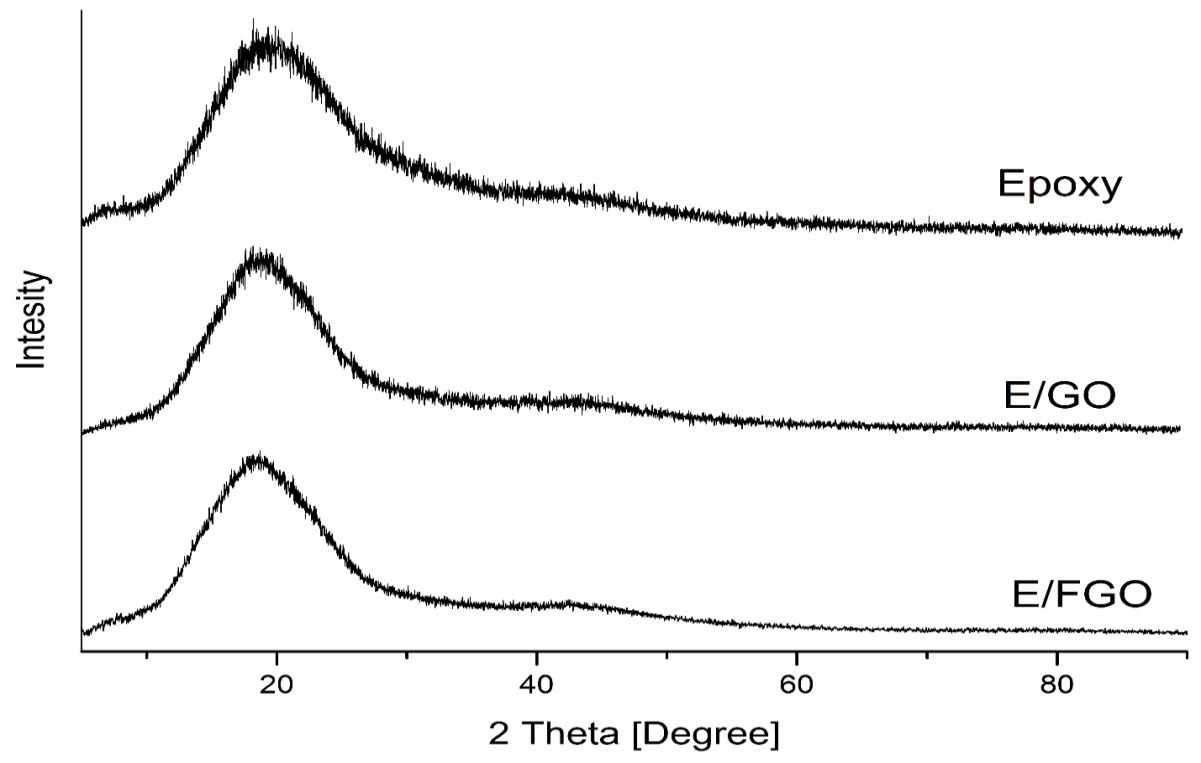

Figure 9.5: XRD patterns of Epoxy, E/GO and E/FGO composites.

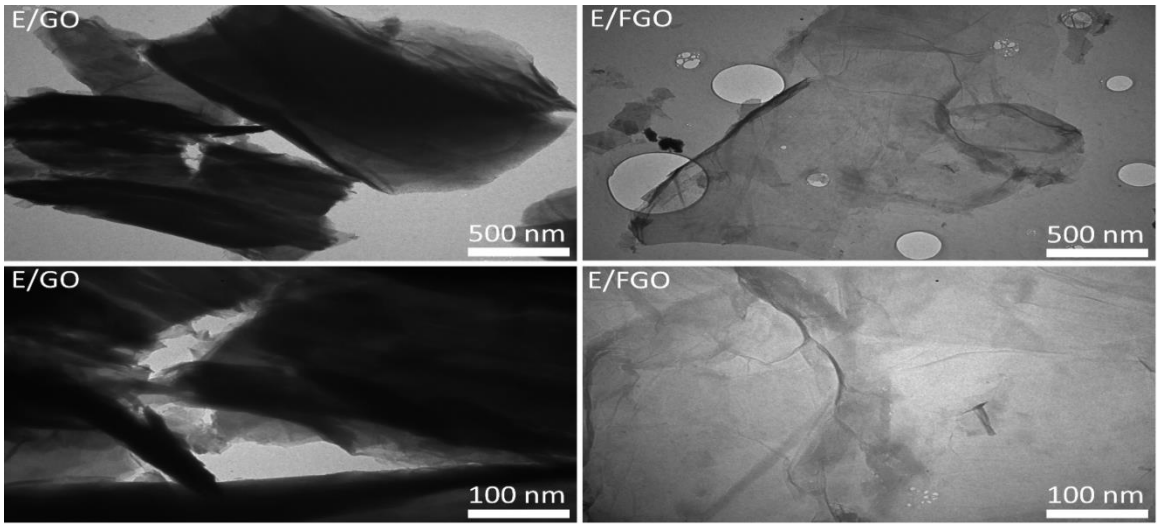

Figure 9.6: TEM images of E/GO and E/FGO.

9.3.2 Coating Adhesion

The main objective of coating metal substrates is to protect the coated metals from corrosion by aggressive corrosion agents in the surrounding environment. However, poor interface adhesion between the metal substrates and the protective coating may result in void spaces at the interface between the coating and the coated substrate, where corrosive elements might accumulate and accelerate the corrosion process. Therefore, one of the critical properties of protective coating that needs to be assessed before testing the corrosion resistance ability of a protective coating in corrosive medium is interface adhesion. Here, the interface adhesion between the CRS substrate and the prepared protective composite coatings is examined and evaluated according to ASTM D3359 using adhesion tape test kit. In this test, perpendicular cuts are made on the coating surface using standard blade (11-teeth with teeth spacing of 1 mm) and the adhesion tape is applied on the surface. After peeling off the adhesion tape, the condition of the coating where the cuts were made are examined and the interface adhesion property of the coating is evaluated based on the amount of peeled materials from the coating.

Here, interface adhesion tests were performed after exposing the protective coatings to 3.5% NaCl solution for 90 days at room temperature to confirm the long-term interface adhesion properties of the prepared coatings. Figure 9.7, illustrates the post adhesion test results for Epoxy, E/GO and E/FGO. From the figure, no peelings were observed on any of the coatings and therefore, all coatings were rated at 5B rating (0% peeling) according to ASTM standard.

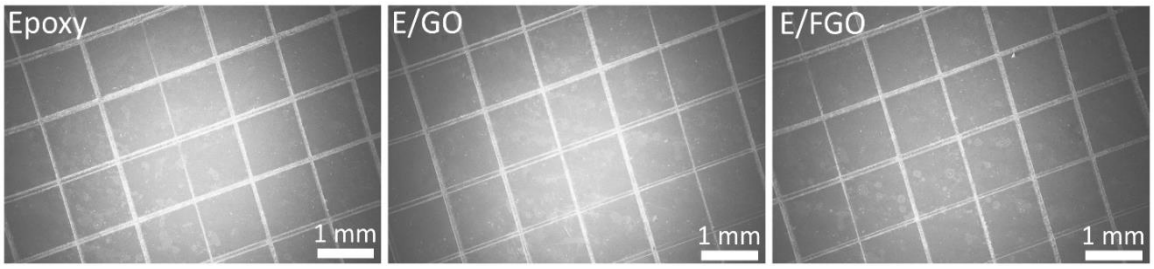

Figure 9.7: SEM images of post-adhesion tests of Epoxy, E/GO and E/FGO coated CRS substrates

9.3.3 Gravimetric Analysis

The long-term corrosion resistance properties of the prepared protective coatings were examined by conducting weight loss measurements in 3.5% NaCl solution at 22° C for 90 days. The study permits the calculation of the corrosion rates (R_{corr}) based on the variations in the initial and final weight of coated CRS substrates after the exposure period using equation (9.1). In addition to the corrosion rates, the weight loss measurements were utilized to calculate the protection efficiency (P_{EF}) of the prepared protective composites coatings by comparing the corrosion rates for bare and coated CRS substrates using equation (9.2).

$$R_{corr} = \frac{W_0 - W}{Axt} \qquad (9.1)$$

$$P_{EF}[\%] = \left(1 - \frac{R_{corr}}{R^{\circ}_{corr}}\right) x100 \qquad (9.2)$$

In the above equations, A is the exposed surface area of the bare and coated CRS substrates (1 cm^2), t is the exposure time (90 days), R_{corr} and R°_{corr} are the corrosion rates of the coated and bare CRS substrates, respectively, while W_0 and W are the weight (mg) before and after exposure to the corrosive medium. The data associated with the weight loss measurements are reported in Table 9.1 and in

addition to the corrosion rates and protection efficiencies, the triplicate measurements allow the calculation of the standard deviation of the corrosion rates ($R_{corr, STD}$).

Table 9.1: Weight loss measurements for bare CRS, Epoxy, E/GO and E/FGO coated CRS substrates in a 3.5 wt.% NaCl solution

Sample	W_0 mg	W mg	R_{corr} $mg.cm^{-2}.d^{-1}$	$R_{corr, STD}$ $mg.cm^{-2}.d^{-1}$	P_{EF} %
CRS	110.3	72.1	0.42	0.02	-
Epoxy	130.5	126.8	0.04	0.04	90.3
E/GO	132.8	131.1	0.018	0.005	95.5
E/FGO	132.1	131.9	0.003	0.001	99.5

The weight loss measurement results reported in Table 9.1 illustrate the possibility of enhancing the corrosion resistance of epoxy coatings by the incorporation of a nanofiller such as GO. This can be clearly observed as descent in corrosion rate in addition to enhancement in corrosion protection efficiency. Furthermore, the results reported in Table 9.1 clearly demonstrate the advantage of GO surface modification, where the incorporation of FGO in the epoxy resin leads to further attenuation in the corrosion rates and further enhancement in protection efficiency. In addition to the enhancement in corrosion resistance, the results illustrate the superior reproducibility of corrosion resistance performance of E/FGO compared to E/GO, which can be observed as lower magnitude of $R_{corr, STD.}$

9.3.4 Impedance Measurements

Electrochemical impedance spectroscopy is one of the main techniques utilized to investigate the electrochemical behavior of bare or coated metal substrates. Here, the electrochemical behavior of bare

and coated CRS is compared to examine the corrosion resistance properties of the prepared protective coatings. An impedance study involves passing an alternative current through electrical circuit that may contain various element such as resistances, insulators and capacitors or a combination of these elements. The observed outcome resistance of passing the alternative current through the circuits is a complex output known as impedance. In corrosion experiments, the alternative current is forced through the bare or coated metal substrates over a range of frequencies and the observed complex output is reported as the impedance of the bare or coated metal substrates. Furthermore, equivalent circuits with specific combination of electrical elements such as resistors, insulator and capacitors can be utilized to fit the raw impedance data, where the order of combination and the magnitude of each element in the equivalent circuit control the feature of the fitting. Once the best fitting of raw impedance data for bare and coated CRS substrates are captured, the variations in the magnitude of the various elements of the equivalent circuits can be used to evaluate the corrosion protection properties of the protective coatings.

After collecting raw impedance data for bare and coated CRS substrates, an equivalent circuit with specific combination as depicted in Figure 9.8 was used to fit the raw impedance data. The type and order of electrical elements in the equivalent circuit was chosen in order to obtain the best fitting for raw impedance data, where R_s represents the resistance of the 3.5% NaCl electrolyte solution, R_{ch} represents the charge transfer resistance of the bare or coated metal substrates and C represents a double layer capacitor. The magnitudes of the different elements in the equivalent circuits in addition to the frequencies of the alternative current signal (ω) were used to fit the raw impedance data using equation (9.3).

$$Z = Z' + jZ'' = R_s \frac{R_{ch}}{1+(R_{ch}\times C\times \omega)^2} + j\frac{{R_{ch}}^2\times C\times \omega}{1+(R_{ch}\times C\times \omega)^2} \qquad (9.3)$$

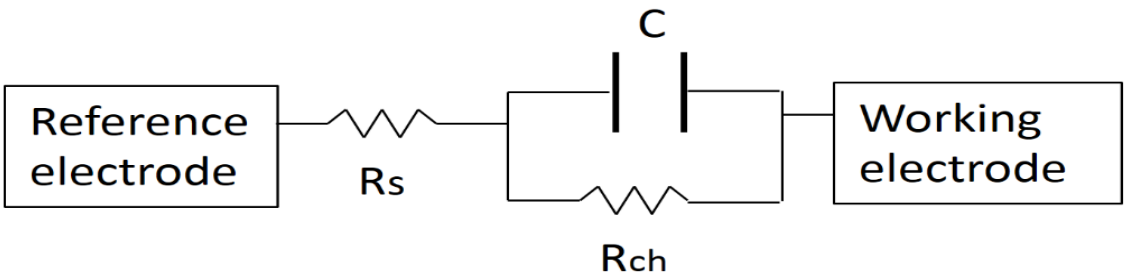

Figure 9.8: Equivalent circuits used to fit raw electrochemical impedance data

The collected raw and fitting impedance data are depicted in Figure 9.9, which is known in corrosion studies as the Nyquist plots, where the real and the imaginary parts of the complex impedance data are reported. In general, an increase in the size of the impedance semi-circle represents an enhancement in corrosion resistance. The Nyquist plots clearly illustrates the possibility of enhancing the corrosion resistance behavior of CRS by coating the metal substrates with Epoxy. Furthermore, the reported results in the Nyquist plots demonstrates that the corrosion protection property of Epoxy can be excelled by the incorporation of GO in the polymeric matrix. Nevertheless, the plots clearly indicate that such an enhancement in corrosion protection can be further surpassed by surface modification of GO. This can be observed for the case of E/FGO composites coatings as a significant increase in the magnitude of the real resistivity parts at the lowest recorded frequencies.

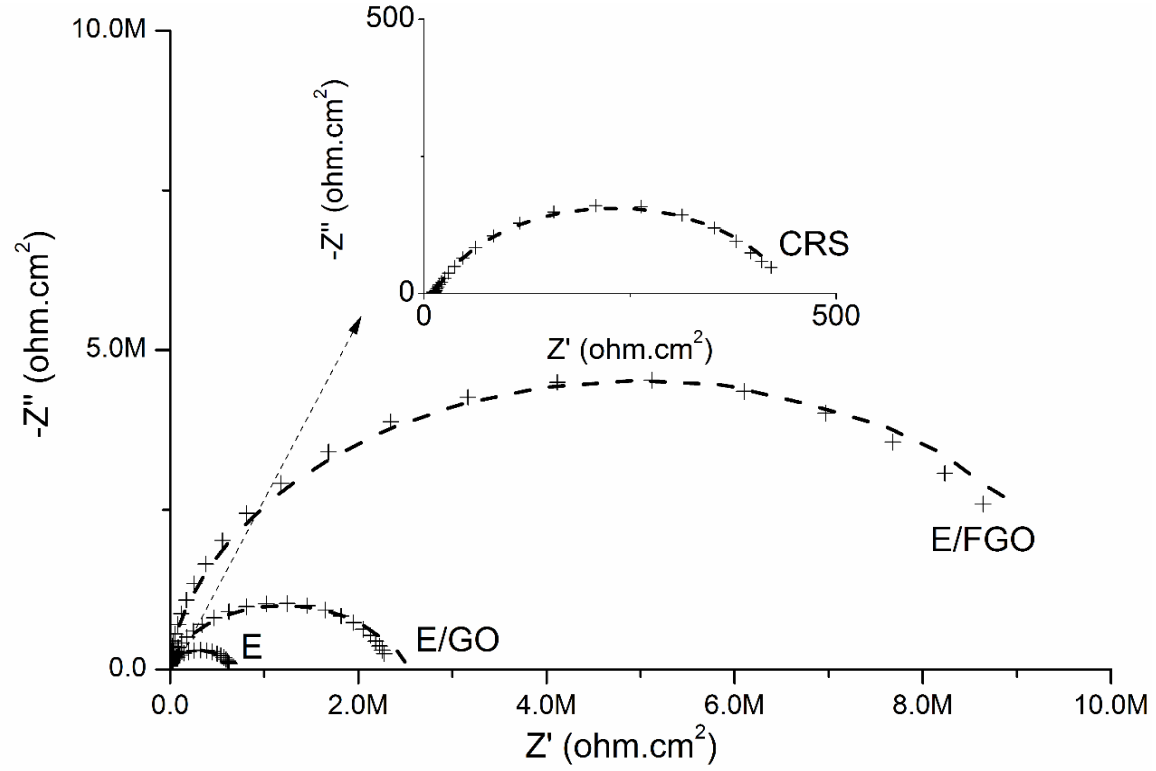

Figure 9.9: Nyquist plots for bare CRS, Epoxy, E/GO and E/FGO coated CRS substrates

In addition to the qualitative analysis of the Nyquist plots, quantitative analysis can be carried out on the magnitudes of the various elements of the equivalent circuits to evaluate the variation in corrosion protection behavior of the prepared protective composite coatings. It is important to note that the choice of the elements in the equivalent circuit in addition to the unique combination of these elements were adopted in order to obtain the best fitting results for the raw impedance data for bare and coated CRS substrates. All raw impedance data were collected in triplicates and therefore, the magnitudes of the mean values of the various elements of the equivalent circuit for all samples are reported in Table 9.2. The reported results noticeably illustrate the advantage of incorporating GO in the Epoxy matrix in the corrosion protection property of Epoxy. However, The results also demonstrates the significant values of functionalization of GO on the corrosion mitigation property, where the charge transfer resistance

increased from 433.6 *ohm.cm²* for bare CRS to 6.5×10^5 *ohm.cm²* for Epoxy, 2.3×10^6 *ohm.cm²* for pristine E/GO and 9.5×10^6 *ohm.cm²* for E/FGO coated CRS. The repeatability of the collected raw impedance data is illustrated by the small values of the standard deviations of the charge transfer resistance ($R_{ch,\ STD}$) for all samples.

Table 9.2: Electrochemical corrosion parameters obtained from equivalent circuit for EIS raw measurements for bare CRS, Epoxy, E/GO and E/FGO coated CRS in 3.5 wt.% NaCl solution.

Sample	R_S Ω.cm²	C F	R_{ch} Ω.cm²	$R_{ch\ ,\ STD}$ Ω.cm²
CRS	18.3	$4.5x10^{-04}$	433.6	4
Epoxy	17.9	$6.7x10^{-11}$	$6.5x10^5$	110
E/GO	18.0	$1.24x10^{-10}$	$2.34x10^6$	700
E/FGO	18.2	$6.3x10^{-11}$	$9.57x10^6$	220

Bode plots are another approach to represent impedance behavior of bare and coated metals and can be utilized to assess the corrosion resistance properties of the prepared protective composite coatings. In Bode plots, the real part of impedance (Z_{real}) is presented versus the entire frequency range of the impedance EIS test in logarithmic scales as depicted in Figure 9.10(a), while Figure 9.10(b) depict the phase plots of raw impedance data. The corrosion resistance property of a coating can be evaluated based on the Z_{real} values at the lowest recorded frequency and comparing the Z_{real} values for the various coatings demonstrate the variation in the corrosion protection properties of the different coatings. The results presented in Figure 9.10(a), illustrates the advantages of incorporating FGO in the Epoxy resin over pristine GO, where the utilization of FOG remarkably increased the value of log Z_{real} at the lowest

frequencies from 2.6 *ohm.cm*^{2} for bare CRS to 5.8 *ohm.cm*^{2} for Epoxy, 6.43 *ohm.cm*^{2} for pristine E/GO and 7.0 *ohm.cm*^{2} for E/FGO coated CRS.

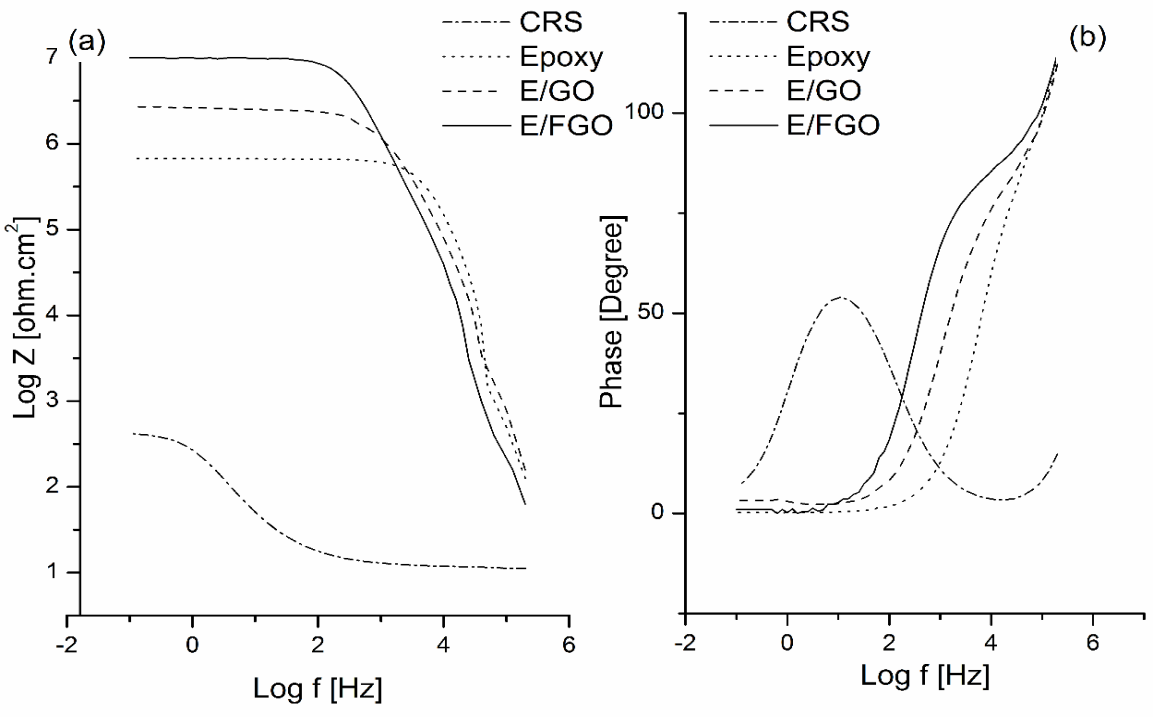

Figure 9.10: (a) Bode and (b) phase plots for bare CRS, Epoxy, E/GO and E/FGO coated CRS substrates

The reported EIS results in various forms illustrates the possibility of prolonging the life span of CRS in a Chloride rich environment by coating the metal substrate with Epoxy. Furthermore, the results show that the corrosion resistance property of Epoxy can be further enhanced by the incorporation of GO as a filler in the polymeric matrix. This enhancement in corrosion protection can be attributed to the superior barrier property of GO sheets [64], which may prolong the pathways corrosion agents follow to reach the interface between the metal substrates and the protective coating. Moreover, the

reported data clearly demonstrates the fact that corrosion property of E/GO composite coating can be further excelled by functionalization of GO. This further enhancement in corrosion resistance property of E/FGO can be attributed to improved dispersion of FGO in the Epoxy matrix, which may further attenuate the corrosion rate by increasing the tortuosity pathway the corrosive agents follow to reach the coated metal substrate.

9.3.5 Cyclic Voltammetry

Another widely utilized electrochemical approach in corrosion studies is cyclic voltammetry (CV) or potentiodynamic measurements, where the potential of the working electrode is scanned over a range of potential difference against the constant potential of the reference electrode in order to examine the anodic and cathodic behavior of the working electrode. After immersing the working electrode in the electrolyte, the potential of the working electrode was allowed to stabilize for 30 min and the stable potential of the working electrode was recorded as the open circuit potential (OCP) before conducting the test. It should be noted that CV is a destructive test and therefore, a new electrolyte solution was prepared for each experiment. Starting from OCP and scanning in the anodic direction, CV test was conducted by scanning the potential of the working electrode from -0.5 V to 0.5 V around the OCP at a rate of 20 mV/Min.

Even though the CV test was conducted over a wide range of potential, only the area where the potential of the working electrode shifts from anodic to cathodic behavior, which is known as the Tafel plots are presented in Figure 9.11. The potentiodynamic results depicted in the figure allow the extraction of significant corrosion parameters such as corrosion potential (E_{corr}) and corrosion current (I_{corr}). Furthermore, the triplicates measurements for each sample facilitate the examination of the reproducibility of the raw data by calculating the standard deviation of E_{corr} ($E_{corr, STD}$) and I_{corr} ($I_{corr, STD}$)

as reported in Table 9.3. Furthermore, the extracted corrosion currents were implemented in equation (9.4), which is known as the Stern-Geary equation to compute the polarization resistances (R_p) of the bare and coated CRS substrates. Finally, the extracted corrosion potential was also utilized and compared to compute the protection efficiency (P_{EF}) of the prepared protective coatings using equation (9.5).

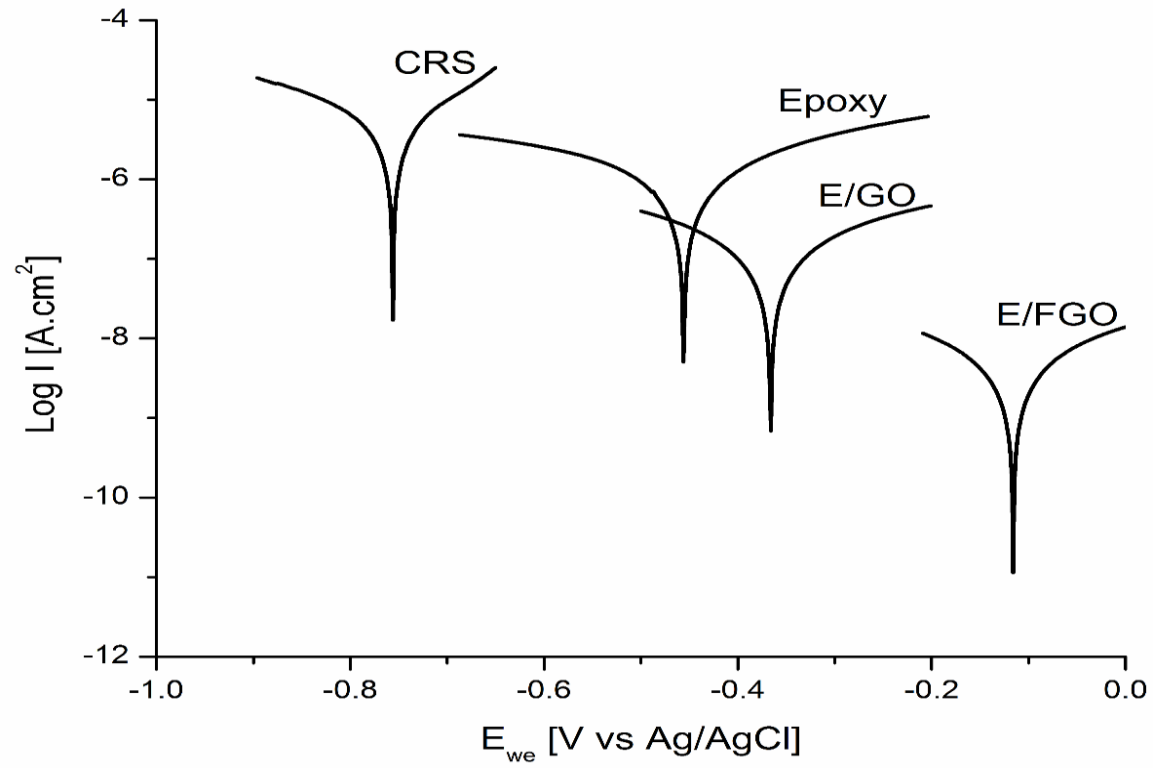

Figure 9.11: Tafel plots for bare CRS, Epoxy, E/GO and E/FGO coated CRS substrates

$$R_P = \frac{(b_a x b_c)}{2.303x(b_a+b_c)xI_{corr}} \qquad (9.4)$$

$$P_{EF}[\%] = (1 - I_{corr}/I^{\circ}_{corr})x100 \qquad (9.5)$$

In the above equation, b_a/b_c are the anodic and the cathodic Tafel slope (dE/dlog I), respectively, where the intersection of the extrapolations of the linear portions of the slopes indicates the corrosion current. In equation (9.5), I°_{corr} and I_{corr} are corrosion current of bare and coated CRS substrates, respectively. The quantitative variations in the corrosion parameters reported in Table 9.3 can be utilized to evaluate the corrosion protection properties of the prepared protective composite coatings. For instance, a positive shift in E_{corr} and R_p in addition to a drop in I_{corr} represents an enhancement in corrosion resistance.

Table 9.3: Electrochemical corrosion parameters obtained from cyclic voltammetry measurements for bare CRS, Epoxy, E/GO and E/FGO coated CRS in a 3.5 wt.% NaCl solution.

Sample	E_{corr} mV vs Ag/AgCl	$E_{corr,STD}$ V vs Ag/AgCl	I_{corr} $\mu A/cm^2$	$I_{corr,STD}$ $\mu A/cm^2$	b_a	b_c	R_P $\Omega.cm^2$	P_{EF} %
CRS	-756	0.03	6.78	0.003	162.6	269.6	6.5	-
Epoxy	-537	1.9	0.55	0.001	293.4	396.5	133.1	91.9
E/GO	-366	8.5	0.099	0.007	219.3	208.8	469.1	98.5
E/FGO	-120	2.1	0.005	0.002	276.3	251.6	11436	99.9

The potentiodynamic measurements results depicted in Figure 9.11 and reported in Table 9.3, illustrates the noble corrosion resistance property of epoxy. In addition, the results demonstrated that the noble corrosion resistance of epoxy can be further enhanced by the incorporation of GO as a filler in the polymeric matrix. Furthermore, such an imperative property of a protection coating can be further

excelled by functionalization of GO and this can be clearly observed in the case of using E/FGO, where the utilization of FGO leads to remarkable positive shift in E_{corr} and R_p in addition to a significant attenuation in I_{corr}.

It is worth noting, even though E/GO enhances corrosion protection over pristine epoxy resin, the triplicate measurements indicate the poor reproducibility of the CV results for E/GO as indicated by the higher magnitude of $E_{corr,\ STD}$. On the other hand, the superior corrosion mitigation property of E/FGO was combined with a remarkable reproducibility as indicated by the by the small E_{corr} value as reported in Table 9.3. The advanced corrosion protection property of E/FGO can be attributed to the shielding property of FGO as well as the improved degree of dispersion of the filler in E/FGO as indicated by the TEM images, while the highly dispersed FGO sheets might be responsible for the noble reproducibility of the CV results.

9.3.6 Thermal Stability

The influences of the incorporated GO and FGO in the thermal stability of the prepared composites coatings are evaluated using DSC and TGA techniques. DSC was utilized to examined the influences of GO and FGO on the glass transition temperature (T_g) of the composites and the results are depicted in Figure 9.12. From the figure, it can be observed that the incorporation of GO slightly increases the T_g from 80.5 to 82.6° C, while the incorporation of FGO causes a more significant increase in T_g to 86.8° C. The influence of GO and FGO on T_g can be attributed to the restriction of the mobility of the polymer chains by the filler [84]. In addition to T_g, the impacts of the fillers on the thermal degradation of E/GO and E/FGO composite coatings were examined using TGA and here too, the incorporation of the fillers enhances the thermal stability of the composites as indicated by increase in the onset temperature (T_{onset}), which is the temperature at which the composites degrade by 5% of the initial

weight as depicted in Figure 9.13. Moreover, the TGA results indicates that functionalization of GO further excels the thermal stability of the epoxy composite, where T_{onset} increased from 354.5 ˚C for Epoxy to 359.4 ˚C and 362.3 ˚C for E/GO and E/FGO, respectively.

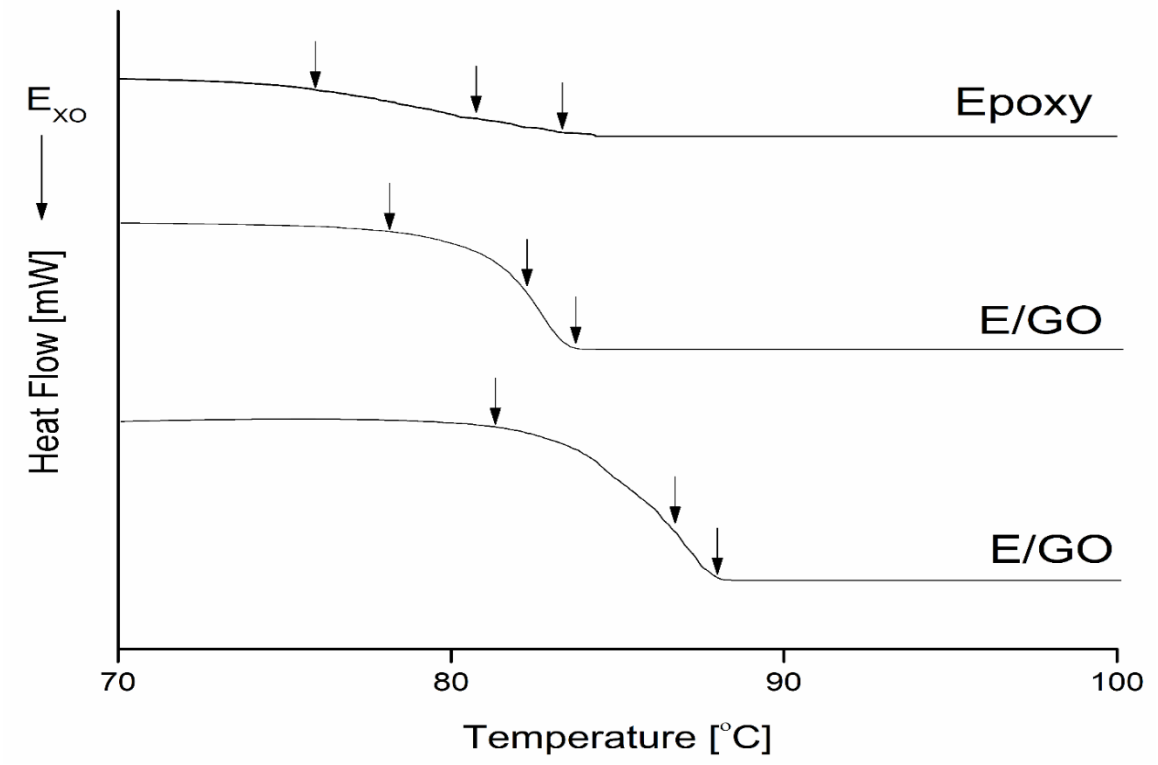

Figure 9.12: DSC thermograms of Epoxy, E/GO and E/FGO composites coatings

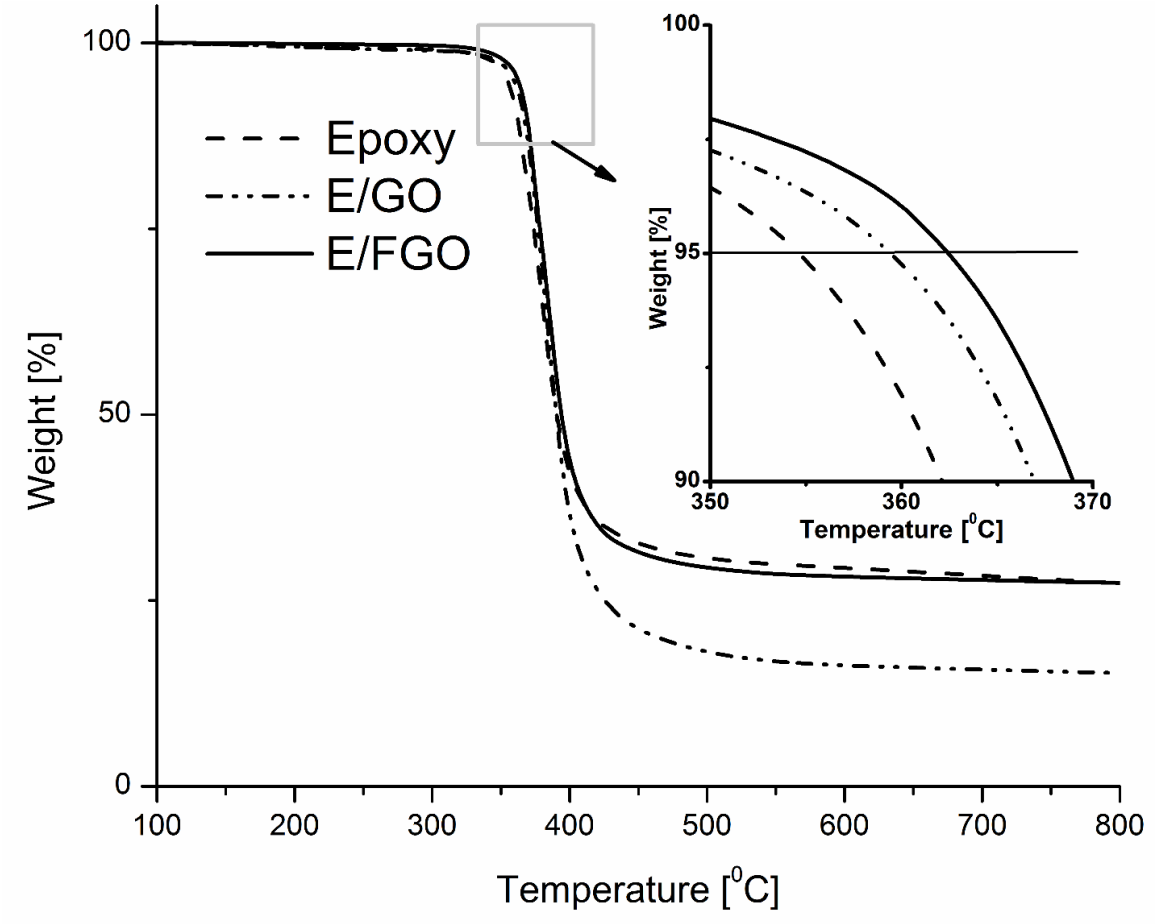

Figure 9.13: TGA thermograms of Epoxy, E/GO and E/FGO composites coatings

Table 9.4: Thermal analysis results for Epoxy, E/GO and E/FGO composites

Sample	Initial weight	T_{onset}	$T_{50\%}$	Residue	T_g
	mg	°C	°C	%	°C
Epoxy	41.1	354.5	390.5	27.31	80.5
E/GO	31.2	359.4	390.4	15.22	82.7
E/FGO	35.02	362.3	394.04	27.35	86.8

The positive impacts of GO and FGO can also be attributed to the restriction in chain's mobility in addition to the possible interaction between the amino group in epoxy with the epoxy/ hydroxyl groups on GO or the possible direct bonding between the grafted amino group on FGO and Epoxy.

9.3.7 Impact resistance

Impact resistance of a protective composite coating is another property that can be examined in addition to corrosion resistance and thermal stability in order to evaluate the durability of the coatings and the possibility of utilizing the coatings in various applications, where the coatings might be exposed to sudden impacts. The impact test was conducted according to the ASTM D2794 to analyze the influences of GO and FGO on the impact resistance of E/GO and E/FGO composites. Several previous studies have examined the effect of GO and graphene on the mechanical properties of epoxy composites [82], [87]–[89], however; the objective here is to examine the impacts of GO functionalization on the resistance of epoxy composite to sudden deformation. Figure 9.14 depicts the elevations at which the composites coatings fail five times. The impact resistance results revealed that the incorporation of GO in the epoxy matrix may enhances the impact resistance property of the resin. Moreover, the surface modification of GO further improves the impact resistance as observed in the case of E/FGO. These effects of GO and FGO on the impact resistance of epoxy can be attributed to the increase/decrease of toughness/elasticity of the epoxy composite after the incorporation of the fillers.

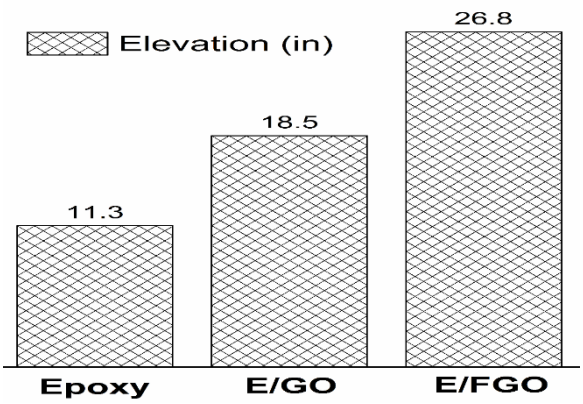

Figure 9.14: Impact resistance test results for Epoxy, E/GO and E/FGO composites coatings

9.4 Conclusion

E/GO and E/FGO composites were synthesized using situ pre-polymerization approach and evaluated as protective coatings on CRS substrates. The study demonstrates that the corrosion resistance property of Epoxy coating can be excelled by the incorporation of pristine GO sheets in the resin, where the GO sheets may shield corrosive agents such as Oxygen and Chloride ions. Furthermore, surface functionalization of GO sheets with diamine may further enhance the corrosion protection properties. This enhancement in the corrosion protection properties may be attributed to the interaction between the amino group in the diamine and the epoxide group in the Epoxy resin, which improve the degree of dispersion of FGO in the polymeric matrix and consequently prolong the pathways corrosive agents follow to reach the coated metal substrate. Moreover, the surface modification of GO and the interaction between the FGO sheets and the Epoxy resin may also enhance thermal stability of the composites as well as resistance to sudden deformation.

Chapter 10

Conclusions and Future Work

10.1 Summary of Contributions and Concluding Remarks

A number of corrosion protection polymer composites based coatings product were synthesized and evaluated on different metal substrates that are utilized in oil and gas industry in addition to a wide range of applications. The protective coatings products studied in this research project and the contributions of the studies on the different products can be listed and summarized as follow.

- Polyetherimide-Graphene (PEI/G) composites on Copper substrates:
    - Enhanced the inhibition of copper corrosion by coating with polyetherimide-graphene nanocomposite containing a very low loading of graphene.
    - Analyzed the electrochemical behavior of bare copper, copper coated with polyetherimide, and copper coated with polyetherimide-graphene nanocomposites.
    - Discussed the mechanism by which graphene enhances the anticorrosion performance of the coating.
    - Evaluated the adhesion and the long term performances of the prepared protective coatings.
    - Illustrated the variation in the performances of the prepared coatings as well as the drawbacks associated with varying the load of Graphene.

- Epoxy-Graphene (E/G) composites on Stainless Steel type 304 (SS304):
    - Study the influences of an epoxy coating on the electrochemical behavior of Stainless Steel 304.
    - Evaluated the possibility of enhancing the corrosion protection property of epoxy by the incorporation of graphene.
    - Investigated the variation in the corrosion protection efficiencies of epoxy/graphene coatings at different loads of graphene.
    - Demonstrated the impacts of the load of graphene on imperative properties of epoxy such as interface adhesion, flexibility, impact and UV resistances.
    - Evaluated the influences of graphene on thermal behavior of epoxy.
    - Illustrated how the degree of dispersion in the polymeric matrix may vary with the load of graphene.
- Electro-active Epoxy-Glass Flake (EE/GF) composites on Cold Rolled Steel (CRS):
    - Studied the influences of an electroactive Epoxy coating on the electrochemical behavior of CRS.
    - Evaluated the possibility of enhancing the corrosion protection property of electroactive Epoxy by the incorporation of Glass Flake.
    - Investigated the variation in the corrosion protection efficiencies of electroactive Epoxy/Glass Flake coatings at different loads of Glass Flake.

- Demonstrated the impacts of the load of Glass Flake on imperative properties of electroactive epoxy such as interface adhesion, impact resistance and UV degradation.
- Illustrated how the degree of dispersion in the polymeric matrix may vary with the load of Glass Flake.

- Epoxy-Functional Glass Flake (E/FGF) composites on Cold Rolled Steel (CRS):
  - Studied the influences of an Epoxy coating on the electrochemical behavior of Cold rolled steel (CRS).
  - Evaluated the possibility of enhancing the corrosion protection property of Epoxy by the incorporation of Glass Flake (GF).
  - Investigated the variation in the corrosion protection efficiencies of Epoxy/GF coatings at different loads of GF.
  - Demonstrated the possibility of modifying the surface of GF by attaching Amino grafted saline functional group and study the role of the functionalization of GF on corrosion mitigating properties of Epoxy/Functional Glass Flake (E/FGF) composites.
  - Studied the influences of the load of FGF on the corrosion protection properties of E/FGF composites.
  - Illustrated the role of functionalization of GF on the degree of dispersion in the polymeric matrix.
  - Examined interface adhesion between Epoxy. E/GF and E/FGF E coatings and CRS substrates and illustrates the influences of the load of GF/FGF on such a significant property.

- Evaluated the influences of the incorporation and the load of GF/FGF on thermal behavior of Epoxy.

- Epoxy-Functional Graphene (E/FGO) composites on Cold Rolled Steel (CRS):
  - Examined the corrosion protection property of an Epoxy coating on Cold rolled steel (CRS).
  - Evaluated the possibility of enhancing the corrosion protection property of Epoxy by the incorporation of Graphene Oxide (GO).
  - Investigated the variation in the corrosion protection efficiencies of Epoxy/GO coating.
  - Demonstrated the possibility of modifying the surface of GO by attaching Amino grafted functional group and study the role of the functionalization of FGO on corrosion mitigating properties of Epoxy/Functional Graphene Oxide (E/FGO) composites.
  - Studied the influences of the load of FGO on the corrosion protection properties of E/FGO composites.
  - Illustrated the role of functionalization of GO on the degree of dispersion in the polymeric matrix.
  - Examined interface adhesion between Epoxy. E/GO and E/FGO coatings and CRS substrates.
  - Evaluated the influences of the incorporation of GO/FGO on thermal behavior of Epoxy.

10.2 Future Work

A variety of polymer based composites protective coatings products have been examined and evaluated for corrosion mitigation purposes. The current studies can be further extended to evaluate the prepared protective coatings in different environment. For instance, a salt spray chamber can be utilized in the future to evaluate the long-term corrosion resistance properties of the coatings with artificial defects. In addition, studies can be extended to illustrate the influences of the incorporation of Graphene or Glass Flakes materials on the biofouling property of Epoxy and other polymer resin. In particular, a number of studies in the literature have investigated Graphene based materials for water treatment and the possibility of using Graphene based materials for water purification. A biofouling study requires immersing coated samples in natural sea or ocean water for a long period of time while exposing the testing environment to natural sunlight. Such a study can be conducted in collaboration with a research facility in an area where the exposing the samples to sea or ocean water around the year is possible. In addition to biofouling study, the influences of the incorporated fillers in the mechanical properties of the different types of polymer resin can be evaluated. In this research, studies focused on impact resistance and bending properties, but further testing can be conducted to evaluate properties such as tensile strength and tensile modulus.

Bibliography

[1] G. H. Koch, M. P. H. Brongers, N. G. Thompson, Y. P. Virmani, and J. H. Payer, "Corrosion costs and preventive strategies in the united states. report by cc technologies laboratories, inc. to federal highway administration (fhwa), office of infrastructure research and development," *Off. Infrastruct. Res. Dev. Rep. FHWA-RD-01-156*, 2001.

[2] G. X. Shen, Y. C. Chen, and C. J. Lin, "Corrosion protection of 316 L stainless steel by a TiO2 nanoparticle coating prepared by sol-gel method," *Thin Solid Films*, vol. 489, no. 1–2, pp. 130–136, 2005.

[3] L. Cecchetto, D. Delabouglise, and J. P. Petit, "On the mechanism of the anodic protection of aluminium alloy AA5182 by emeraldine base coatings. Evidences of a galvanic coupling," *Electrochim. Acta*, vol. 52, no. 11, pp. 3485–3492, 2007.

[4] M. L. Zheludkevich, R. Serra, M. F. Montemor, I. M. Miranda Salvado, and M. G. S. Ferreira, "Corrosion protective properties of nanostructured sol-gel hybrid coatings to AA2024-T3," *Surf. Coatings Technol.*, vol. 200, no. 9, pp. 3084–3094, 2006.

[5] G. Moretti, F. Guidi, and G. Grion, "Tryptamine as a green iron corrosion inhibitor in 0.5 M deaerated sulphuric acid," *Corros. Sci.*, vol. 46, no. 2, pp. 387–403, 2004.

[6] J. E. Gray and B. Luan, "Protective coatings on magnesium and its alloys — a critical review," *J. Alloys Compd.*, vol. 336, no. 1, pp. 88–113, 2002.

[7] B. V. Appa Rao, M. Yakub Iqbal, and B. Sreedhar, "Self-assembled monolayer of 2-(octadecylthio)benzothiazole for corrosion protection of copper," *Corros. Sci.*, vol. 51, no. 6, pp. 1441–1452, 2009.

[8] M. Stratmann, R. Feser, and A. Leng, “Corrosion protection by organic films,” *Electrochim. Acta*, vol. 39, no. 8–9, pp. 1207–1214, 1994.

[9] M. I. Redondo and C. B. Breslin, “Polypyrrole electrodeposited on copper from an aqueous phosphate solution: Corrosion protection properties,” *Corros. Sci.*, vol. 49, no. 4, pp. 1765–1776, 2007.

[10] V. K. Mittal *et al.*, “Formation and characterization of bi-layer oxide coating on carbon-steel for improving corrosion resistance,” *Thin Solid Films*, vol. 517, no. 5, pp. 1672–1676, 2009.

[11] M. Segarra *et al.*, “Copper and CuNi alloys substrates for HTS coated conductor applications protected from oxidation,” *Mater. Sci. Forum*, vol. 426–432, no. 4, pp. 3511–3516, 2003.

[12] S. F. Guo, H. J. Zhang, Z. Liu, W. Chen, and S. F. Xie, “Corrosion resistances of amorphous and crystalline Zr-based alloys in simulated seawater,” *Electrochem. commun.*, vol. 24, no. 1, pp. 39–42, 2012.

[13] B. E. Conway, E. Yeager, and R. E. White, “Comprehensive Treatise of Electrochemistry, vol. 4.” Plenum Press, New York, 1981.

[14] H.-H. Strehblow and H.-D. Speckmann, “Corrosion and layer formation of passive copper in alkaline solutions,” *Mater. Corros.*, vol. 35, no. 11, pp. 512–519, 1984.

[15] G. Kilinççeker, B. Yazici, A. B. Yilmaz, and M. Erbil, “Effect of phosphate ions on electrochemical behaviour of copper in sulphate solutions,” *Br. Corros. J.*, 2013.

[16] M. Kabasakaloğlu, T. Kiyak, O. Şendil, and A. Asan, “Electrochemical behavior of brass in 0.1 M NaCl,” *Appl. Surf. Sci.*, vol. 193, no. 1–4, pp. 167–174, 2002.

[17] C.-H. Lee, M. Kato, and A. Usuki, “Preparation and properties of bio-based polycarbonate/clay

nanocomposites," *J. Mater. Chem.*, vol. 21, no. 19, p. 6844, 2011.

[18] A. Usuki, N. Hasegawa, M. Kato, and S. Kobayashi, "Polymer-clay nanocomposites," in *Inorganic polymeric nanocomposites and membranes*, Springer, 2005, pp. 135–195.

[19] P. Pötschke *et al.*, "Improvement of carbon nanotube dispersion in thermoplastic composites using a three roll mill at elevated temperatures," *Compos. Sci. Technol.*, vol. 74, pp. 78–84, 2013.

[20] M. L. Minus, H. G. Chae, and S. Kumar, "Polyethylene crystallization nucleated by carbon nanotubes under shear," *ACS Appl. Mater. Interfaces*, vol. 4, no. 1, pp. 326–330, 2011.

[21] X.-L. Hu, G.-M. Hou, M.-Q. Zhang, M.-Z. Rong, W.-H. Ruan, and E. P. Giannelis, "A new nanocomposite polymer electrolyte based on poly (vinyl alcohol) incorporating hypergrafted nano-silica," *J. Mater. Chem.*, vol. 22, no. 36, pp. 18961–18967, 2012.

[22] J. H. Chen, M. Z. Rong, W. H. Ruan, and M. Q. Zhang, "Interfacial enhancement of nano-SiO 2/polypropylene composites," *Compos. Sci. Technol.*, vol. 69, no. 2, pp. 252–259, 2009.

[23] B. Hojjati and P. A. Charpentier, "Synthesis of TiO 2-polymer nanocomposite in supercritical CO 2 via RAFT polymerization," *Polymer (Guildf).*, vol. 51, no. 23, pp. 5345–5351, 2010.

[24] C.-W. Tang, B. Li, L. Sun, B. Lively, and W.-H. Zhong, "The effects of nanofillers, stretching and recrystallization on microstructure, phase transformation and dielectric properties in PVDF nanocomposites," *Eur. Polym. J.*, vol. 48, no. 6, pp. 1062–1072, 2012.

[25] A. K. Geim and K. S. Novoselov, "The rise of graphene," *Nat. Mater.*, vol. 6, no. 3, pp. 183–191, 2007.

[26] M. Losurdo, M. M. Giangregorio, P. Capezzuto, and G. Bruno, "Graphene CVD growth on

copper and nickel: role of hydrogen in kinetics and structure," *Phys. Chem. Chem. Phys.*, vol. 13, no. 46, pp. 20836–20843, 2011.

[27] S. Park and R. S. Ruoff, "Chemical methods for the production of graphenes," *Nat. Nanotechnol.*, vol. 4, no. 4, p. 217, 2009.

[28] S. Stankovich *et al.*, "Synthesis of graphene-based nanosheets via chemical reduction of exfoliated graphite oxide," *Carbon N. Y.*, vol. 45, no. 7, pp. 1558–1565, 2007.

[29] H. Talsma, M. J. Van Steenbergen, J. C. H. Borchert, and D. J. A. Crommelin, "A novel technique for the one-step preparation of liposomes and nonionic surfactant vesicles without the use of organic solvents. Liposome formation in a continuous gas stream: the ﬠbubbleﬠmethod," *J. Pharm. Sci.*, vol. 83, no. 3, pp. 276–280, 1994.

[30] C. J. Watkinson and J. H. Elvidge, "Method and apparatus for forming glass flakes." Google Patents, 1991.

[31] K.-C. Chang *et al.*, "Room-temperature cured hydrophobic epoxy/graphene composites as corrosion inhibitor for cold-rolled steel," *Carbon N. Y.*, vol. 66, pp. 144–153, 2014.

[32] H. Alhumade, A. Abdala, A. Yu, A. Elkamel, and L. Simon, "Corrosion inhibition of copper in sodium chloride solution using polyetherimide/graphene composites," *Can. J. Chem. Eng.*, 2016.

[33] B. P. Singh, B. K. Jena, S. Bhattacharjee, and L. Besra, "Development of oxidation and corrosion resistance hydrophobic graphene oxide-polymer composite coating on copper," *Surf. Coatings Technol.*, vol. 232, pp. 475–481, 2013.

[34] H. Alhumade, A. Yu, A. Elkamel, L. Simon, and A. Abdala, "Enhanced protective properties

and UV stability of epoxy/graphene nanocomposite coating on stainless steel," *Express Polym. Lett.*, vol. 10, no. 12, p. 1034, 2016.

[35] T. Kuilla, S. Bhadra, D. Yao, N. H. Kim, S. Bose, and J. H. Lee, "Recent advances in graphene based polymer composites," *Prog. Polym. Sci. Vol.*, vol. 35, no. 11, pp. 1350–1375, 2010.

[36] R. K. Singh Raman *et al.*, "Protecting copper from electrochemical degradation by graphene coating," *Carbon N. Y.*, vol. 50, no. 11, pp. 4040–4045, 2012.

[37] A. R. BOCCACCINI *et al.*, "The electrophoretic deposition of inorganic nanoscaled materials a review," *J. Ceram. Soc. Japan*, vol. 114, no. 1325, pp. 1–14, 2006.

[38] O. O. der Biest and L. J. Vandeperre, "Electrophoretic deposition of materials," *Annu. Rev. Mater. Sci.*, vol. 29, no. 1, pp. 327–352, 1999.

[39] D. J. Hourston and J. M. Lane, "The toughening of epoxy resins with thermoplastics: 1. Trifunctional epoxy resin-polyetherimide blends," *Polymer (Guildf).*, vol. 33, no. 7, pp. 1379–1383, 1992.

[40] A. J. Crosby and J.-Y. Lee, "Polymer nanocomposites: the ﷺnano﷽ effect on mechanical properties," *Polym. Rev.*, vol. 47, no. 2, pp. 217–229, 2007.

[41] A. K. Noor and S. L. Venneri, *Flight-vehicle Materials, Structures, and Dynamics: Advanced metallics, metal-matrix and polymer-matrix composites*, vol. 2. American Society of Mechanical Engineers, 1994.

[42] Z. Yu *et al.*, "Preparation of graphene oxide modified by titanium dioxide to enhance the anti-corrosion performance of epoxy coatings," *Surf. Coatings Technol.*, vol. 276, pp. 471–478, 2015.

[43] Z. Yang, W. Sun, L. Wang, S. Li, T. Zhu, and G. Liu, "Liquid-phase exfoliated fluorographene as a two dimensional coating filler for enhanced corrosion protection performance," *Corros. Sci.*, vol. 103, pp. 312–318, 2016.

[44] M. Ehsani, H. A. Khonakdar, and A. Ghadami, "Progress in Organic Coatings Assessment of morphological , thermal , and viscoelastic properties of epoxy vinyl ester coating composites : Role of glass flake and mixing method," *Prog. Org. Coatings*, vol. 76, no. 1, pp. 238–243, 2013.

[45] M. Nematollahi, M. Heidarian, M. Peikari, S. M. Kassiriha, N. Arianpouya, and M. Esmaeilpour, "Comparison between the effect of nanoglass flake and montmorillonite organoclay on corrosion performance of epoxy coating," *Corros. Sci.*, vol. 52, no. 5, pp. 1809–1817, 2010.

[46] S. Sathiyanarayanan, S. S. Azim, and G. Venkatachari, "Corrosion protection coating containing polyaniline glass flake composite for steel," vol. 53, pp. 2087–2094, 2008.

[47] G. Wang and J. Yang, "Progress in Organic Coatings Influences of glass flakes on fire protection and water resistance of waterborne intumescent fire resistive coating for steel structure," *Prog. Org. Coatings*, vol. 70, no. 2–3, pp. 150–156, 2011.

[48] J. J. Santana, S. González, and R. M. Souto, "Progress in Organic Coatings Resistance of metallic substrates protected by an organic coating containing glass flakes," vol. 68, pp. 240–243, 2010.

[49] H. Alhumade, A. Yu, A. Elkamel, and L. Simon, "Optimizing Corrosion Protection of Stainless Steel 304 by Epoxy-Graphene Composite using Factorial Experimental Design," pp. 1105–1112, 2016.

[50] D. Wang and G. P. Bierwagen, “Progress in Organic Coatings Sol – gel coatings on metals for corrosion protection,” vol. 64, pp. 327–338, 2009.

[51] G. Kang, Q. Kan, J. Zhang, and Y. Sun, “Time-dependent ratchetting experiments of SS304 stainless steel,” vol. 22, pp. 858–894, 2006.

[52] Y. Tsutsumi, A. Nishikata, and T. Tsuru, “Pitting corrosion mechanism of Type 304 stainless steel under a droplet of chloride solutions,” vol. 49, pp. 1394–1407, 2007.

[53] Z. Xu and M. J. Buehler, “Geometry controls conformation of graphene sheets: membranes, ribbons, and scrolls,” *ACS Nano*, vol. 4, no. 7, pp. 3869–3876, 2010.

[54] B. P. Singh, B. K. Jena, S. Bhattacharjee, and L. Besra, “Development of oxidation and corrosion resistance hydrophobic graphene oxide-polymer composite coating on copper,” *Surf. Coatings Technol.*, vol. 232, pp. 475–481, 2013.

[55] D. Prasai, J. C. Tuberquia, R. R. Harl, G. K. Jennings, and K. I. Bolotin, “Graphene: corrosion-inhibiting coating,” *ACS Nano*, vol. 6, no. 2, pp. 1102–1108, 2012.

[56] D. Dobos and S. Wawzonek, “Electrochemical data,” *J. Electrochem. Soc.*, vol. 123, no. 10, p. 348C--348C, 1976.

[57] F. Bellucci, L. Nicodemo, T. Monetta, M. J. Kloppers, and R. M. Latanision, “A study of corrosion initiation on polyimide coatings,” *Corros. Sci.*, vol. 33, no. 8, pp. 1203–1226, 1992.

[58] D. Roy, G. P. Simon, M. Forsyth, J. Mardel, and others, “Towards a better understanding of the cathodic disbondment performance of polyethylene coatings on steel,” *Adv. Polym. Technol.*, vol. 21, no. 1, pp. 44–58, 2002.

[59] C. Bao *et al.*, “Graphite oxide, graphene, and metal-loaded graphene for fire safety applications

of polystyrene," *J. Mater. Chem.*, vol. 22, no. 32, pp. 16399–16406, 2012.

[60] J. R. Potts, O. Shankar, L. Du, and R. S. Ruoff, "Processing--morphology--property relationships and composite theory analysis of reduced graphene oxide/natural rubber nanocomposites," *Macromolecules*, vol. 45, no. 15, pp. 6045–6055, 2012.

[61] J. S. F. Barrett, A. A. Abdala, and F. Srienc, "Poly (hydroxyalkanoate) elastomers and their graphene nanocomposites," *Macromolecules*, vol. 47, no. 12, pp. 3926–3941, 2014.

[62] C. H. Chang *et al.*, "Novel anticorrosion coatings prepared from polyaniline/graphene composites," *Carbon N. Y.*, vol. 50, no. 14, pp. 5044–5051, 2012.

[63] K. C. Chang *et al.*, "Room-temperature cured hydrophobic epoxy/graphene composites as corrosion inhibitor for cold-rolled steel," *Carbon N. Y.*, vol. 66, pp. 144–153, 2014.

[64] K. C. Chang *et al.*, "Advanced anticorrosive coatings prepared from electroactive polyimide/graphene nanocomposites with synergistic effects of redox catalytic capability and gas barrier properties," *Express Polym. Lett*, vol. 8, pp. 243–255, 2014.

[65] D. Prasai, J. C. Tuberquia, R. R. Harl, G. K. Jennings, and K. I. Bolotin, "Graphene: Corrosion-inhibiting coating," *ACS Nano*, vol. 6, no. 2, pp. 1102–1108, 2012.

[66] J. Liang *et al.*, "Molecular-level dispersion of graphene into poly (vinyl alcohol) and effective reinforcement of their nanocomposites," *Adv. Funct. Mater.*, vol. 19, no. 14, pp. 2297–2302, 2009.

[67] M. Stern and A. L. Geary, "Electrochemical Polarization," *J. Electrochem. Soc.*, vol. 104, no. 9, p. 559, 1957.

[68] J. O. Bockris and A. K. N. Reddy, *Modern Electrochemistry 2B: Electrodics in Chemistry,*

Engineering, Biology and Environmental Science, vol. 2. Springer Science & Business Media, 2001.

[69] B. R. V Dennis, L. T. Viyannalage, and V. Anil, "Graphene nanocomposite coatings for protecting low- alloy steels from corrosion," 1945.

[70] M.-H. Tsai, I. Tseng, Y.-F. Liao, J.-C. Chiang, and others, "Transparent polyimide nanocomposites with improved moisture barrier using graphene," *Polym. Int.*, vol. 62, no. 9, pp. 1302–1309, 2013.

[71] S.-M. Park and J.-S. Yoo, "Peer reviewed: electrochemical impedance spectroscopy for better electrochemical measurements," *Anal. Chem.*, vol. 75, no. 21, p. 455--A, 2003.

[72] D. Wang, B. Xiang, Y. Liang, S. Song, and C. Liu, "Corrosion control of copper in 3.5 wt.% NaCl solution by domperidone: experimental and theoretical study," *Corros. Sci.*, vol. 85, pp. 77–86, 2014.

[73] K. F. Khaled, "Studies of the corrosion inhibition of copper in sodium chloride solutions using chemical and electrochemical measurements," *Mater. Chem. Phys.*, vol. 125, no. 3, pp. 427–433, 2011.

[74] F. Zucchi, V. Grassi, A. Frignani, C. Monticelli, and G. Trabanelli, "Electrochemical behaviour of a magnesium alloy containing rare earth elements," *J. Appl. Electrochem.*, vol. 36, no. 2, pp. 195–204, 2006.

[75] M. Li, X. Huang, C. Wu, H. Xu, P. Jiang, and T. Tanaka, "Fabrication of two-dimensional hybrid sheets by decorating insulating PANI on reduced graphene oxide for polymer nanocomposites with low dielectric loss and high dielectric constant," *J. Mater. Chem.*, vol. 22,

no. 44, pp. 23477–23484, 2012.

[76] J. Longun and J. O. Iroh, "Nano-graphene/polyimide composites with extremely high rubbery plateau modulus," *Carbon N. Y.*, vol. 50, no. 5, pp. 1823–1832, 2012.

[77] K.-H. Liao, Y. T. Park, A. Abdala, and C. Macosko, "Aqueous reduced graphene/thermoplastic polyurethane nanocomposites," *Polymer (Guildf).*, vol. 54, no. 17, pp. 4555–4559, 2013.

[78] K. C. Chang *et al.*, "Advanced anticorrosive coatings prepared from electroactive polyimide/graphene nanocomposites with synergistic effects of redox catalytic capability and gas barrier properties," *Express Polym. Lett.*, vol. 8, no. 4, pp. 243–255, 2014.

[79] S. Liu, L. Gu, H. Zhao, J. Chen, and H. Yu, "Corrosion Resistance of Graphene-Reinforced Waterborne Epoxy Coatings," *J. Mater. Sci. Technol.*, vol. 32, no. 5, pp. 425–431, 2016.

[80] C.-H. Chang *et al.*, "Novel anticorrosion coatings prepared from polyaniline/graphene composites," *Carbon N. Y.*, vol. 50, no. 14, pp. 5044–5051, 2012.

[81] Y. Chen, H.-B. Zhang, Y. Huang, Y. Jiang, W.-G. Zheng, and Z.-Z. Yu, "Magnetic and electrically conductive epoxy/graphene/carbonyl iron nanocomposites for efficient electromagnetic interference shielding," *Compos. Sci. Technol.*, vol. 118, pp. 178–185, 2015.

[82] Y.-J. Wan, W.-H. Yang, S.-H. Yu, R. Sun, C.-P. Wong, and W.-H. Liao, "Covalent polymer functionalization of graphene for improved dielectric properties and thermal stability of epoxy composites," *Compos. Sci. Technol.*, vol. 122, pp. 27–35, 2016.

[83] F. Wang, L. T. Drzal, Y. Qin, and Z. Huang, "Enhancement of fracture toughness, mechanical and thermal properties of rubber/epoxy composites by incorporation of graphene nanoplatelets," *Compos. Part A Appl. Sci. Manuf.*, vol. 87, pp. 10–22, 2016.

[84] K.-H. Liao, S. Aoyama, A. A. Abdala, and C. Macosko, "Does Graphene Change T g of Nanocomposites?," *Macromolecules*, vol. 47, no. 23, pp. 8311–8319, 2014.

[85] L.-C. Tang *et al.*, "The effect of graphene dispersion on the mechanical properties of graphene/epoxy composites," *Carbon N. Y.*, vol. 60, pp. 16–27, 2013.

[86] A. Ghasemi-Kahrizsangi, J. Neshati, H. Shariatpanahi, and E. Akbarinezhad, "Improving the UV degradation resistance of epoxy coatings using modified carbon black nanoparticles," *Prog. Org. Coatings*, vol. 85, pp. 199–207, 2015.

[87] M. A. Rafiee, J. Rafiee, Z. Wang, H. Song, Z.-Z. Yu, and N. Koratkar, "Enhanced mechanical properties of nanocomposites at low graphene content," *ACS Nano*, vol. 3, no. 12, pp. 3884–3890, 2009.

[88] S. Chandrasekaran, N. Sato, F. Tölle, R. Mülhaupt, B. Fiedler, and K. Schulte, "Fracture toughness and failure mechanism of graphene based epoxy composites," *Compos. Sci. Technol.*, vol. 97, pp. 90–99, 2014.

[89] D. R. Bortz, E. G. Heras, and I. Martin-Gullon, "Impressive fatigue life and fracture toughness improvements in graphene oxide/epoxy composites," *Macromolecules*, vol. 45, no. 1, pp. 238–245, 2011.

[90] E. P. Giannelis, "Polymer layered silicate nanocomposites," *Adv. Mater.*, vol. 8, no. 1, pp. 29–35, 1996.

[91] Y. Wei, J. Wang, X. Jia, J.-M. Yeh, and P. Spellane, "Polyaniline as corrosion protection coatings on cold rolled steel," *Polymer (Guildf).*, vol. 36, no. 23, pp. 4535–4537, 1995.

[92] K. Shah and J. Iroh, "Electrochemical synthesis and corrosion behavior of poly (N-ethyl aniline)

coatings on Al-2024 alloy," *Synth. Met.*, vol. 132, no. 1, pp. 35–41, 2002.

[93] Z. Y. Wang *et al.*, "Electroactive polyimides derived from amino-terminated aniline trimer," *Macromolecules*, vol. 31, no. 8, pp. 2702–2704, 1998.

[94] W. Lu, X. Sheng Meng, and Z. Yuan Wang, "Electrochemical behavior of a new electroactive polyimide derived from aniline trimer," *J. Polym. Sci. Part A Polym. Chem.*, vol. 37, no. 23, pp. 4295–4301, 1999.

[95] D. Chao *et al.*, "Electroactive hyperbranched polyamide synthesized by oxidative coupling polymerization within an A2+ B3 Strategy," *Macromol. Chem. Phys.*, vol. 208, no. 6, pp. 658–664, 2007.

[96] K.-Y. Huang, Y.-S. Jhuo, P.-S. Wu, C.-H. Lin, Y.-H. Yu, and J.-M. Yeh, "Electrochemical studies for the electroactivity of amine-capped aniline trimer on the anticorrosion effect of as-prepared polyimide coatings," *Eur. Polym. J.*, vol. 45, no. 2, pp. 485–493, 2009.

[97] K.-C. Chang *et al.*, "Nanocasting technique to prepare lotus-leaf-like superhydrophobic electroactive polyimide as advanced anticorrosive coatings," *ACS Appl. Mater. Interfaces*, vol. 5, no. 4, pp. 1460–1467, 2013.

[98] D. Chao *et al.*, "New method of synthesis of electroactive polyamide with amine-capped aniline pentamer in the main chain," *J. Polym. Sci. Part A Polym. Chem.*, vol. 44, no. 1, pp. 477–482, 2006.

[99] D. Chao *et al.*, "Design, synthesis and characterization of novel electroactive polyamide with amine-capped aniline pentamer in the main chain via oxidative coupling polymerization," *J. Appl. Polym. Sci.*, vol. 104, no. 3, pp. 1603–1608, 2007.

[100] D. Chao, X. Lu, J. Chen, X. Liu, W. Zhang, and Y. Wei, “Synthesis and characterization of electroactive polyamide with amine-capped aniline pentamer and ferrocene in the main chain by oxidative coupling polymerization,” *Polymer (Guildf).*, vol. 47, no. 8, pp. 2643–2648, 2006.

[101] C.-J. Weng *et al.*, “Advanced anticorrosive coatings prepared from the mimicked xanthosoma sagittifolium-leaf-like electroactive epoxy with synergistic effects of superhydrophobicity and redox catalytic capability,” *Chem. Mater.*, vol. 23, no. 8, pp. 2075–2083, 2011.

[102] H.-Y. Huang *et al.*, “Advanced anticorrosive materials prepared from amine-capped aniline trimer-based electroactive polyimide-clay nanocomposite materials with synergistic effects of redox catalytic capability and gas barrier properties,” *Polymer (Guildf).*, vol. 52, no. 11, pp. 2391–2400, 2011.

[103] Y.-C. Chou *et al.*, “Synthesis and anticorrosive properties of electroactive polyimide/SiO2 composites,” *Polym. Compos.*, vol. 35, no. 3, pp. 617–625, 2014.

[104] C.-J. Weng, J.-Y. Huang, K.-Y. Huang, Y.-S. Jhuo, M.-H. Tsai, and J.-M. Yeh, “Advanced anticorrosive coatings prepared from electroactive polyimide--TiO 2 hybrid nanocomposite materials,” *Electrochim. Acta*, vol. 55, no. 28, pp. 8430–8438, 2010.

[105] M. Nematollahi, M. Heidarian, M. Peikari, S. M. Kassiriha, N. Arianpouya, and M. Esmaeilpour, “Comparison between the effect of nanoglass flake and montmorillonite organoclay on corrosion performance of epoxy coating,” *Corros. Sci.*, vol. 52, no. 5, pp. 1809–1817, 2010.

[106] Y. Wei, C. Yang, and T. Ding, “A one-step method to synthesize N, N’-bis (4’-aminophenyl)-1, 4-quinonenediimine and its derivatives,” *Tetrahedron Lett.*, vol. 37, no. 6, pp. 731–734, 1996.

[107] X. Hou, Y. Wang, G. Sun, R. Huang, and C. Zhang, “Effect of polyaniline-modified glass flakes on the corrosion protection properties of epoxy coatings,” *High Perform. Polym.*, vol. 29, no. 3, pp. 305–314, 2017.

[108] Z. Li *et al.*, “Control of the functionality of graphene oxide for its application in epoxy nanocomposites,” *Polym. (United Kingdom)*, vol. 54, no. 23, pp. 6437–6446, 2013.

[109] J. Manna, B. Roy, and P. Sharma, “Efficient hydrogen generation from sodium borohydride hydrolysis using silica sulfuric acid catalyst,” *J. Power Sources*, vol. 275, pp. 727–733, 2015.

[110] M.-Y. Jiang, L.-K. Wu, J.-M. Hu, and J.-Q. Zhang, “Silane-incorporated epoxy coatings on aluminum alloy (AA2024). Part 1: Improved corrosion performance,” *Corros. Sci.*, vol. 92, pp. 118–126, 2015.

[111] M.-Y. Jiang, L.-K. Wu, J.-M. Hu, and J.-Q. Zhang, “Silane-incorporated epoxy coatings on aluminum alloy (AA2024). Part 2: Mechanistic investigations,” *Corros. Sci.*, vol. 92, pp. 127–135, 2015.

[112] B. D. Mert, “Corrosion protection of aluminum by electrochemically synthesized composite organic coating,” *Corros. Sci.*, vol. 103, pp. 88–94, 2016.

[113] S. Hiromoto, “Self-healing property of hydroxyapatite and octacalcium phosphate coatings on pure magnesium and magnesium alloy,” *Corros. Sci.*, vol. 100, pp. 284–294, 2015.

[114] S. Pour-Ali, C. Dehghanian, and A. Kosari, “Corrosion protection of the reinforcing steels in chloride-laden concrete environment through epoxy/polyaniline--camphorsulfonate nanocomposite coating,” *Corros. Sci.*, vol. 90, pp. 239–247, 2015.

[115] A. Ghanbari and M. M. Attar, “A study on the anticorrosion performance of epoxy

nanocomposite coatings containing epoxy-silane treated nano-silica on mild steel substrate," *J. Ind. Eng. Chem.*, vol. 23, pp. 145–153, 2015.

[116] S. S. Golru, M. M. Attar, and B. Ramezanzadeh, "Studying the influence of nano-Al 2 O 3 particles on the corrosion performance and hydrolytic degradation resistance of an epoxy/polyamide coating on AA-1050," *Prog. Org. Coatings*, vol. 77, no. 9, pp. 1391–1399, 2014.

[117] L. Liu and J. Xu, "A study of the erosion--corrosion behavior of nano-Cr 2 O 3 particles reinforced Ni-based composite alloying layer in aqueous slurry environment," *Vacuum*, vol. 85, no. 6, pp. 687–700, 2011.

[118] M. J. Palimi, M. Rostami, M. Mahdavian, and B. Ramezanzadeh, "A study on the corrosion inhibition properties of silane-modified Fe2O3 nanoparticle on mild steel and its effect on the anticorrosion properties of the polyurethane coating," *J. Coatings Technol. Res.*, vol. 12, no. 2, pp. 277–292, 2015.

[119] S. K. Dhoke, A. S. Khanna, and T. J. M. Sinha, "Effect of nano-ZnO particles on the corrosion behavior of alkyd-based waterborne coatings," *Prog. Org. Coatings*, vol. 64, no. 4, pp. 371–382, 2009.

[120] M. K. Sahnesarayi, H. Sarpoolaky, and S. Rastegari, "Effect of heat treatment temperature on the performance of nano-TiO 2 coating in protecting 316L stainless steel against corrosion under UV illumination and dark conditions," *Surf. Coatings Technol.*, vol. 258, pp. 861–870, 2014.

[121] J. Li, L. Ecco, M. Fedel, V. Ermini, G. Delmas, and J. Pan, "In-situ AFM and EIS study of a solventborne alkyd coating with nanoclay for corrosion protection of carbon steel," *Prog. Org. Coatings*, vol. 87, pp. 179–188, 2015.

[122] B. P. Singh, S. Nayak, K. K. Nanda, B. K. Jena, S. Bhattacharjee, and L. Besra, "The production of a corrosion resistant graphene reinforced composite coating on copper by electrophoretic deposition," *Carbon N. Y.*, vol. 61, pp. 47–56, 2013.

[123] N.-W. Pu *et al.*, "Graphene grown on stainless steel as a high-performance and ecofriendly anti-corrosion coating for polymer electrolyte membrane fuel cell bipolar plates," *J. Power Sources*, vol. 282, pp. 248–256, 2015.

[124] S. Chen *et al.*, "Oxidation resistance of graphene-coated Cu and Cu/Ni alloy," *ACS Nano*, vol. 5, no. 2, pp. 1321–1327, 2011.

[125] Y.-W. Son, M. L. Cohen, and S. G. Louie, "Half-metallic graphene nanoribbons," *Nature*, vol. 444, no. 7117, pp. 347–349, 2006.

[126] J. S. Bunch *et al.*, "Impermeable atomic membranes from graphene sheets," *Nano Lett.*, vol. 8, no. 8, pp. 2458–2462, 2008.